Loss of function mutation of the receptor guanylyl cyclase B (GC-B) leads to changes in features of auditory processing

Dissertation

der Mathematisch-Naturwissenschaftlichen Fakultät

der Eberhard Karls Universität Tübingen

zur Erlangung des Grades eines

Doktors der Naturwissenschaften

(Dr. rer. nat.)

vorgelegt von

Steffen Wolter

aus Weimar

Tübingen

2019

Gedruckt mit Genehmigung der Mathematisch-Naturwissenschaftlichen Fakultät der Eberhard Karls Universität Tübingen.

Tag der mündlichen Qualifikation:	03.07.2019
Dekan:	Prof. Dr. Wolfgang Rosenstiel
1. Berichterstatter:	Prof. Dr. Jan Benda
2. Berichterstatter:	Prof. Dr. Marlies Knipper

Ich erkläre hiermit, dass ich die zur Promotion eingereichte Arbeit mit dem Titel: „Loss of function mutation of the receptor guanylyl cyclase B (GC-B) leads to changes in features of auditory processing“ selbstständig verfasst, nur die angegebenen Quellen und Hilfsmittel benutzt und wörtlich oder inhaltlich übernommene Stellen (alternativ: Zitate) als solche gekennzeichnet habe. Ich erkläre, dass die Richtlinien zur Sicherung guter wissenschaftlicher Praxis der Universität Tübingen (Beschluss des Senats vom 25.05.2000) beachtet wurden. Ich versichere an Eides statt, dass diese Angaben wahr sind und dass ich nichts verschwiegen habe. Mir ist bekannt, dass die falsche Abgabe an Eides statt mit Freiheitsstrafe bis zu drei Jahren oder mit Geldstrafe bestraft wird.

Acknowledgements

Ich möchte mich bei Prof. Dr. Marlies Knipper für die Möglichkeit in ihrer Gruppe zu arbeiten, sowie für die vielen anregenden Diskussionen und Ideen und die vielfältige Unterstützung auch über meine Zeit in Tübingen hinaus bedanken.

Mein Dank gilt auch apl. Prof. Dr. Lukas Rüttiger für seine umfassenden Erklärungen und die kritische Sicht auf mein Experimente.

Besonders möchte ich mich bei meinen wundervollen Kollegen Dorit, Marie, Philipp „Lanewalker“ A., Benedikt, Philipp E., Wibke, Dario, Lewis, Kun, Yan, Giulia und Satish für all die Unterstützung, die tolle Zusammenarbeit und die zahlreichen linguistischen, kulinarischen und nerdigen Erfahrungen bedanken.

Vielen Dank an die fleißigen Bienen Karin, Iris und Hyun-Soon für den ausgezeichneten technischen Support ,Ulli für die hilfreichen Vorschläge zur grafischen Darstellung wissenschaftlicher Daten, sowie Monika und Kerstin für die Hilfe bei administrativen Fragen.

Besonderer Dank gilt meiner Familie und besonders meinen Liebsten Lena und Tim für das Verständnis, die fortwährende Unterstützung und Hingabe während einer intensiven Zeit voller Veränderungen. Ohne euch wäre diese Arbeit nicht zustande gekommen.

Table of Contents

Abbreviations

ABR	auditory brainstem response
AC	auditory cortex
AN	auditory nerve
ANP	atrial natriuretic peptide
aVCN	anteroventral cochlear nucleus
BNP	B-type natriuretic peptide
CF	carrier frequency
ChAT	choline acetyltransferase
CN	cochlear nucleus
CNP	C-type natriuretic peptide
cGMP	cyclic guanosine monophosphate
cGKIα	cyclic guanosine monophosphate-dependent protein kinase Iα
CSG	cranial sensory ganglion
CtBP2	c-terminal-binding protein 2
CTRL	control
DCN	dorsal cochlear nucleus
DPOAE	distortion product otoacoustic emissions
DRG	dorsal root ganglion
EF-LOC	efferent innervation from the lateral olivary complex
EF-MOC	efferent innervation from the medial olivary complex
GABA	γ-aminobutyric acid
gVII/VIII	acousticofacial ganglion
gVIII	vestibuloacoustic ganglion
HET	heterozygous
IC	inferior colliculus
IHC	inner hair cell
I-O function	input-output function
ITD	interaural time difference
KO	knockout
LL	lateral lemniscus
LOC	lateral olivocochlear complex
MET	mechanoelectrical transduction

MF	modulation frequency
MGB	medial geniculate body
MNTB	medial nuclei of the trapezoid body
MOC	medial olivocochlear complex
nAChR	α9/α10-nicotinic receptors
NF	neurofilament protein
NO	nitric oxide
NO-GC	NO-sensitive soluble guanylyl cyclase
NPR	natriuretic peptide receptor
OC	organ of Corti
OHC	outer hair cell
PFA	paraformaldehyde
PG	pontine grey
PPF	prepulse facilitation
PPI	prepulse inhibition
PRN	pontine reticular nuclei
pVCN	posteroventral cochlear nucleus
SGN	spiral ganglion neuron
SNR	signal-to-noise ratio
SOC	superior olivary complex
SR	spontaneous firing rate
VAMP2	vesicle-associated membrane protein isotype 2
VCN	ventral cochlear nucleus
vGlut3	vesicular glutamate transporter 3
VGN	vestibular ganglion neuron
WT	wildtype

Symbols

Ca^{2+}	calcium
dB	decibel
E	embryonal day
f_1	primary frequency 1
f_2	primary frequency 2
H	hertz
kHz	kilohertz
K^+	potassium
L_1	primary 1 stimulus level
mm	micrometer
ms	milliseconds
n.s.	not significant
P	postnatal day
S.D.	standard deviation
S.E.M.	standard error of the mean
SL	sensation level
SPL	sound pressure level
µm	micrometer

Summary

The guanylyl cyclase B (GC-B) was recently shown to be important for proper wiring of sensory axons of dorsal root ganglions (DRGs) as well as cranial sensory ganglions (CSGs) as genetic deletion of GC-B and other components of the GC-B signaling pathway resulted in failure of T-like branches in the spinal cord and the hindbrain, respectively (Schmidt et al. 2007; Schmidt et al. 2009; Schmidt and Rathjen 2010; Ter-Avetisyan et al. 2014). First studies shed light on impaired bifurcation of spiral ganglion neurons (SGNs), whose axons form the auditory nerve (AN), showed disturbed tonotopic representation on the level of the cochlear nucleus (CN) and impaired reliance of AN activity but basic hearing function seemed to be normal (Lu et al. 2014). In contrast, the present study found for the first time that a loss of function mutation of the GC-B gene lead to a basal hearing phenotype using standardized methods for investigation of auditory thresholds, namely auditory brainstem responses (ABRs) and distortion products of the otoacoustic emission (DPOAEs). The discovered loss of sensitivity to recognize acoustic stimuli was not caused by impaired sound transmission in the middle ear but changed outer hair cell (OHC) sensitivity following sound stimulation. Analysis of GC-B expression patterns in the cochlea and the brainstem point to intact cochlear hair cells and supports the abundance of fully differentiated and functional inner and outer hair cells (IHCs and OHCs, respectively). Strikingly, morphological and functional analysis of retrocochlear innervation, which drives efferent feedback control of active cochlear amplification and overall cochlear output, points to reduced efferent innervation and changed efferent modulation of hair cell activity. This argument is supported by disclosure of greatly delayed signal transmission along the afferent auditory pathway with misproportion of synchronous activity in the involved auditory nuclei. Reliance and precision of very fast auditory processing was revealed as detection of amplitude-modulated sounds, especially close to detection threshold, and temporal features regarding acoustic startle response (ASR) and prepulse inhibition (PPI) were changed in constitutive GC-B knockout (KO) mice. First experiments with conditional GC-B and cGKI KO mice confirmed the neuronal basis of the observed auditory threshold phenotype of constitutive GC-B KO mice. Concluded, a severe impairment of wiring of AN fibers within the CN during formation of the ascending auditory pathway leads to a profound hearing phenotype, including deficits in temporal resolution of auditory signals.

Zusammenfassung

Kürzlich veröffentlichte Studien haben gezeigt, dass der Rezeptor Guanylylcyclase B (GC-B) für eine ordnungsgemäße Verschaltung von Axonen spinaler und kranialer sensorischer Neurone im Rückenmark notwendig sind, da eine genetische Deletion des GC-B Gens und andere Komponenten der GC-B-abhängigen Signalkaskade und anderer Komponenten zu einem Verlust der Verzweigung afferenter Nerven im im Rückenmark bzw. im Hinterhirn führt (Schmidt et al. 2007; Schmidt et al. 2009; Schmidt and Rathjen 2010; Ter-Avetisyan et al. 2014). Eine erste Studie hat gezeigt, dass genetische Inaktivierung von GC-B zu gestörter Bifurkation von Spiralganglionneuronen führt, deren Axone den Hörnerv bilden was eine gestörte tonotope Repräsentation auf Ebene des CN und eine reduzierte Zuverlässigkeit der Signalübertragung im Hörnerv zur Folge hatte (Lu et al. 2014). Im Gegensatz dazu zeigt die vorliegende Studie zum ersten Mal mithilfe standardisierter klinischer und wissenschaftlicher Messmethoden zur Ermittlung von Hörschwellen, dass ein Funktionsverlust von GC-B zu einem basalen Hörphänotyp führt. Der offengelegte Empfindlichkeitsverlust bei der Detektion akustischer Reize konnte nicht mit einer beeinträchtigten der Schallübertragung im Mittelohr in Verbindung gebracht werden, sondern ist wahrscheinlich durch Veränderungen in der Empfindlichkeit äusserer Haarzellen bedingt. Die Analyse der Expressionsmuster in der Kochlea und im Hirnstamm weist auf intakte und funktionstüchtige Haarzellen hin. Die veränderte Empfindlichkeit kochleärer Haarzellen ist wahrscheinlich durch Veränderungen in der Rückkopplungskontrolle der aktiven Signalverstärkung und infolgedessen einer Erhöhung der Gesamtaktivität des Hörnervs bedingt. Diese Hypothese wird durch die Offenlegung einer stark verzögerten und unsynchronen Signalübertragung in der aufsteigenden Hörbahn unterstützt. Die Zuverlässigkeit und Präzision der sehr schnellen Verarbeitung akustischer Reize scheint gestört zu sein, was sich in subtilen Veränderungen in der Erkennung amplitudenmodulierter Stimuli nahe der Hörschwelle und in Eigenschaften der akustischen Schreckreaktion widerspiegelt. Der basale Hörphänotyp konnte im konditionalen Mausmodell betätigt werden, was für eine neuronale Grundlage spricht. Die Erkenntnisse der vorliegenden Studie weisen daher stark auf eine tiefgreifende Störung in der zeitlichen Präzision der Erkennung akustischer Reiz hin, wenn die ordnungsgemäße Ausbildung der Verzweigungen des Hörnervs gestört ist.

List of publications

Accepted Papers

Möhrle D*, Reimann K*, **Wolter S***, Wolters M, Varakina K, Mergia E, Eichert N, Geisler HS, Sandner P, Ruth P, Friebe A, Feil R, Zimmermann U, Koesling D, Knipper M, Rüttiger L (2017) NO-sensitive guanylate cyclase isoforms NO-GC1 and NO-GC2 contribute to noise-induced inner hair cell synaptopathy. Molecular Pharmacology 92:375-388.

Wolter S*, Möhrle D*, Schmidt H, Pfeiffer S, Zelle D, Eckert P, Krämer M, Feil R, Pilz PKD, Knipper M, Rüttiger L (2018) GC-B deficient mice with axon bifurcation loss exhibit compromised precision of auditory processing. Frontiers Neural Circuits 12:65.

*: equal contributions

1. Introduction

The auditory system is able to detect sound waves by transformation into mechanical deflections, neurotransmitter release and generation of neuronal signals, which are processed and used for adequate reactions to the environment, for interindividual and interspecific communication or navigation. Sound is ubiquitous and exists in infinite variations of modulated frequencies and amplitudes, for which reason the auditory system has to be able to extract meaningful content precisely and reliably in the frequency and time domain and to process them in the appropriate auditory nuclei in the brain. If functional, the auditory system can detect differences in the arrival time of sound between two ears in the microsecond range (interaural time differences, ITDs) (Brand et al. 2002; G. Klumpp and R. Eady 1956). If auditory processing is compromised, the accessibility of this essential information may get lost. According to WHO estimates, 432 million people suffer from disabling hearing loss (6.1 % of the world's population) which is therefore the most frequent sensory impairment in humans (Mathers et al. 2000). Impaired hearing can lead to disturbed speech perception, thus restricting communication and social interactions of affected individuals with significant consequences for language acquisition, education, employment and overall wellbeing (Graydon et al. 2019). Human auditory defects have been intensively studied in animal models, in particular mouse models, which allow for genetic manipulations of genes associated with deafness in humans. So far, little is known about the effects of impaired neuronal wiring on the level of the cochlear nucleus (CN) under control of the CNP/GC-B/cGMP/cGKI-signaling cascade (Lu et al. 2014; Ter-Avetisyan et al. 2014) for the integrity and reliability of the auditory system.

1.1 Anatomy of the cochlea and the auditory pathway

The origin of the hearing impairments discussed in this study is anchored in early development but studied in the mature auditory system. Therefore, organization of the auditory pathway and relevant proteins involved in adequate wiring of ascending fibers are briefly described in the following chapter.

1.1.1 Organization of the inner ear

Sound is propagated through the outer and the middle ear into the inner ear, where the sensory epithelium is localized. Within the inner ear, sound is perceived and converted into electrical signals by the cochlear hair cells, which are embedded in a structure called the organ of Corti (OC, Fig. 1). Sound vibrates the liquid-filled scalae and the vibrations are transduced into deflections of stereocilia at the apex of the hair cells. Due to their organization in interconnected hair bundles and embedded mechanoelectrical transducer (MET) channels, which open and close according to the orientation of their deflections, sound vibrations can be coded in respect to their sound pressure level (SPL) by graded changes in membrane potential within the hair cells (Fettiplace 2017; Knipper et al. 2013).

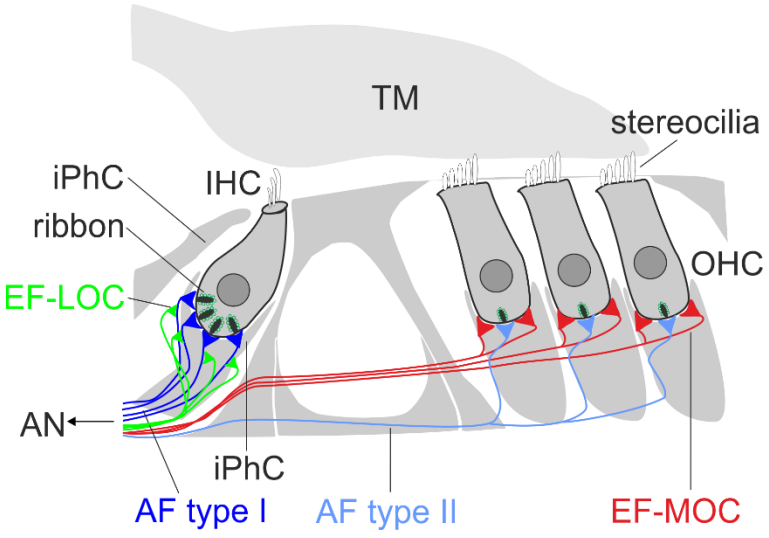

Fig. 1. Mature afferent and efferent innervation pattern of cochlear hair cells. Schematic drawing of the organ of Corti (grey). IHCs are innervated by dendritic processes of afferent fibers (AF) type I (dark blue). OHCs are innervated by dendritic processes of AF type II (bright blue). AF type I below IHCs receive efferent input via efferent fibers from the lateral olive (EF-LOC, bright green), while OHCs are directly innervated by efferent fibers from the medial olive (EF-MOC, red). Hair cell presynapses are characterized by synaptic ribbons (dark green). *Modified from (Knipper et al. 2013).*

Cochlear hair cells can be divided into two subgroups with distinct morphology and function, and are organized tonotopically, with high frequencies coded at the base and low frequencies coded at the apex of the cochlea (Von Békésy 1960). In rodents as well as in humans, three rows of outer hair cells (OHCs, Fig. 1) are specialized to shorten and enlengthen following incoming sound, thereby amplifying basilar membrane deflections according to their frequency composition. By that, sensitivity for auditory thresholds is greatly enhanced, why this OHC-based active amplification process is also referred to as the cochlear amplifier. The intrinsic electromotility of OHCs is due to the motor protein prestin, which is densely packed in the lateral walls of mature OHCs (Dallos 2008). Transduction of mechanical deflections into electrical signals is performed by the true sensory cells in the OC, the inner hair cells (IHCs, Fig. 1). Changes in membrane potential trigger release of the neurotransmitter glutamate into synaptic cleft between IHCs and their afferent neuronal contacts with spiral ganglion neurons (SGNs). Densely packed vesicles bound to very specialized structures, called ribbon synapses (Fig. 1), enable for coding of sound intensity with high temporal precision by graded vesicle release (Glowatzki and Fuchs 2002; Moser et al. 2006; Nouvian et al. 2006). Like hair cells, SGNs can be subdivided into two distinct classes regarding their mature innervation pattern and myelinization. Myelinated SGN afferent fibers (AF) type I contact IHCs (Fig. 1) (Kiang et al. 1982), while mainly unmyelinated AF type II are contacting OHCs (Fig. 1) (Berglund and Ryugo 1987). Further, AF type I are distinguishable in their response characteristics to acoustic stimuli, with high spontaneous firing rate (SR) fibers (high-SR fibers) having narrow dynamic ranges (are already saturated at low SPLs) and low thresholds (0-20 dB SPL), and low-SR fibers having wider dynamic ranges (are saturated at higher SPLs) and higher thresholds (40 dB SPL) (Liberman 1978, 1980; Sachs and Abbas 1974). This diversity in response characteristics allows for precise temporal and frequency coding, covering a wide range of stimulus intensities (Buran et al. 2010; Knipper et al. 2013). In contrast, AF type II are still discussed to be involved in acoustic nociception. In addition to their afferent innervation, mature OHCs and IHCs maintain efferent contacts with neurons located in the olivocochlear nuclei within the auditory brainstem. OHCs are primarily innervated by medial olivocochlear (MOC) efferent fibers (EF-MOC, Fig. 1), that originate in the medial part of the ipsi- and contralateral superior olivary complex (SOC) and are currently discussed to protect from traumatic injury following noise overexposure (Maison et al. 2013a; Maison et al. 2013b) and

contrast enhancement in noisy environments (Kawase et al. 1993). MOC-efferent fibers act on OHCs via release of the neurotransmitter acetylcholine, which is recognized by specific cholinergic receptors at the postsynaptic membrane, inducing Ca^{2+}-dependent efflux of K^{+}. Consequently, OHCs hyperpolarize and become less responsive to acoustic stimuli, reducing their electromotility which in turn results in reduced active cochlear amplification and loss of cochlear gain (Elgoyhen and Katz 2012; Guinan 2006, 2018). On the other hand, AF type I contacting IHCs receive mainly ipsilateral efferent innervation from lateral olivary complex (EF-LOC) fibers (Guinan 2006, 2010; Knipper et al. 2013) and are supposed to modulate their firing rates (Rabbitt and Brownell 2011). For instance, proper adjustment of firing rates is important for integration of binaural information underlying e.g. sound localization (Darrow et al. 2006) or protection from noise-induced overexcitation (Darrow et al. 2007).

1.1.2 Organization of the auditory pathway

This study focused on auditory processing in the auditory periphery and the auditory brainstem. To understand the phenotypes found in this study, the structure of the ascending auditory pathway will be explained briefly with focus on the nuclei in the auditory brainstem (Fig. 2). The axons of the SGNs form the auditory nerve (AN) which target several regions within the cochlear nucleus (CN), the first relay on the ascending auditory pathway (Cant and Benson 2003).

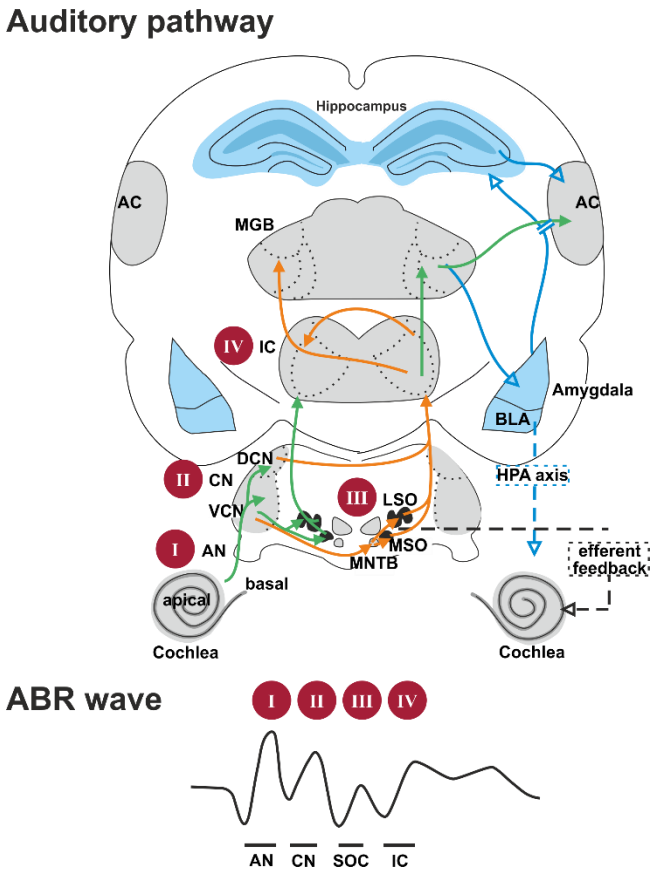

Fig. 2. Schematic drawing of the auditory pathway and correlated ABR wave deflections. Acoustic information is transduced into electrical signals in the cochlea and then propagated through the auditory nerve (AN). The AN bifurcates into an ascending branch, innervating the DCN and a descending branch innervating the VCN. Information is split at this point, with the DCN propagating auditory information to the IC, while the VCN feeds information in to the nuclei of the SOC (LSO, MSO, MNTB). ABR wave deflections can be roughly correlated to evoked activity in the AN (ABR wave I), CN (ABR wave II), SOC (ABR wave III) and IC (ABR wave IV). *Modified from (Knipper et al. 2013).*

AN fibers bifurcate into the anterior (ascending) branch and the posterior (descending) branch, innervating the three main subdivisions of the CN, the anteroventral cochlear nucleus (aVCN), posteroventral cochlear nucleus (pVCN) and the dorsal cochlear nucleus (DCN) (Brawer et al. 1974). The target neurons in the VCN themselves heavily innervate distinct nuclei in the ipsi- and contralateral SOC, e.g. the lateral and the medial olive (LSO and MSO) and the medial nuclei of the trapezoid body (MNTB, Fig. 2). In mammals with specialized high frequency hearing (e.g. rodents or bats), the LSO and MNTB are more prominent than in species with less specialization in high frequency hearing (as e.g. humans). On the other hand, the MSO is less developed in the first species (Malmierca and Ryugo 2012). The nuclei of SOC are currently discussed to be involved in sound localization. VCN neurons themselves innervate the nuclei of the lateral lemniscus (LL), which can be seen as a relay station to the inferior colliculus (IC). The IC is a higher order integration center of the ascending auditory pathway, as it integrates information from the contralateral DCN, as well as from ipsilateral and contralateral input from the SOC. The IC projects to the medial geniculate body (MGB) of the thalamus which relays the signal to the auditory cortex (AC) on the temporal lobe (Malmierca and Merchán 2004). Reliable and precise

processing of auditory information in the ascending auditory pathway is essential for maintenance of hearing function and can be critically challenged by traumatic noise exposure, genetic mutations or aging (Salvi et al. 2000). Auditory brainstem response (ABR) is a powerful tool for diagnosis of impaired evoked auditory activity within the ascending auditory pathway (Melcher and Kiang 1996)) in humans (Gu et al. 2012), as well as in animals (Rüttiger et al. 2013; Singer et al. 2013).

1.2 Role of the cGMP/cGKI-dependent signaling cascade in the auditory system

(Jaumann et al. 2012) recently tackled the question, if the intracellular second messenger molecule cyclic guanosine monophosphate (cGMP)/cGMP-dependent protein kinase I (cGKI) signaling cascade is involved in maintenance of hearing function and otoprotection after noise injury on the level of sensory hair cells. Although cGMP-dependent signaling is involved in a variety of physiological processes in the cardio-vascular, immune, genitourinary, muscular, neuronal and sensory systems (Kemp-Harper and Feil 2008), the generators upstream of cGMP responsible for the otoprotective effects found in (Jaumann et al. 2012) are still unknown. Potential candidates are the cytosolic soluble nitric-oxide-sensitive guanylyl cyclase (NO-GC/sGC) and members of the membrane-bound (particulate) guanylyl cyclases A and B (GC-A/NprA/Npr1 and GC-B/Npr2/NprB), which are themselves activated by atrial, B-type or C-type natriuretic peptides (ANP, BNP, CNP), respectively (Friebe and Koesling 2003; Kemp-Harper and Feil 2008; Kuhn 2003, 2009; Schmidt et al. 2007; Schmidt et al. 2009; Schulz 2005). The significance lies in pharmacological intervention of sensorineural hearing loss caused by deafferentation of sensory hair cells and subsequent auditory fiber loss.

1.2.1 cGMP/cGKI signaling in formation of the ascending auditory pathway

Sensory axons of dorsal root ganglia (DRG) and cranial sensory ganglia (CSG), including cochlear spiral ganglion neurons (SGN) and vestibular ganglion neurons (VGN), undergo a T-shaped branching (bifurcation, Fig. 3) before the formation of collaterals, that synapse onto second-order neurons in the spinal cord or hindbrain. The importance of CSG axon bifurcation is currently not understood. Recently it has been shown that axons of the DRG, CSG or SGN fail to bifurcate in the absence of members of the CNP/GC-B/cGMP/cGKI signaling cascade (Lu et al. 2014; Schmidt et al. 2007; Schmidt et al. 2009; Ter-Avetisyan et al. 2014).

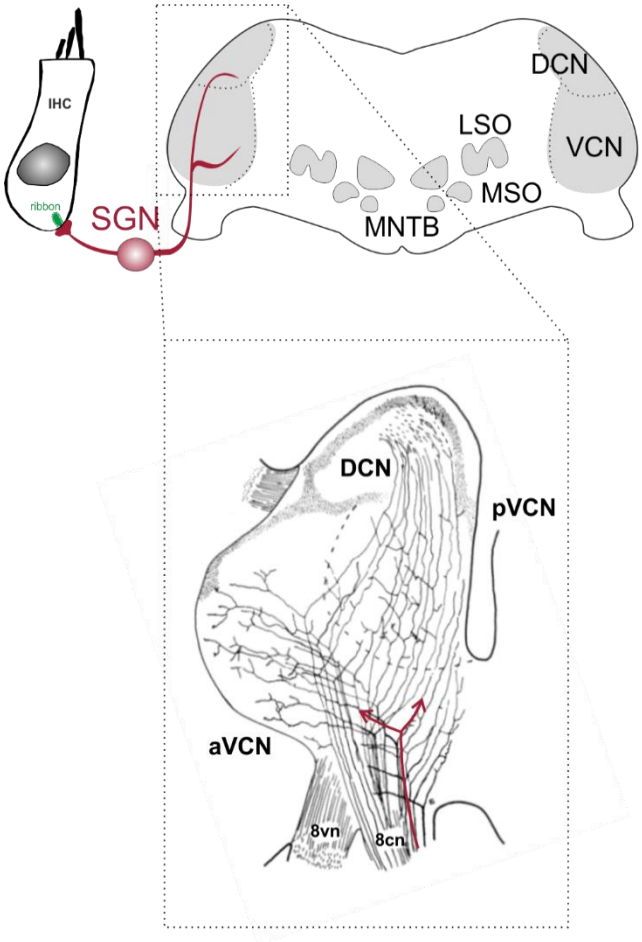

Fig. 3. Schematic drawing of the peripheral connections of the ascending auditory pathway and SGN central axon bifurcation within the CN. IHCs are afferently innervated by SGN (red) dendrites. SGN central axons bifurcate in the entry zone of the CN (red arrows in enlarged section), innervating target neurons in the dorsal (DCN), anteroventral (aVCN) and posteroventral (pVCN) portions of the CN. *Modified from (Knipper et al. 2013) and (Malmierca and Ryugo 2012).*

1.2.2 Guanylyl cyclase B (GC-B/Npr2) in the auditory system

The transmembrane receptor GC-B activates a cGMP-dependent signaling cascade (Fig. 4) upon binding of its ligand CNP, which is expressed dorsally along the length of the embryonic neural tube (Potter et al. 2006; Schmidt et al. 2009). High cytosolic cGMP levels induce bifurcation mediated by cGKI activity, but the exact mode of action is so far not known. Bifurcation loss of SGN axons due to a point mutation in the *GC-B* gene of mutant mice (*Npr2*$^{cn/cn}$) led to only subtle changes in auditory function, but deficits in the tonotopic organization typical of central auditory circuits were striking (Lu et al. 2014), affecting all innervated divisions of the CN (anterior ventral cochlear nucleus, aVCN, posterior ventral cochlear nucleus, pVCN, and dorsal cochlear nucleus, DCN, see Fig. 3). Besides the disrupted tonotopic organization, also the convergence of SGN inputs to multipolar cells in the CN may be altered in GC-B deficient mice, as T-Stellate cells in the VCN maintained a limited dynamic range of response growth to gradual increasing electrical stimulation (Lu et al. 2014). This indicates, that reliability of sound integration and encoding is disturbed. Strikingly, the multipolar cells in the VCN have been proposed as the interneurons for the cholinergic efferent feedback to OHCs, thereby controlling cochlear amplification via the EF-MOC fibers (de Venecia et al. 2005). Further it has been shown, that planar multipolar neurons in the VCN project to the ventral nucleus of the trapezoid body (MNTB), where they formed synapses with MOC neurons (Darrow et al. 2012). So far, consequences for the cochlear efferent feedback system have not yet been examined in GC-B deficient mice.

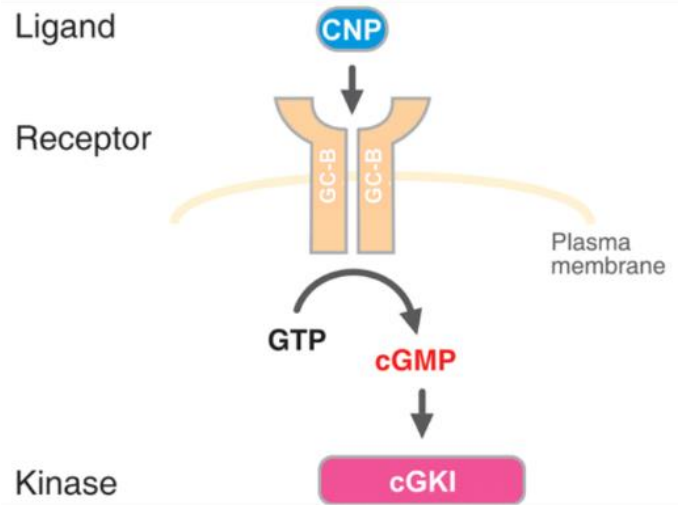

Fig. 4. Schematic figure of the known cGMP-dependent signaling pathway components involved in sensory axon bifurcation. Binding of CNP, the ligand of GC-B induces cGMP production. Cytosolic cGMP activates the cGMP-dependent protein kinase Iα (cGKI). *Modified from (Schmidt et al. 2009).*

1.2.3 Other guanylyl cyclases in the auditory system

Besides the critical role of GC-B for proper development of sensory axon bifurcation (Schmidt et al. 2007; Schmidt et al. 2009; Ter-Avetisyan et al. 2014), guanylyl cyclases are suspected to modulate cochlear function, as indicated by otoprotective effects found in (Jaumann et al. 2012). Until now, the involved cGMP generator is still unknown. Potential candidates, besides GC-B, are the particulate receptor GC-A and the NO-sensitive soluble NO-GC (Möhrle et al. 2017). NO may modulate inner ear function via different pathways, since studies showed contrary effects. Thus, NO was shown to harm cochlear function after critical noise overexposure (Ohinata et al. 2003; Shi et al. 2002). On the other hand, otoprotective effects of NO were observed on the level of cochlear hair cells, as NO-GC counteracted stressor-triggered Ca^{2+} influx (Shen et al. 2003; Shen et al. 2005; Shen et al. 2006; Takeda-Nakazawa et al. 2007; Yukawa et al. 2005). NO is synthesized by NO synthase and activates two different isoforms of NO-GC (Takumida and Anniko 2002). Both isoforms share a β1-subunit, that forms dimers with the α1-subunit or α2-subunit for NO-GC1 and NO-GC2 isoforms, respectively (Russwurm and Koesling 2002). Recently, the function of NO/NO-GC/cGMP/cGKI signaling in hearing has been specifically addressed in the mature auditory system NO-GC1 and NO-GC2 knockout mice (Möhrle et al. 2017). Another potential candidate for modulation of cochlear function is GC-A, a particulate guanylyl cyclase with well-studied function in the cardiovascular system (Kuhn 2009). First studies found evidence for the existence of ANP/GC-A signaling in SGNs contacting mature IHCs (AF type I) and OHCs (AF type II), as well as in perineuronal satellite glial cells, and suggested a possible role during neurotransmission within the spiral ganglion (Sun et al. 2014).

1.5 Aim of the study

In the present study a closer investigation of a constitutive *GC-B* knockout model (*Npr2*$^{lacZ/lacZ}$), that was created by insertion of a *lacZ* expression cassette into exon 1 of the *GC-B* gene (Ter-Avetisyan et al. 2014) was carried out to understand the consequences of impaired wiring on the level of the CN for processing of auditory information, as proper integration of sound relies on precise and reliable signal transmission in the afferent and efferent auditory pathway. Sensitive methods for hearing screening in animal models as well as in humans were used, namely auditory brainstem responses (ABRs) and distortion products of the otoacoustic emission (DPOAEs) on anesthetized mice. Fast retrocochlear modulation of OHC activity was investigated by using the primary-tone phase variation (PTPV) approach with continuous and pulsed primary presentation to test for very fast ipsilateral adaptation of the DPOAEs. Further, fast auditory processing was tested using amplitude and latency analysis of click-evoked supra-threshold ABRs. Also, auditory steady state responses (ASSR) were analyzed, as very fast changes of the envelope of amplitude-modulated tones need proper processing in the time domain. Finally, behavioral experiments with awake mice were performed to test for one of the fastest (acoustic) reflexes in mammals, the acoustic startle response (ASR) The findings suggest a role of axon bifurcation for the establishment of feedback control and precise temporal auditory processing. In particular, it was investigated: **(i)** how proper formation of the auditory pathway is affected by genetic deletion of *GC-B* in a constitutive knockout mouse model (*Npr2*$^{LacZ/LacZ}$), affecting innervation of the dorsal (DCN) and ventral cochlear nucleus (VCN). Further, **(ii)** the findings were confirmed with first experiments in conditional knockout mouse models for GC-B (*Npr2*$^{fl/fl}$*;Wnt1*^{Cre} and *cGKI*$^{fl/fl}$*;Wnt1*^{Cre}).

2. Materials and methods

2.1 Animals

Mice were housed in the animal care facility of the institute, where noise levels did not exceed 50-60 dB sound pressure level (SPL). Mice were held in groups of one (only fighting males) to five in standard Macrolon cages containing nesting material under a 12-h light-dark schedule (lights on at 7 am) and received food and tap water ad libitum. The cages were in an air-conditioned room with the temperature set at 24±1 °C and the humidity held at 60±5 %. Animal care, procedures, and treatments were performed in accordance with institutional and national guidelines following approval by the University of Tübingen, Veterinary Care Unit, and the Animal Care and Ethics Committee of the regional board of the Federal State Government of Baden-Württemberg, Germany, and followed the guidelines of the EU Directive 2010/63/EU for animal experiments.

2.1.1 Generation of $Npr2^{lacZ/lacZ}$ mice

$Npr2^{lacZ/lacZ}$ mice were generated by injection of an ES-cell line (129/Ola background) into C57Bl/6J blastocysts. Successful transmission of the mutant *Npr2-lacZ* gene was achieved by identification of chimeras by backcrossing of *$Npr2^{lacZ/+}$* males with C57BL/6J females. Additional backcrossing was performed for at least 5 generations before the mouse line was transferred to pool breeding and generation of experimental animals. Genotyping procedures of mutant alleles were conducted as described before (Ter-Avetisyan et al. 2014). For hearing measurements, behavioral experiments and molecular analysis, adult 1-to-6-month-old mice of either sex were used in this study. For behavioral experiments, a second group of 2-to-4-month-old mice was recruited.

2.1.2 Generation of $Npr2^{fl/fl};Wnt1^{Cre}$ and $cGKI^{fl/fl};Wnt1^{Cre}$ mice

Generation of *$Npr2^{fl/fl};Wnt1^{Cre}$* and *$cGKI^{fl/fl};Wnt1^{Cre}$* mice was performed by crossing *$Npr2^{fl/fl}$* (Tröster et al. 2018) or *$cGKI^{fl/fl}$* (Wegener et al. 2002) mice with *$Wnt1^{Cre}$* (Danielian et al. 1998) mice as described in detail in (Tröster et al. 2018). For hearing measurements, adult 1-to-3-month-old mice of either sex were used in this study.

2.2 Hearing measurements

If not otherwise stated, mice were anaesthetized for hearing tests using a blend of ketamine hydrochloride (75 mg/kg body weight, Ketavet, Pharmacia Pfizer, Karlsruhe, Germany), xylazine hydrochloride (5 mg/kg body weight, Rompun 2 %, Bayer, Leverkusen, Germany), atropine sulfate (0.2 mg/kg body weight, Atropinsulfat, B.Braun, Melsungen, Germany) diluted in water (Ampuwa, Fresenius KABI, Bad Homburg, Germany) administered intraperitoneally with a dosage of 5 ml/kg body weight. Initial level of anesthesia was monitored by reflex tests for toe-pinch, eye lid and cornea and monitored over der duration of the experiments by heart rate and breathing rate. If maintenance of anesthesia was needed, maximally one third of the initial dose was applied subcutaneously in 20-minute-intervals. ABRs, DPOAEs, and ASSRs were recorded in a soundproof chamber (IAC, Niederkrüchten, Germany) as previously described. ((Engel et al. 2006; Knipper et al. 2000; Möhrle et al. 2016; Rüttiger et al. 2013), see also Fig. 2F in (Wolter et al. 2018)).

2.2.1 Auditory brainstem response (ABR)

When the auditory system is stimulated with a transient acoustic (broadband or pure tone) stimulus, evoked auditory brainstem responses (ABR) can be recorded as changes in electrical potential over time in the first 10-15 ms in form of typically-shaped successive wave (voltage) amplitude deflections by placing subcutaneous silver electrodes behind the ear, onto the vertex and a ground on the back near the tail neck of the animal. These changes in electrical potential are known to be correlated to synchronous spiking activity of distinct auditory neuron populations along the ascending auditory pathway (Burkard and Don 2007). ABR thresholds and ABR wave fine structure (amplitudes and onset latencies of distinct wave deflections) can be interpreted in the context of hearing screening tests in humans as well as animal models. In this study, the recorded click-, noise- and pure-tone-ABRs were preprocessed by amplification (100 dB), band-pass-filtering (0.2–5 kHz) and averaging of the raw signal for a minimum of 128 repetitions (Rüttiger et al. 2013). For determination of click (100 µs), noise burst (1 ms, random phase frozen noise) and pure tone (3 ms, including 1 ms cosine squared rise and fall envelope, 2-32 kHz with 2 steps per octave) ABR thresholds, the lowest sound pressure was chosen that produced potentials visually distinct from noise level.

2.2.2 Distortion product otoacoustic emission (DPOAE)

In short, OHC function can be assessed by stimulation of the cochlea with two pure tone stimuli (primaries, f_1 and f_2) followed by recording of the returned signal within the ear canal. In the recent study, the growth function and the DP-gram of the $2f_1$-f_2 DPOAE (Engel et al. 2006; Knipper et al. 2000) were investigated. The $2f_1$–f_2 DPOAE were measured for f_2=1.24*f_1 and L_2=L_1–10 dB and the maximum amplitude of DPOAEs were determined at L_1=50 dB SPL in the frequency range of 4-32 kHz to ensure for good positioning of the coupler inside the ear canal. The $2f_1$–f_2 DPOAE amplitudes for f_2=11.3 kHz and L_1 between 0-65 dB SPL were analyzed. Threshold was determined as the L_1 sound pressure that could evoke a $2f_1$–f_2 DPOAE signal reliably exceeding 5 dB above noise level. For assessment of MOC-efferent adaptation of DPOAEs, the ear was exposed with f_2=11.3 kHz and f_1=9.11 kHz to elicit DPOAEs in the ipsilateral ear. Both primaries were switched on synchronously and presented simultaneously for 100 ms or with continuous presentation of f_1 and pulsed presentation of f_2 (five pulses with 20 ms duration each, 20 ms pause between pulses). Stimulus onset and offset contained cosine-shaped ramps of 2 ms length. Stimuli were presented 128 times (sweeps) using 500 ms recording intervals with two presentations per second. Primaries were presented in combinations of phase-varied pairs of stimulus phases rotated by 90° (f_1) and 180° (f_2) for each subsequent presentation (primary tone phase variation, PTPV) to cancel the primary components in the response of either four summated single presentations (Dalhoff et al. 2015; Whitehead et al. 1996). DPOAE amplitudes were successfully reduced for SPLs of L_1=60–70 dB SPL (Kujawa and Liberman 2001). The 128 sweeps were band-pass filtered (1/8 octave) around the $2f_1$-f_2 DPOAE frequency, digitally amplified (40 dB), averaged, and Hilbert-transformed to extract the envelope of the $2f_1$-f_2 DPOAE response in the time signal (SingleSweep custom software, University of Tübingen, ANSI C-code based on LabWindows-CVI, National Instruments, Austin, TX, USA). Amplitudes of the extracted DPOAE signals were further analyzed using Microsoft Excel 2016 (Microsoft Cooperation, Redmond, WA, USA) software, by normalization to the noise plateau (in dB) at the end of the recording (120 ms for simultaneous primary presentation or 200 ms for pulsed primary presentation, respectively). Adaptation (Δ_{amp}, in dB) was defined as the difference between the maximum amplitude (amp_{max}, in dB) in a time window at the non-adapted onset of the response (10 ms for simultaneous primary presentation or 2 ms for pulsed

primary presentation, respectively) and the adapted average amplitude (amp_{adapt}, in dB) at 80-100 ms (simultaneous primary presentation) or at 16-18 ms (pulsed primary presentation). At first, the amplitude values amp_{max} and Δ_{amp} were compared for GC-B WT and GC-B HET mice. Both groups were combined to make a solid control group (GC-B CTRL) for the GC-B KO mice and to gain statistical power because of the small *n*, since both genotypes maintain no SGNs bifurcation deficit (Ter-Avetisyan et al. 2014) and since no difference in respect to the measured parameters was found. For simultaneous primary presentation, initial DPOAE amplitudes (amp_{max}) and adaptation (Δ_{amp}) in GC-B CTRL and GC-B KO mice were then analyzed by 1-sided Student's t-test, subsequently certified by a resampling procedure (Bootstrapping statistics) to control for random statistical outcomes that may be confounded by the small *n*. Experimental data were rearranged in 20 repetitions, each with 10,000 resamplings, and analyzed for randomness of *p* values. For pulsed primary presentation, initial DPOAE amplitudes (amp_{max}) and adaptation (Δ_{amp}) in GC-B CTRL and GC-B KO mice were analyzed by multiple t tests corrected for multiple comparisons (Bonferroni-Dunn method). A $p<0.05$ was considered statistically significant.

2.2.3 Auditory steady state response (ASSR)

For auditory steady-state response measurements, amplitude modulated sinusoidal stimuli, built from an 11.3 kHz carrier and modulation frequencies between 64-2048 Hz with one step per octave, were used. The stimuli were modulated at 100 % and presented at 40 dB above threshold (dB sensation level, dB SL) unless otherwise stated. At a fixed modulation frequency of 512 Hz, responses to modulation depths between 0 % (unmodulated), and 0.78 % to 100% modulation indices were recorded in half-octave steps. For I-O functions the carrier level ranged from -10-60 dB SL.

2.2.4 Acoustic startle response (ASR) and prepulse inhibition (PPI)

Acoustic startle response was performed on five adult GC-B WT (2 male, 3 female) and seven GC-B KO (4 male, 3 female) mice after an adaptation period in the colony room of the startle measuring facility of 14 days before testing. Since differences in age (2 or 4-month-old, ANOVA F-test $F<1$), gender (ANOVA F-test $F<1$) and weight (GC-B WT: 20–33 g, GC-B KO: 10–20 g, Pearson correlation $R^2=0.016$, $p>0.6$) had no significant impact on standard startle stimuli (105 dB) in a pretest on day one, all data were statistically analyzed for the factor genotype without further specification. All

startle tests were performed during the light period (8:30 am to 15:30 pm). Startle responses were measured inside a sound-attenuated chamber by a movement-sensitive piezo accelerometer platform (Startle-Messsystem, University of Tübingen) as described in (Wolter et al. 2018). All startle stimuli were presented as broadband white noise stimuli. For calculation of the ASR I-O function, startle stimuli had a duration of 20 ms and were presented 24 times at 75, 85, 95, 105 and 115 dB SPL, summed up for a total of 120 repetitions. For temporal summation of the ASR, startle stimuli of 105 dB SPL were presented 20 times with a duration of 0.5, 1, 2, 4, 5, 6, 7 or 8 ms and 60 times with a duration of 20 ms, unless otherwise stated. Prepulse inhibition tests were executed using additional white noise stimuli (65 dB SPL) presented 3, 6, 12, 25, 50, 100, 200 or 400 ms before onset of the startle stimulus (lead time) with a duration of 20 ms if the lead time was >20 ms, or they lasted until startle stimulus began. Each prepulse lead time was presented 20 times. As a control, a startle stimulus without a preceding prepulse was presented 60 times. For Gap PPI, a constant background noise of 65 dB SPL was given. Prepulses were gaps with a leadtime of 50 ms and had durations of 1.5, 5 and 50 ms, respectively. The noise in the gap had a SPL of 31 dB, and in addition 45 and 55 dB for the durations 5 and 50 ms. Each gap type was presented 20 times. As a control, a startle stimulus without a preceding prepulse was presented 40 times.

2.3 Histological analysis

2.3.1 Tissue preparation

For immunohistochemistry on cochlear sections, cochleae were isolated, fixed by immersion in 2 % paraformaldehyde (PFA), 125 mM sucrose in 100 mM phosphate buffered saline, pH 7.4, for 2 hours and then decalcified for 45 minutes in RDO rapid decalcifier (Apex Engineering Products Corporation, Aurora, IL, USA), cryosectioned at 10 µm, and mounted on SuperFrost*/plus microscope slides before storage at -20°C or immediate use as previously described (Knipper et al. 1996; Knipper et al. 2000). For cochlear whole-mounts, the temporal bone of mature mice was dissected on ice, fixed and stained as described (Duncker et al. 2013). For ossicle preparations, GC-B HET (*n*=3) and GC-B KO (*n*=3) mice were deeply anesthetized with CO_2 and decapitated. Temporal bones were carefully removed to ensure the bullae were still attached, transferred into 4 % PFA and fixed for at least 2 h. Temporal bones were

shortly rinsed (PBS), carefully cleared from soft tissue (glands, muscles, nerves) under visual control of a Leica MZ FL III stereomicroscope (Leica, Wetzlar, Germany) mounted with a camera (Soft Imaging System CC12, Olympus) via a microscope objective/camera adapter (0.63x10446261, Leica). Subsequently, the bullae were opened bit by bit using an ear canal approach to prevent damage to the tympanum. The tympanum was carefully removed after inspection and the bulla was further opened and finally removed to access the ossicles. The ossicles were removed one by one and photographed using CellSens software (version 1.8.1, Olympus Software Imaging Solutions, Olympus).

2.3.2 Immunohistochemistry

For immunohistochemistry, mouse cochlear sections were stained as previously described (Tan et al. 2007). For hair cell phenotyping, antibodies directed against C-terminal-binding protein 2 (CtBP2/RIBEYE, American Research Products, Waltham, MA, United States), otoferlin (LifeSpan Biosciences, Seattle, WA, United States), anti-vGlut3 (Synaptic Systems, Göttingen, Germany), potassium voltage-gated channel subfamily KQT member 4 (KCNQ4, StressMarq Biosciences, Victoria, BC, Canada) and prestin (Squarix Biotechnology, Marl, Germany (Weber et al. 2002)), were used (Table 1). For labeling of afferent and efferent innervation of inner hair cells (IHCs) and OHCs, antibodies directed against choline acetyltransferase (ChAT, Millipore, Temecula, CA, United States), Synaptobrevin (vesicle-associated membrane protein isotype 2, VAMP2, Synaptic Systems, Göttingen, Germany), large conductance Ca^{2+}-activated KC channel (BK, Alomone Labs, Jerusalem, Israel), and Neurofilament 200 (Nf200, Sigma-Aldrich, St. Louis, MO, United States) were used (Table 1). Primary antibodies were detected using appropriate Cy3- (1:1500, Jackson Immuno Research Laboratories, West Grove, PA, United States) or Alexa488-conjugated secondary antibodies (1:500, Invitrogen Molecular Probes, Paisley, United Kingdom). For double labeling studies, pairs of antibodies were simultaneously incubated for identical time periods. Sections were analyzed by high-resolution fluorescence deconvolution microscopy (Zampini et al. 2010) using an Olympus BX61 microscope (Olympus, Hamburg, Germany) equipped with epifluorescence illumination. Images were acquired using an Olympus XM10 CCD monochrome camera and analyzed with cellSens Dimension software (OSIS GmbH, Münster, Germany). To increase spatial resolution, slices were imaged using an image-stack along the z-axis (z-stack) followed

by 3-dimensional deconvolution using cellSens Dimension's built-in algorithm (ADVMLE, CellSens, Olympus, Hamburg, Germany) and displayed as maximum intensity projection over z. Each immunohistochemical labeling was done in replicate of at least three in three independent experiments. Immunofluorescent staining of embryonic tissues was performed as described previously (Schmidt et al. 2007; Schmidt and Rathjen 2011). The following primary antibodies were used in combination with appropriate fluorophore-conjugated secondary antibodies: rabbit anti-β-gal (1:20000; Cappel) and guinea pig anti-cGKIα (1:25000) to the N-terminal region of mouse cGKIα (amino acid residues 2–89) (Ter-Avetisyan et al. 2014). For X-gal staining in whole-mount preparations anti-β-galactosidase monoclonal antibody was used (mouse, 1:100, Promega, catalogue number Z3781, Madison, WI, United States). Immunohistochemical staining of cochlear sections were quantified as described (Wolter et al. 2018) by integrating density values of color pixels for each single specimen using ImageJ software (U. S. National Institutes of Health, Bethesda, Maryland, USA). The density values of all specimens stained within the same experiment were then normalized to the group mean (i.e., all sections of all cochlear turns stained in the same experiment gave an average value of 1.0). This correction allowed to compensate for the high inter-trial variation of staining intensity. Within every single experiment, the same number of GC-B WT and GC-B KO sections were stained by the same experimenter. These sections were in parallel exposed to the identical solutions, antibody concentration, temperature, and environmental variations. All sections from one mouse were then averaged and entered the statistical evaluation as n=1.

Table 1. List of primary antibodies used for immunohistochemistry on cochlear sections.

Target	***Host***	***Provider***	***Catalogue number***	***Dilution***
CtBP2	rabbit	American Research Products	10-P1554	1:1500
otoferlin	mouse	LifeSpan Biosciences	LS-C153337	1:100
anti-vGlut3	rabbit	Synaptic Systems	135 203	1:100
KCNQ4	mouse	StressMarq Biosciences	SMC-309D	1:50
prestin	rabbit	*not commercial*	(Weber et al. 2002)	1:3000
ChAT	rabbit	Millipore	AB5042	1:100
VAMP2	mouse	Synaptic Systems	104211	1:200
BK	rabbit	Alomone Labs	APC-021	1:400
Nf200	mouse	Sigma-Aldrich	N0142	1:8000

2.4 Data analysis

2.4.1 Supra-threshold ABR wave fine structure analysis

Supra-threshold ABRs were analyzed for successive amplitude deflections (waves). Each wave was defined by an initiating negative (n) peak, followed by a positive (p) peak. Peak amplitudes of click-stimulus-evoked ABR wave SP, I, II, III and IV were extracted with customized computer programs as previously described (Rüttiger et al. 2013). ABR peak-to-peak (wave) amplitude input-output (I-O) growth functions were constructed using Microsoft Excel 2013 (Microsoft Cooperation, Redmond, WA, USA) for each individual ear and increasing stimulus levels from 0-65 dB SL (referenced to individual ABR thresholds).

2.4.2 Statistical analysis

Results for ABR thresholds, DPOAE thresholds, DPOAE I-O functions and ABR fine structure analysis from the two individual ears of each animal were averaged and the statistical analysis was run based on the number of animals as described (Wolter et al. 2018). Unless otherwise stated, all data are presented as group mean ± S.D. or ± standard error of the mean (S.E.M.) for *n* animals per experimental group. Differences of the means were compared for statistical significance either by Mann-Whitney test, Student's t-test, 1-way ANOVA or 2-way ANOVA tests using Microsoft Excel 2013 and 2016 (Microsoft Cooperation, Redmond, WA, USA) or GraphPad Prism 6.07 (La Jolla, USA). 1-way and 2-way ANOVA tests were followed by *post hoc* t-tests with correction of α level of 0.05 for multiple comparisons after Bonferroni. Differences of the slopes built by linear regression were compared by ANCOVA. For statistical analysis of the ASR, the startle responses were averaged for each day, stimulus condition, and mouse. Parametric statistics were calculated and presented as mean ± S.E.M.. For the prepulse effect (prepulses and gaps), the mean response amplitude for each prepulse condition (ASRPP) and mouse was first calculated relative to the startle stimulus alone (ASR0) condition as described (Wolter et al. 2018):

$$Relative\ ASR\ =\ (ASRPP\ -\ ASR0\ /\ ASR0)\mathrm{RelativeASR} = (\mathrm{ASRPP} - \mathrm{ASR0})/\mathrm{ASR0} \qquad (1)$$

A negative Relative ASR is then referred to as prepulse inhibition (in %). Positive Relative ASR describes prepulse facilitation. For the effect of startle stimulus duration, response amplitudes for each duration (ASRDur) and mouse were calculated relative to the response to 20 ms (ASR20) lasting startle stimuli:

$$Relative\ ASR\ =\ ASRDur\ /\ ASR20 \qquad (2)$$

Differences for prepulse and gap measures and startle stimulus duration were statistically compared using the relative measurements. Statistical tests were done with JMP (SAS institute, version 13). For statistical evaluation of integrated density from immunohistochemical stainings, the unpaired 2-sided Student's t-test for independent samples was used. Data are presented as group mean ± S.D.. Statistical difference between group means was evaluated, until otherwise stated, by the unpaired two-sided Statistical significance level α=0.05 and resulting *p* values are reported in the figure legends. (*): $p<0.1$; *: $p<0.05$; **: $p<0.01$; ***: $p<0.001$; n.s.: not significant.

3. Results

3.1 Basal hearing function analysis of Npr2$^{lacZ/lacZ}$ mice

To understand how deterioration of afferent auditory pathway formation affects basal hearing capability in the auditory periphery as well as central auditory processing, parts of the experiments conducted in (Wolter et al. 2018) were summarized in the following chapter. In this study, a constitutive knockout mouse mutant with loss of function mutation of the GC-B gene was used, whose embryonal inactivation of GC-B affects formation of tonotopic contacts in the CN (Lu et al. 2014) and the other cranial nerve terminals (Ter-Avetisyan et al. 2014) as well as in the spinal cord (Schmidt et al. 2007). Discussion of results is focused on of basal hearing function, because constitutive *GC-B* knockout severely affects survival of the mutants, prohibiting challenging noise exposure protocols due to longer lasting experiments. GC-B KO mice maintained a bone growth phenotype (Fig. 5A), as reported before (Ter-Avetisyan et al. 2014). For quantification, naso-anal length was measured for 1-to-2-month-old mice (GC-B WT: 1.5±0.5 months, *n*=11; GC-B HET: 1.4±0.4 months, *n*=12; GC-B KO: 1.2±0.2 months, *n*=10).

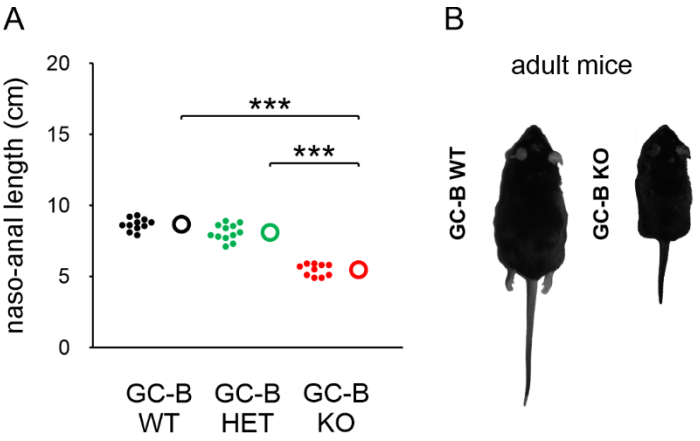

Fig. 5: GC-B KO mice maintain a bone growth phenotype. (A) Mean ± S.D. naso-anal length was significantly different for GC-B KO (red open circle) compared to GC-B WT (black open circle) and GC-B HET (green open circle) mice. Filled dots represent individual mice. **(B)** Depiction of anesthetized GC-B WT (*Npr2*$^{+/+}$) and GC-B KO (*Npr2*$^{lacZ/lacZ}$) mice shortly before awakening after performed hearing measurements.

GC-B KO mice were significantly smaller when compared to GC-B WT and GC-B HET mice (1-way ANOVA, $p<0.0001$, $F(2,30)=129$). In average, GC-B KO mice were 3.2 cm and 2.6 cm shorter when compared to GC-B WT (Bonferroni's multiple comparisons test, $p<0.0001$) and GC-B HET mice ($p<0.0001$), respectively. GC-B HET mice were in average 0.6 cm smaller compared to GC-B WT mice. This difference was also significant (Fig. 5B, Bonferroni's multiple comparisons test, $p=0.0249$). As a first step it was evaluated, if basic hearing function was affected in GC-B KO mice.

3.1.1 Analysis of ABR thresholds

To determine basic hearing function of mutant mice lacking functional GC-B in all sensory neurons (Ter-Avetisyan et al. 2014; Wolter et al. 2018), adult GC-B WT (*n*=16), GC-B HET (*n*=17) and GC-B KO (*n*=18) mice were investigated first using ABRs. Broadband and pure tone stimuli were chosen to get a measure for the whole frequency-hearing range of the auditory system, with click stimuli mainly covering lower frequencies and noise burst stimuli covering also high frequencies of the mouse hearing range due to producing high sound pressure levels (SPLs) in lower or higher frequencies, respectively. Pure tone stimuli evoke maximal auditory responses at their corresponding tonotopic place in the cochlea and can be therefore used for frequency-specific testing of mouse hearing function. Since heterozygous inactivation of GC-B did not lead to disturbed bifurcation of the auditory nerve (Ter-Avetisyan et al. 2014), no change in basal hearing function of GC-B HET mice was assumed.

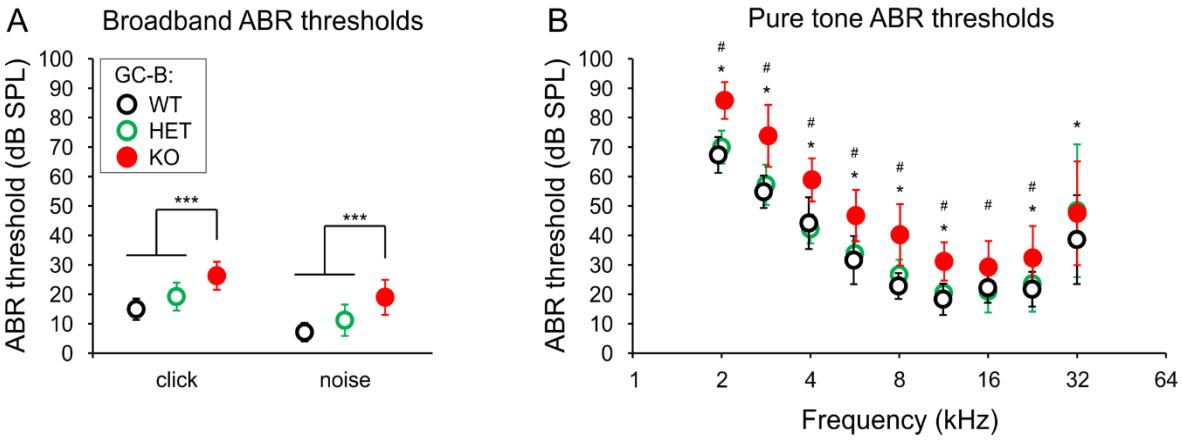

Fig. 6. Mild elevation of ABR thresholds in GC-B KO mice. (A) Mean ± standard deviation (S.D.) click- and noise-evoked ABR thresholds were significantly elevated for GC-B KO (red filled circle) compared to GC-B WT (black open circle) and GC-B HET (green open circle) mice. **(B)** Pure tone-evoked ABR thresholds significantly differed for GC-B KO and GC-B WT mice (2 to 11.31 kHz and 22.6 to 32 kHz, asterisks) and for GC-B KO and GC-B HET mice (2 to 22.6 kHz, hash signs). The legend keys in **(A)** apply for **(A+B)**. *Modified from (Wolter et al. 2018)*.

Analysis of ABR thresholds revealed a significant elevation of click-, noise burst- and pure tone-evoked ABR thresholds in GC-B KO mice when compared with GC-B WT and GC-B HET mice, primarily in the low to middle frequency range (Fig. 6A left, click: threshold loss of 11.4 dB when compared to GC-B WT and 7.1 dB when compared to GC-B HET mice, respectively, 1-way ANOVA, $p<0.0001$, $F=(2,48)=20.19$, Bonferroni's multiple comparisons test $p<0.0001$ and $p=0.0007$, Fig. 6A right, noise: threshold loss of 12.4 dB and 8.4 dB when compared to GC-B WT and GC-B HET mice, respectively,

1-way ANOVA, $p<0.0001$, $F(2,43)=22.39$, Bonferroni's multiple comparisons test $p<0.0001$ and $p=0.0001$, and Fig. 6B, pure tones: threshold loss of on average 13.3 dB when compared to GC-B WT and 11.7 dB when compared to GC-B HET mice, respectively, see Table 2). As expected, ABR thresholds of GC-B WT and GC-B HET mice did not differ significantly for click- (Bonferroni's multiple comparisons test, $p=0.0721$), noise burst- (Bonferroni's multiple comparisons test, $p=0.0767$), and pure tone-evoked ABR thresholds for the frequency range between 2-22.6 kHz (Bonferroni's multiple comparisons test see Table 2). At 32 kHz, the highest pure tone frequency tested using ABRs, revealed significant difference between GC-B WT and GC-B HET mice but also high interindividual scatter of ABR thresholds in any genotype which resulted in high S.D. of the averaged ABR thresholds. The high variance of ABR thresholds at 32 kHz complicates interpretation of hearing function for very high frequencies, therefore further analysis and interpretation of hearing measurements were focused on the low to middle frequency range. Taken together, significant mild elevation of hearing thresholds in this particular constitutive knockout model for GC-B was observed (Wolter et al. 2018), a phenotype which was not reported before (Lu et al. 2014).

Table 2. Statistical comparison of pure tone ABR thresholds from GC-B WT (*n*=14-16), GC-B HET (*n*=16-17) and GC-B KO (*n*=12-13) mice.

Pure tone ABR thresholds

Frequency (kHz)	**2**	**2.83**	**4**	**5.66**	**8**	**11.31**	**16**	**22.6**	**32**
WT vs KO	<0.0001 ***	<0.0001 ***	<0.0001 ***	<0.0001 ***	<0.0001 ***	0.0006 ***	0.1182 n.s.	0.0061 **	0.0344 *
delta |dB|	18.5	19.0	14.7	15.1	17.4	12.9	7.0	10.6	8.9
HET vs KO	<0.0001 ***	<0.0001 ***	<0.0001 ***	0.0004 ***	0.0002 ***	0.0047 **	0.0455 *	0.0281 *	>0.999 n.s.
delta |dB|	15.8	16.6	16.7	12.9	13.6	10.7	8.2	8.8	0.9
WT vs HET	>0.999 n.s.	>0.999 n.s.	>0.999 n.s.	>0.999 n.s.	0.6959 n.s.	>0.999 n.s.	>0.999 n.s.	>0.999 n.s.	0.0092 **
delta |dB|	2.7	2.4	2.0	2.2	3.8	2.2	1.2	1.8	9.8

Bonferroni corrected *p* values: ***$p<0.001$, **$p<0.01$, *$p<0.05$, n.s. not significant

3.1.2 Analysis of DPOAE thresholds

Sound waves, propagated by vibrations of the tympanic membrane and movements of the ossicular chain, deflects the basilar membrane within the scala media and shears the stereocilia of the hair cells. Activation of OHCs actively amplifies basilar membrane deflections at the tonotopic frequency place of the frequencies the sound is composed of. A byproduct of this process are otoacoustic emissions, which can be used as an objective indicator of active cochlear amplification by OHCs (Avan et al. 2013; Brownell 1990) and is regularly used for clinical hearing screening especially in newborns (Barker et al. 2000; Xia and Li 1998). In mice, the cubic ($2f_1$-f_2) distortion products of the otoacoustic emission (DPOAE) can be comfortably recorded and analyzed because of its pronounced amplitudes.

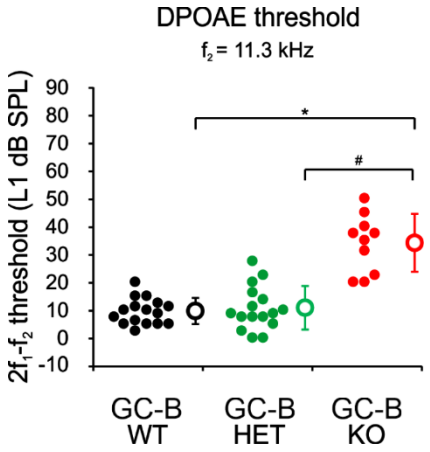

Fig. 7. Mild elevation of DPOAE thresholds in GC-B KO mice. Mean ± S.D. $2f_1$-f_2 DPOAE threshold (open circles with error bars) at the stimulus frequency f_2=11.3 kHz of GC-B KO mice was significantly elevated when compared to GC-B WT and GC-B HET mice (filled dots: thresholds of individual mice). *Modified from (Wolter et al. 2018)*.

$2f_1$-f_2 DPOAE thresholds were significantly elevated for the stimulation frequency of f_2=11.3 kHz in GC-B KO (Fig. 7 and (Wolter et al. 2018), one-way ANOVA, p<0.0001, F(2,192)=38.42) when compared to GC-B WT (Bonferroni corrected p value, p<0.0001, GC-B WT: n=16, GC-B KO: n=10) and GC-B HET mice (Bonferroni corrected p value, p<0.0001, GC-B HET: n=16).

Conclusion: The observed elevated ABR thresholds in GC-B KO mice are likely resulting from reduced detection sensitivity of OHCs following sound stimulation.

3.1.3 Analysis of sound conduction through the middle ear

A loss of GC-B function impairs endochondral ossification, resulting in dwarfism (Tsuji and Kunieda 2005). To exclude that the DPOAE responses and threshold differences were confounded by malformations of the ossicles, sound conductance of the middle ear ossicular chain and the morphology of the bony middle ear were studied in more detail. It has been shown, that slopes of DPOAE Input-Output (I-O) functions change when sound conductance is impaired (Qin et al. 2010; Turcanu et al. 2009).

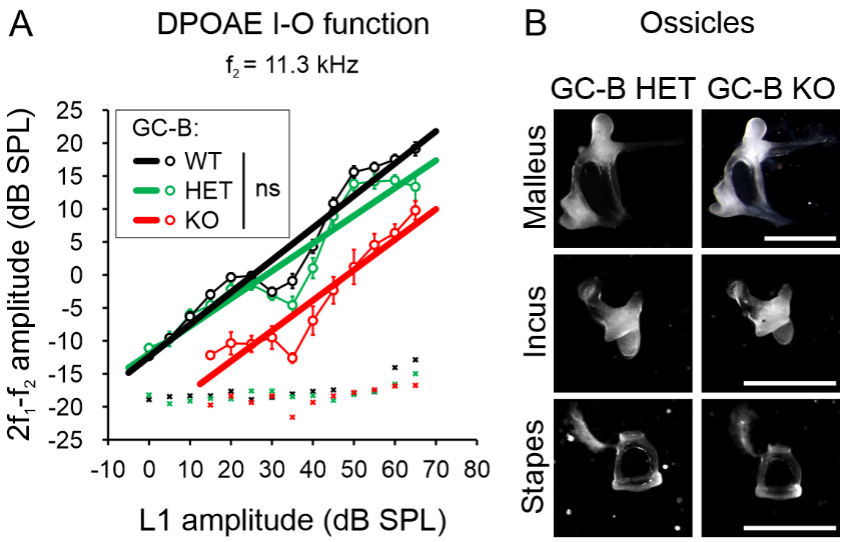

Fig. 8. Functional and morphological analysis of the DPOAE I-O functions and the bony middle ear reveal no significant conductive contribution to the basal hearing phenotype. (A) Mean ± S.D. $2f_1$-f_2 DPOAE Input-Output (I-O) functions (circles connected by a thin line) for f_2=11.3 kHz of GC-B WT, GC-B HET and GC-B KO mice. The DPOAE threshold difference in (Fig. 7) was reflected by a right-shift of the I-O curve in GC-B KO mice. No significant difference was found for the linear fit of I-O functions of either genotype (GC-B WT: y=0.4883x-12.399, R^2=0.9363, GC-B HET: y=0.4191x-11.986, R^2=0.8851, GC-B KO: y=0.4607x-22.291, R^2=0.8818, bold lines), indicating no damping effect due to conductive problems in the middle ear. **(B)** Representative pictures of GC-B HET and GC-B KO ossicles did not show obvious malformation or size differences. Ossicle preparations were performed in triplicate for both genotypes (*n*=3). Scale bars in **(B)**: 1000 µm. *Modified from (Wolter et al. 2018)*.

The primary frequency f_2=11.3 kHz was chosen for functional analysis of middle ear conduction, because highest sensitivity (lowest hearing thresholds) normally is centered around 11.3kHz in mice (see GC-B WT mice in Fig. 6B) and because this particular primary frequency was affected significantly in GC-B KO mice (see Fig. 7). For emission signals evoked at f_2=11.3 kHz, linear regression analysis did not reveal a difference in DPOAE I-O function slopes for GC-B KO when compared to GC-B WT (Fig. 8A, ANCOVA, *p*=0.6813, *F*(1,21)=0.173) or GC-B KO and GC-B HET mice

(Fig. 8A, p=0.5755, F(1,21)=0.323). Further, no obvious size differences or malformations of the ossicles were observed by microscopic inspection in GC-B KO mice (Fig. 8B, representative for GC-B HET: n=3 mice, GC-B KO: n=3 mice).

Conclusion: Indistinguishable slopes of DPOAE I-O growth functions and inconspicuous morphology and size of the middle ear ossicles suggest that the reduced sensitivity of OHCs to sound stimulation in GC-B KO mice is unlikely caused by sound conduction impairments in the middle ear.

3.2 Analysis of auditory pathway morphology of Npr2$^{lacZ/lacZ}$ mice

3.2.1 Analysis of GC-B expression in the auditory pathway

For verification of coinciding GC-B expression during the bifurcation event of central SGN neuron axons, as well as involvement and localization of compartments of the CNP/GC-B/cGMP/cGKIα signaling cascade in this process, wholemounts and parasagittal cochlear sections of *Npr2*$^{lacZ/+}$ (GC-B HET) embryos were analyzed using X-gal-staining (E11.5, Fig. 9A) and immunohistochemical co-staining with antibodies targeting nuclear β-gal and cytosolic cGKIα (E12.5, Fig. 9B), respectively. The acousticofacial ganglion (gVII/VIII) showed GC-B expression (Fig. 9A+B), which was partially overlapping with cGKIα expression (Fig. 9B). This ganglion contains the somata of the neurons which innervate the auditory hair cells in the organ of Corti (OC) and vestibular hair cells in the cristae ampullaris, the utricle and the saccule (Whitfield 2015). Additionally, cGKIα expression was found in the central axons of the sensory ganglion neurons, but not in their innervation targets within the CN (Fig. 9B) (Ter-Avetisyan et al. 2014).

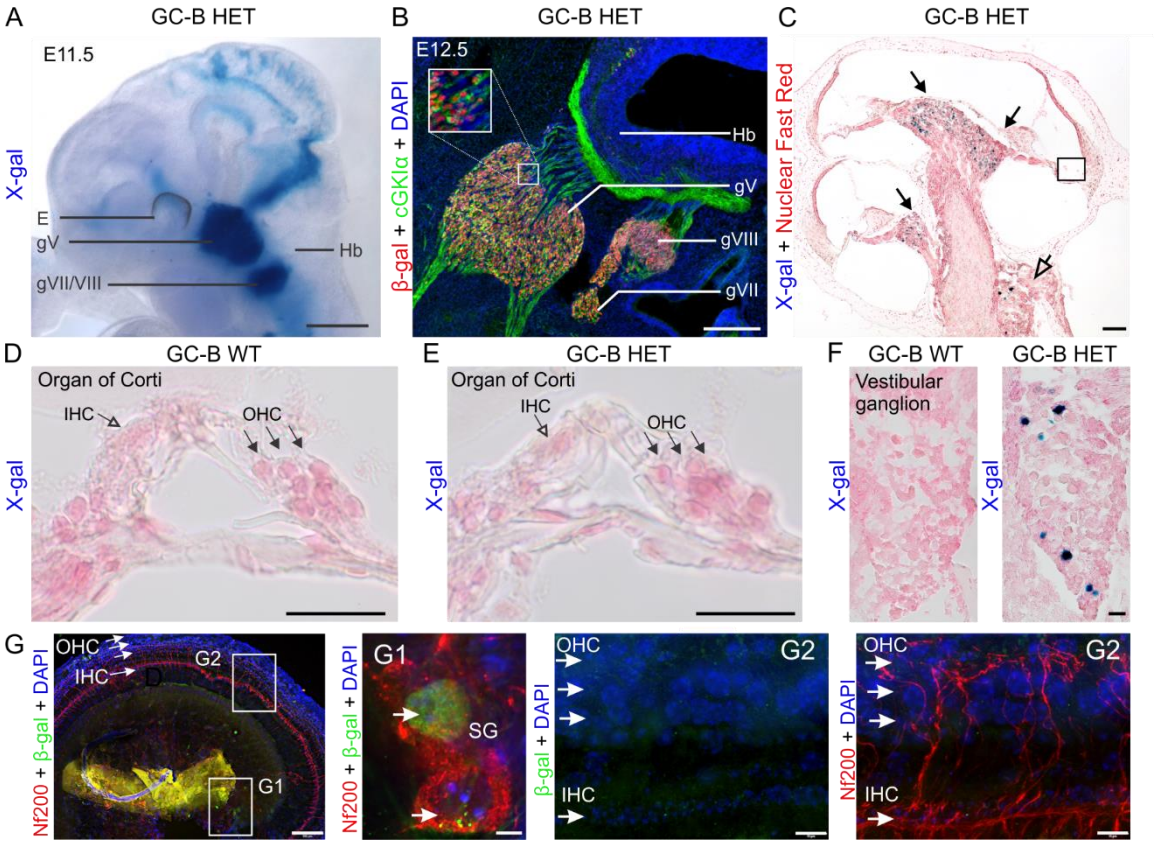

Fig. 9. Expression analysis of GC-B in the inner ear by X-gal staining and by immunohistochemical staining using antibodies targeting β-gal. (A) β-gal activity in *Npr2*$^{lacZ/+}$ (GC-B HET) embryonal wholemounts (E11.5) reveals sites of GC-B expression is restricted to the nuclei of GC-B expressing cells (due to the presence of a nuclear localization signal). X-gal staining points to intense expression of GC-B in all cranial sensory ganglia (Ter-Avetisyan et al. 2014), including the trigeminal (gV) and acousticofacial ganglion (gVII/VIII). **(B)** Immunohistochemical β-gal detection in parasagittal sections of the hindbrain region from E12.5 *Npr2*$^{lacZ/+}$ embryos, coimmunostained with cGKIα, shows an overlapping distribution of β-gal with cGKIα expression in the cranial sensory ganglions at the level of cranial sensory ganglia gV (trigeminal), gVII (facial), gVIII (vestibuloacoustic) and cGKIα expression in cranial sensory axons. **(C)** Cochlear section of a 10-week-old GC-B HET mouse stained for X-gal (blue) and Nuclear Fast Red (red) with the apex oriented upwards. X-gal-positive cells in GC-B HET mice are indicated by filled (SGNs) or open (VGNs) arrows. **(D,E)** No X-gal staining was found in the OC, neither in IHCs nor OHCs (**E** shows a magnification from boxed areas in **C**). IHCs are indicated by open arrowheads and OHCs by filled arrowheads. **(F)** X-gal staining of sections from vestibular ganglia show a number of X-gal positive nuclei in the inner ear of GC-B HET mice (right panel). (**G**) Whole-mount preparations of an adult GC-B HET mouse immunhistochemically stained with anti NF200 (red) and anti-β-gal (green). **(G1)** and **(G2)** show a magnification of boxed areas for spiral ganglion neurons and OC, respectively. E, Eye; g, ganglion; Hb, hindbrain. Nuclei in **(B+G)** were stained with 4',6-diamidin-2-phenylindol (DAPI; blue). Scale bars: 1 mm **(A);** 25 µm **(B);** 100 µm **(C);** 25 µm (**D-F**); **100** µm (**G**); 10 µm **(G1,G2)**. *Modified from (Wolter et al. 2018)*.

In dorsal root ganglion (DRG) neurons of adult mice, another class of sensory neurons which undergo central axonal bifurcation (Schmidt et al. 2007), sparse GC-B expression is still present at P75 (Tröster et al. 2018). To investigate a possible acute effect of GC-B expression in the mature cochlea, the inner ear was analyzed using X-

gal-staining in cochlear sections of adult (10-week-old) *Npr2*$^{+/+}$ (GC-B WT) and *Npr2*$^{lacZ/+}$ (GC-B HET) mice and wholemounts of adult GC-B HET mice. X-gal-positive cells were found in SGNs and VGNs (Fig. 9C, F right panel) of GC-B HET mice, comparable to GC-B expression around P75 in DRG neurons (Tröster et al. 2018). No X-gal-positive cells were observed in GC-B WT OC (Fig. 9D), SGNs (Fig. S1), VGNs (Fig. 9F left panel) and GC-B HET OC, including the sensory hair cells (IHCs and OHCs, Fig. 9E). Immunohistochemical staining of cochlear wholemounts from adult GC-B HET mice using antibodies directed against β-gal showed β-gal-positive SGNs (Fig. 9G, G1, middle panel) and β-gal-negative IHCs and OHCs (Fig. 9G, G2 right panels). For analysis of GC-B expression in the target nuclei in the auditory brainstem, coronal and sagittal cross-sections of P15 GC-B HET brains were stained against X-gal as previously described (Ter-Avetisyan et al. 2014). X-gal staining was absent in regions of the cochlear nucleus (CN) and superior olivary complex (SOC, including MOC and LOC), while positive X-gal staining was restricted to small regions at the level of the vestibular nuclei and the pontine reticular nuclei (PRN, see (Wolter et al. 2018)).

Conclusion: Qualitative analysis of GC-B expression patterns in the cochlea (Fig. 9) and the auditory brainstem (Wolter et al. 2018) revealed abundance of GC-B in the acousticovestibular ganglion around period of the bifurcation event during embryonal development. In the mature inner ear, GC-B expression was found in the acousticovestibular ganglion as well but neither the hair cells within the OC nor innervation targets of SGN central axons in the auditory brainstem exhibited GC-B expression. Therefore, it is implausible that the observed elevated auditory thresholds derive from impaired function of cochlear hair cells or axon bifurcation deficits of central auditory neurons in the auditory brainstem. It is more likely that the observed elevated auditory thresholds derive from a bifurcation deficit of SGNs during embryonal development and its implied consequences for proper formation of the auditory pathway.

3.2.2 Morphological phenotype analysis of cochlear hair cells

The phenotype of OHCs was investigated as a next step to exclude that active cochlear amplification, a prerequisite for proper development and maintenance of hearing sensitivity by reducing auditory thresholds, is affected in GC-B KO mice. Hearing onset is accompanied by establishment of the potassium current $I_{K,n}$ driven by KCNQ4 (Marcotti and Kros 1999), a receptor protein with an expression profile throughout the membrane of immature OHCs, which becomes restricted to the OHC base during their final maturation (Winter et al. 2006). Changes in the KCNQ4 expression profile are indeed linked to progressive hearing loss (Beisel et al. 2000; Jentsch et al. 2000; Leitner et al. 2012). Hearing onset further coincides with redistribution of prestin to the OHC lateral wall (Weber et al. 2002), enabling for OHC electromotility, a underlying requirement for cochlear amplification (Dallos 2008). Additionally, mature and functional OHCs maintain 1-2 CtBP2/Ribeye-positive synaptic contacts with afferent type II fibers at their basal pole (Martinez-Monedero et al. 2016). Therefore, KCNQ4,

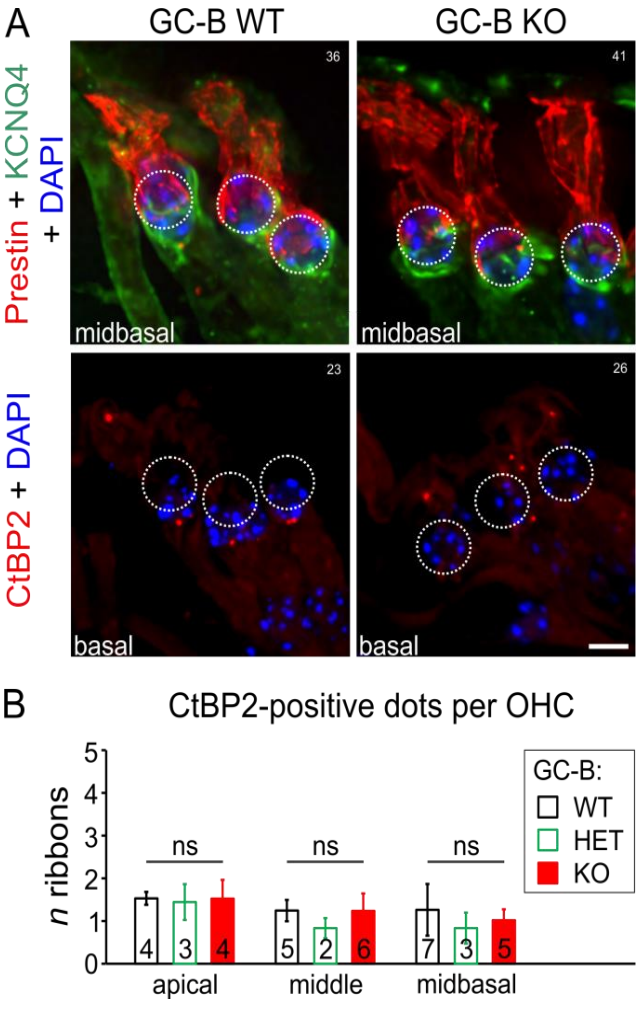

Fig. 10. OHCs of GC-B KO mice did not differ from OHCs of GC-B WT mice as judged on basis of OHC marker protein expression and quantification of CtBP2/Ribeye-positive afferent contacts. **(A)** Immunohistochemical staining of OHCs in the midbasal cochlear turn (representative for the whole cochlea) in GC-B WT (left panels) and GC-B KO (right panels) mice using antibodies targeted against the OHC marker proteins KCNQ4 (green; upper panels) and prestin (red; upper panels). OHC marker protein expression in GC-B KO mice was indistinguishable from that in GC-B WT mice. No differences in number of CtBP2/Ribeye-positive dots at the OHC base (red; lower panels) was observed. **(B)** CtBP2/Ribeye-positive dots, corresponding to OHC ribbons, were quantified in apical, medial and midbasal cochlear turns. The number of OHC synaptic ribbons did not differ significantly between genotypes in all investigated cochlear turns. Bars in **(B)** represent mean ± S.D. ribbons per OHC; numbers in bars indicate the *n* of mice studied. Nuclei in **(A)** were stained with 4',6-diamidin-2-phenylindol (DAPI; blue) and are highlighted by white broken circles. Scale bar in **(A)**: 5 µm. *Modified from (Wolter et al. 2018)*.

prestin and CtBP2/Ribeye-positive contacts were therefore used as correlates for differentiated and mature OHCs. According to performed immunohistochemical staining of cochlear sections, spanning all cochlear turns and shown for midbasal turns, the expression pattern of KCNQ4 (green) and prestin (red) showed a mature distribution in the basal (KCNQ4) and lateral (prestin) OHC membrane and did not differ between GC-B KO and GC-B WT mice over the entire length of the OC (Fig. 10A, upper panels). Final differentiation of OHCs was further confirmed by equal innervation by 1-2 CtBP2/Ribeye-positive afferent fibers type II shown here for GC-B KO and GC-B WT mice (Fig. 10A, lower panels, and quantified for all genotypes in Fig. 10B; 2-way ANOVA, p=0.1864, F(2,30)=1.778, GC-B WT: n=4-7 mice, GC-B HET: n=2-3 mice, GC-B KO: n=4-6 mice).

With assumption of normal OHC mechanoelectrical properties, another potential source for the observed elevated hearing thresholds in GC-B KO mice are alterations in the response pattern of inner hair cells (IHCs). The presence of fully differentiated mature IHCs in GC-B KO mice was investigated by otoferlin distribution analysis, a Ca^{2+}-sensitive scaffold protein found in IHC membranes (Duncker et al. 2013; Hams et al. 2017) in combination with analysis of CtBP2/Ribeye-positive dots as a marker for ribbon synapses. CtBP2/Ribeye-positive particles in ribbon synapses are essential for maintaining a residential vesicle pool (Becker et al. 2018), afferent fiber activity and timing at stimulus onset (Sheets et al. 2017). Following impaired IHC synapse vesicle release properties and deafferentation, the number of CtBP2/Ribeye-positive dots is significantly reduced (Kujawa and Liberman 2009). BK was used as an additional marker protein for fully differentiated and mature IHCs, as upregulation of BK channels with hearing onset is essential to transform immature IHCs (producing spontaneous Ca^{2+}-spikes) into mature functional cells, that are then able to respond to sound stimuli with graded receptor potentials (Marcotti 2012).

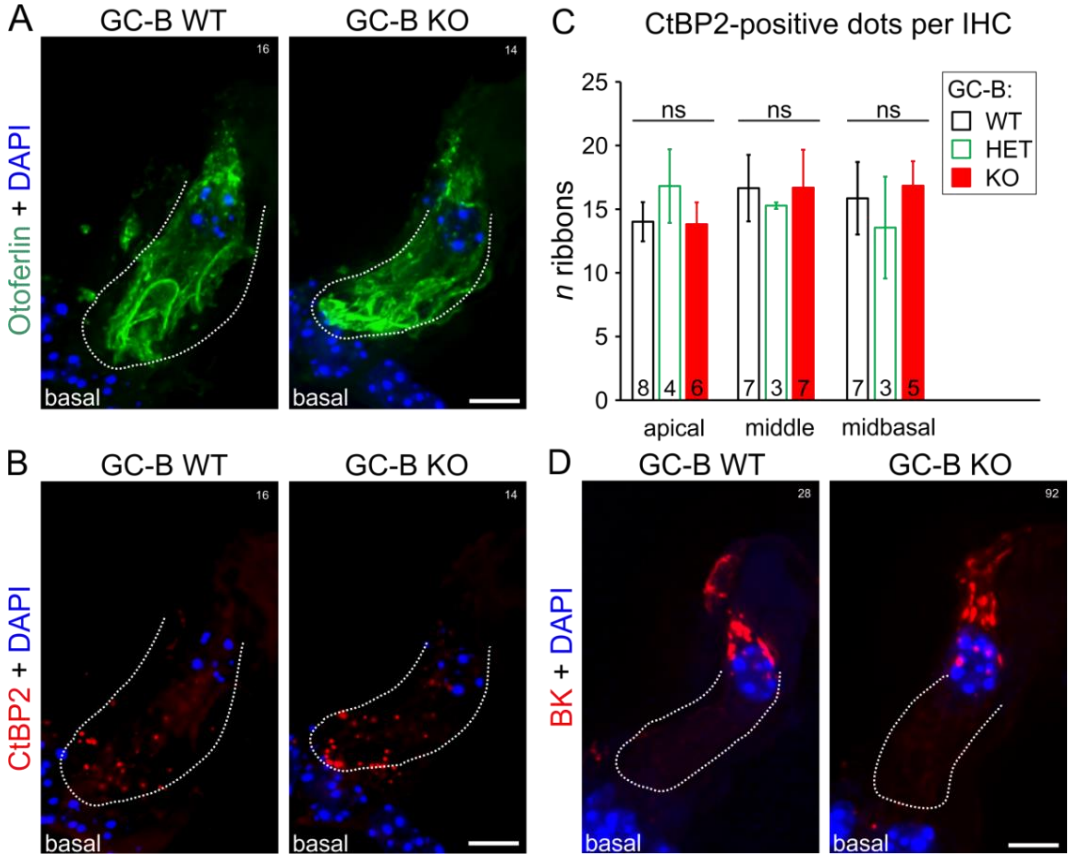

Fig. 11. IHCs of GC-B KO mice did not differ from IHCs of GC-B WT mice as judged on basis of IHC marker protein expression and quantification of CtBP2/Ribeye-positive afferent contacts. (A) Immunohistochemical staining of IHCs in the midbasal cochlear turn (representative for the whole cochlea) in GC-B WT (left panels) and GC-B KO (right panels) mice using antibodies targeted against the otoferlin (**A**, green), CtBP2/Ribeye (**B**, red), and BK (**D**, red). IHC marker protein expression in GC-B KO mice was indistinguishable from that in GC-B WT mice. **(C)** No difference in number of CtBP2/Ribeye-positive dots at the IHC base (red; lower panels) between genotypes was observed in the apical, medial and midbasal cochlear turns, representing low, middle and high frequency coding IHCs, respectively. Bars in **(C)** represent mean ± S.D. ribbons per IHC, numbers in open bars indicate the *n* of mice. Nuclei in **(A, B, D)** were stained with 4',6-diamidin-2-phenylindol (DAPI; blue). IHC membranes are partially highlighted by broken white lines. Scale bars in **(A, B, D)**: 5 µm. *Modified from (Wolter et al. 2018)*.

Representative immunohistochemical staining of midbasal cochlear turns, corresponding to the tonotopic place of high-to-middle frequencies (which were among the most affected by the auditory threshold loss in GC-B KO mice, see 11.3kHz in Fig. 6B and Fig. 7) revealed a normal expression pattern of otoferlin (Fig. 11A). The number of CtBP2/ribeye-positive dots was also not different in GC-B KO mice when compared to GC-B WT mice (Fig. 11B and quantified for all genotypes in Fig. 11C, 2-way ANOVA, p=0.8173, $F(2,41)$=0.2027). Further, the expression profile of BK channels in GC-B KO mice was not different from the expression profile of GC-B WT mice (Fig. 11D).

Conclusion: The mild hearing loss in GC-B KO mice cannot be explained by a simple loss of OHCs nor their impaired differentiation, as the results showed clearly the presence of mature OHCs with an indistinguishable expression pattern of typical marker proteins and corresponding afferent innervation when compared to GC-B WT mice. Analysis of IHC marker proteins clearly points to differentiated and functional IHCs. Therefore, the elevated hearing thresholds observed in mature GC-B KO mice could neither be related to deficits in IHC function nor their afferent innervation by AF type I nor to morphological deficits of the OHCs, indicating an intact active cochlear amplification. Summarizing the comparative immunohistochemical analysis of OHCs and IHCs and their afferent innervation, it can be concluded, that the sensory epithelium in the OC is not directly affected by a knockout of GC-B.

3.2.3 Morphological phenotype analysis of cochlear efferents

Mature cochlear hair cells receive efferent input originating from the SOC in the auditory brainstem. While mature IHCs are efferently innervated by LOC neurons (EF-LOC) (Guinan 2006, 2010; Knipper et al. 2013), mature OHCs receive efferent input from the MOC (EF-MOC) (Guinan 2006; Knipper et al. 2013). It has been shown that hearing thresholds are affected by impaired efferent feedback control onto cochlear hair cells following surgery, pharmacological treatment or acoustic overexposure (Darrow et al. 2007; Jäger and Kössl 2016; Maison et al. 2009). As elevated hearing thresholds in GC-B KO mice cannot be explained by impaired final differentiation of cochlear hair cells, cholinergic efferent olivo-cochlear feedback has been investigated as a next step. Cholinergic nerve terminals contact cochlear hair cells and modulate their outward K^+ currents by release of acetylcholine into the synaptic cleft (Fuchs et al. 2014; Housley et al. 1992; Vetter et al. 2007). Signal-to-noise detection is improved by cholinergic inhibition of cochlear hair cells mediated by Ca^{2+} influx through α9-/α10-nicotinic receptors and subsequent activation of K^+ channels (Hienz et al. 1998; Huang and May 1996; Lustig 2006). Further, efferent modulation of cochlear hair cells is discussed to play a role in protection from auditory threshold loss and cochlear injury after acoustic overexposure (Maison et al. 2013a; Maison et al. 2013b). Therefore, choline acetyltransferase (ChAT) (Kitanishi et al. 2013)) was used as a marker for efferent fibers in combination with synaptobrevin (vesicle-associated membrane protein 2, VAMP2), a marker for membrane-bound proteins found in synaptic vesicles (Barszczewski et al. 2008; S. He and Yang 2011) in GC-B KO mice. For localization of

VAMP2 staining outside of IHCs, cochlear cryosections were co-stained against the (vesicular glutamate transporter 3 (vGlut3), a marker for glutamatergic vesicles found in IHCs (Seal et al. 2008). Loss of vGlut3 is involved in a non-syndromic form of sensorineural deafness (DFNA25, (Ruel et al. 2008)).

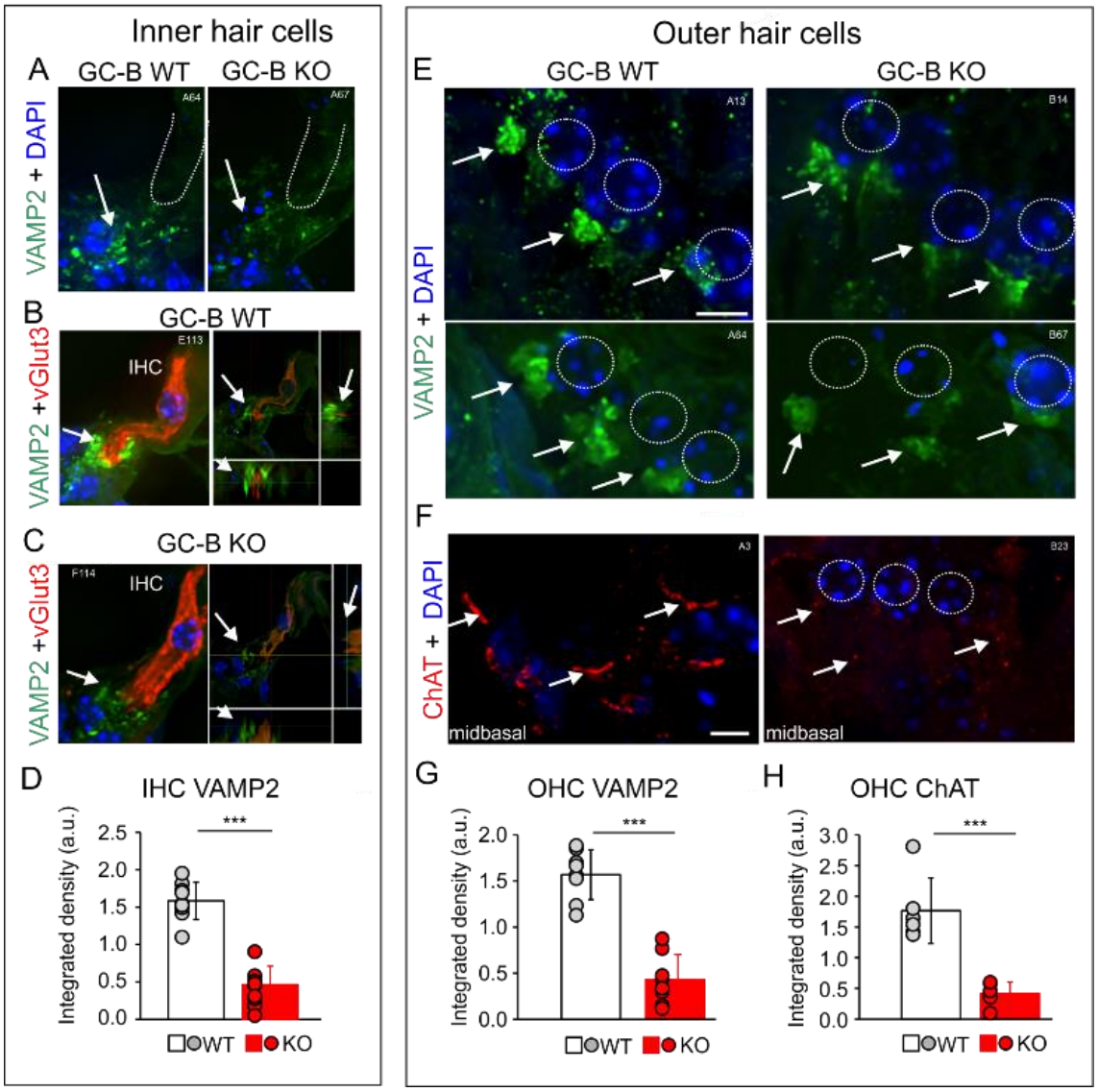

Fig. 12. Reduction of efferent innervation of OHCs and IHCs in GC-B KO mice. (A,B,C,E) Representative immunohistochemical staining with antibodies against synaptobrevin (vesicle-associated membrane protein isotype 2; VAMP2; green), a marker for membrane bound proteins found in synaptic vesicles of efferent synaptic contacts. **(A)** VAMP2 was reduced in efferent synaptic contacts with IHCs in GC-B KO compared to GC-B WT mice shown for *n* = 2 mice (quantification in **D**, *n*=9). **(B, C)** IHCs were co-stained with the vesicular glutamate transporter 3 (vGlut3, red) to show VAMP2 outside of IHCs. **(E)** VAMP2 expression is reduced below OHCs in GC-B KO mice shown *n*=2 mice (quantification in **G**, *n*=8). **(F)** Neuronal dendritic processes of cholinergic cochlear efferents near the basal pole of OHCs were stained with antibodies against choline acetyltransferase (ChAT; red). ChAT staining near the basal pole of OHCs was greatly reduced in GC-B KO mice (quantification in **H**, *n*=6). Nuclei were stained with 4',6-diamidin-2-phenylindol (DAPI; blue). Scale bars: 5 µm; applies for **(A-F)**. *******: *p*<0.001, 2-sided Student's t-test. *From (Wolter et al. 2018)*.

Analysis of cochlea cryosections stained with antibodies targeted against VAMP2 revealed less intense VAMP2 staining below IHCs in GC-B KO mice (indicated for two different section levels in Fig. 12B and (Wolter et al. 2018)) compared to GC-B WT mice (indicated for two different section levels in Fig. 12A and (Wolter et al. 2018)), suggesting less efferent innervation of IHCs within the midbasal cochlear turn in GC-B KO mice. Quantification of the integrated VAMP2 staining density for n=9 mice revealed a significant reduction in GC-B KO mice when compared to GC-B WT mice (p<0.0001, Fig. 12C and (Wolter et al. 2018)). On the other hand, co-staining with vGlut3 was not noticeably different between GC-B WT and GC-B KO mice (Fig. 12A+B and (Wolter et al. 2018)). VAMP2 was also reduced in GC-B KO OHCs (Fig. 12B and (Wolter et al. 2018)) when compared to GC-B WT OHCs (Fig. 12A and (Wolter et al. 2018)). Quantification of the integrated VAMP2 staining density for n=8 mice revealed a significant reduction in GC-B KO mice when compared to GC-B WT mice (p<0.0001, Fig. 12C and (Wolter et al. 2018)). ChAT staining below OHCs in the midbasal cochlear turn was also reduced in GC-B KO mice as judged n basis of qualitative (Fig. 12F and (Wolter et al. 2018)) and quantitative analysis (Fig. 12H and (Wolter et al. 2018), n=6, p<0.001).

Conclusion: As cochlear hair cells in GC-B KO mice seem to fully differentiate into an adult stage (see Fig. 10 and Fig. 11) and given the disturbed SGN central axon bifurcation (Ter-Avetisyan et al. 2014) it can be assumed that retrocochlear feedback onto IHCs and OHCs is reduced in GC-B KO mice.

3.3 Analysis of functional correlates of auditory processing of Npr2$^{lacZ/lacZ}$ mice

Changed basal hearing capability and reduced retrocochlear contacts of auditory feedback loops with cochlear hair cells raised the question, if processing of fast auditory signals is impaired in GC-B KO mice. Therefore, it was tested in the following chapter whether features of ABR Waves I-IV, fast amplitude-modulated stimuli (auditory steady state response, ASSR), fast adaptation of cubic DPOAEs following ipsilateral stimulation (MOC-reflex) and features of the acoustic startle reflex (ASR) are affected by genetic inactivation of GC-B.

3.3.1 Analysis of auditory signal processing in the afferent auditory pathway

Since sound conduction through the middle ear and marker protein expression in sensory hair cells were inconspicuous and therefore most probably not affected by the functional GC-B knockout, the mild threshold elevation observed in GC-B KO mice may be linked to processing deficits in the auditory brainstem and its retrocochlear feedback loops. Gross sound processing up to the auditory midbrain can be estimated by analyzing evoked ABR responses, as synchronicity of action potential generation in auditory nerve fibers and the number of spiking fibers is positively correlated with ABR wave amplitudes (D. H. Johnson and Kiang 1976). Additionally, ABR peak latencies (absolute latencies) provide information about fast auditory processing and are typically calculated as the time of occurrence of distinct peaks with reference to stimulus onset (Burkard and Don 2007).Thus, sound processing deficits can be located at distinct processing units, e.g. IHC stereocilia, AN and nuclei in the auditory brainstem (Fig. 13A).

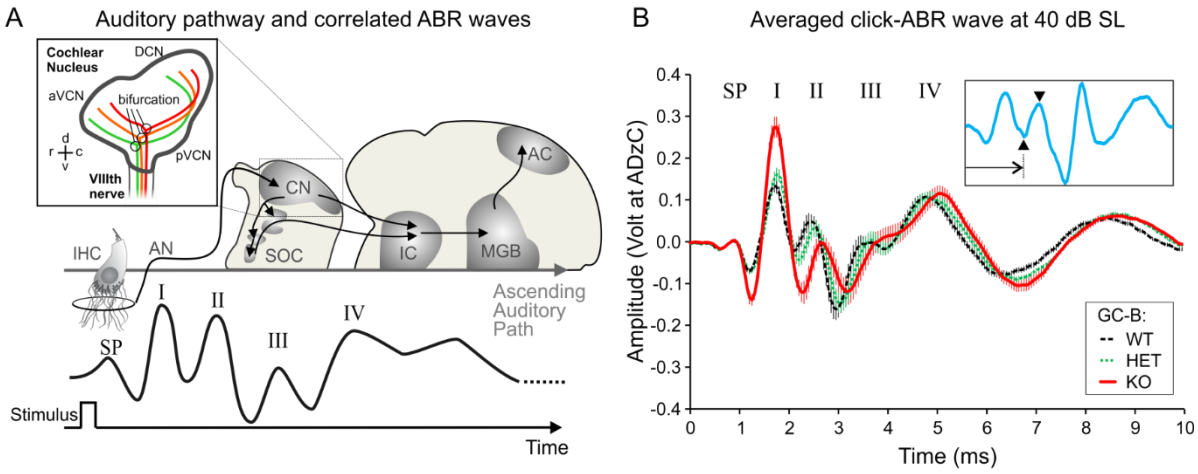

Fig. 13. ABR Waves I-IV are correlated to stimulus-evoked neuronal activity along the ascending auditory pathway and were discovered to be changed in GC-B KO mice.
(A) Schematic illustration of the ascending auditory pathway and correlated evoked deflections of ABR waves SP, I, II, III and IV after onset of an acoustic stimulus. The inset highlights axon bifurcation of AN fibers from the VIIIth nerve in the CN with color-coded axonal projections of afferent fibers type I with tonotopic organization from low (green) to high (red) frequencies (*modified from (Lu et al. 2014)*). d: dorsal, v: ventral, r: rostral, c: caudal, aVCN: anterior part of the ventral cochlear nucleus, pVCN: posterior part of the ventral cochlear nucleus, DCN: dorsal cochlear nucleus. **(B)** Mean ± standard error of the mean (S.E.M.) click-evoked ABR waves recorded at 40 dB SL for GC-B WT (black; *n*=18), GC-B HET (green; *n*=20) and GC-B KO (red; *n*=18) mice. The waves corresponding to the summating potential (SP), wave I, II, III and IV are marked. The inset shows a representative GC-B HET mouse ABR waveform (blue line) to illustrate definitions for wave latencies and amplitudes: wave latencies were defined as the time point of the minimum respective to stimulus onset (arrow) and amplitudes were calculated from the difference between minimum and subsequent maximum of each ABR wave (arrowheads). *Modified from (Wolter et al. 2018)*.

Analysis of supra-threshold click-evoked ABR waves uncovered changed ABR waves, representatively shown for a stimulus intensity of 40 dB SL in GC-B KO mice (*n*=18 ears/mice) when compared to GC-B WT (*n*=18 ears/mice) and GC-B HET mice (*n*=20 ears/mice) (Fig. 13B). Next, those differences in early (peripheral) and late (central) ABR wave amplitudes and latencies were quantified for click-evoked averaged ABRs with increasing stimulus level, normalized to the ABR thresholds of every individual ear of every mouse (dB sensation level, dB SL). Peripheral waves correspond to the summating potential of MET channel activity in IHCs (SP) (Durrant et al. 1998) and sound-evoked neuronal activity in the auditory nerve (AN; wave I), and central waves corresponding to sound-evoked activity in the cochlear nucleus (CN; wave II), in the superior olivary complex (SOC; wave III) and in the lateral lemniscus and inferior colliculus (LL & IC; wave IV) (Melcher and Kiang 1996). The first negative deflection in the ABR waveform fine structure provides an estimate for the SP (Fig. 13) and therefore for mechanoelectrical transduction (MET) channel currents in IHCs (Patuzzi et al. 1989; Rüttiger et al. 2017; Tasaki et al. 1954). Quantitative analysis of SP wave amplitude I-O growth functions (Fig. 14A; 2-way ANOVA, p=0.3599, F(2,1350)=1.023, GC-B WT: n=19-26 ears, GC-B HET: n=18-31 ears, GC-B KO: n=18-31 ears) and SP wave latency I-O growth functions (Fig. 14B; 2-way ANOVA, p=0.1266, F(2,1241)=2.070, GC-B WT: n=25-26 ears, GC-B HET: n=30-31 ears, GC-B KO: n=18-31 ears) revealed no significant differences between genotypes. On the other hand, ABR wave I amplitude and latency I-O growth functions were significantly different between genotypes (GC-B WT: n=18 mice, GC-B HET: n=20 mice, GC-B KO: n=18 mice; amplitudes: 2-way ANOVA, p<0.0001, F(2,1457)=354.2; latencies: 2-way ANOVA, p<0.0001, F(2,1340)=63.20). ABR wave I amplitudes for the middle and high stimulus levels (Fig. 14C) were significantly increased in GC-B KO compared to GC-B WT and GC-B HET mice (Bonferroni's multiple comparisons test see Table 3). *Post hoc* tests (Bonferroni's multiple comparisons test see Table 4) also revealed significantly increased ABR wave I latencies at hearing threshold and for high stimulus levels and progressively elevated ABR wave I amplitudes for medium to high stimulus levels in GC-B KO mice when compared to GC-B WT and GC-B HET mice, respectively (Fig. 14D). In contrast, ABR wave I amplitudes were not found to be different between GC-B HET and GC-B WT mice up to 65 dB SL (see Table 3) and ABR wave I latencies were not significantly different for any measured stimulus level between GC-B HET and GC-B WT mice, respectively (Table 4).

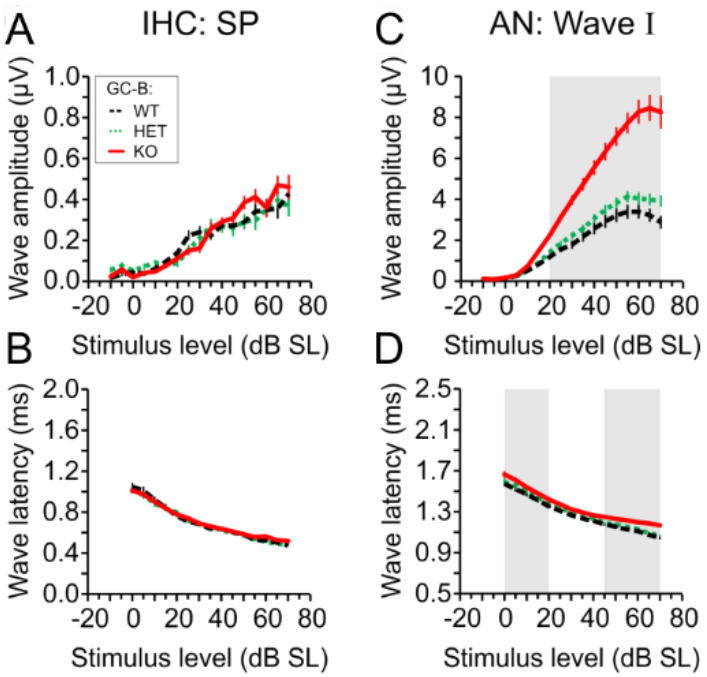

Fig. 14. The click-evoked SP wave remained unchanged but ABR wave I was increased and delayed in GC-B KO mice. (A+C, upper panels) Mean ± S.E.M. I-O functions of maximum peak-to-peak amplitudes of the SP **(A)** and ABR wave I **(C)**. SP amplitude was not significantly different between genotypes **(A)** but summed neuronal activity of the AN was significantly elevated in GC-B KO (**C**, red lines**)** compared to GC-B WT (**C**, black lines) and to GC-B HET (**C**, green lines) mice. Note that ABR wave amplitudes are plotted from -10 to 70 dB SL (normalization to threshold) and that the amplitude scale differs for SP and ABR wave I amplitudes. **(B+D, lower panels)**. Mean ± S.E.M. I-O functions of ABR wave latencies corresponding to the analyzed peak amplitudes in the upper panels of the corresponding wave deflections. SP wave latency did not differ between genotypes at any measured stimulus intensity **(B)**. ABR wave I latencies **(D)** were significantly delayed in GC-B KO compared GC-B WT and GC-B HET mice. Grey-shaded areas in **(A-D)** correspond to stimulus intensities with significant differences between GC-B WT and GC-B KO mice. Statistical comparisons are listed in detail in Table 3 and Table 4. The legend keys in **(A)** apply for **(A-D)**. *Modified from (Wolter et al. 2018)*.

The elevated and delayed ABR wave I in GC-B KO mice leads to the assumption, that activity in the ascending auditory pathway is increased and less synchronized to auditory input in case of a loss of function mutation of GC-B. Therefore, central ABR waves were also examined for indicators of changed auditory processing in the auditory brainstem (ABR waves II and III) and neuronal output into the inferior colliculus (ABR wave IV). Quantitative analysis of the central supra-threshold ABR-wave I-O growth functions of GC-B KO (n=18 mice), GC-B WT (n=18 mice) and GC-B HET mice (n=20 mice) revealed significant differences between genotypes for ABR wave amplitudes (Fig. 15A, ABR wave II: 2-way ANOVA, p<0.0001, F(2,1100)=130.0; Fig. 15C, ABR wave III: 2-way ANOVA, p<0.0001, F(2,1460)=48.31; Fig. 15E, ABR wave IV: 2-way ANOVA, p<0.0001, F(2,1447)=26.34) and ABR wave latencies (Fig. 15B, ABR wave II: 2-way ANOVA, p<0.0001, F(2,1001)=48.57; Fig. 15D, ABR

wave III: 2-way ANOVA, p<0.0001, F(2,1350)=168.2; Fig. 15F, ABR wave IV: 2-way ANOVA, p<0.0001, F(2,1336)=230.2) between genotypes. *Post hoc* tests revealed significantly increased ABR wave II-IV amplitudes for the middle and high stimulus levels (Fig. 15A,C,E) in GC-B KO compared to GC-B WT mice and ABR wave II-III amplitudes compared to GC-B HET mice (Bonferroni's multiple comparisons test see Table 3). Furthermore, the central ABR waves II-IV were progressively delayed in GC-B KO mice, with significant delay of ABR wave II already at hearing threshold (Fig. 15B, Table 4) and even more prominent significant delay spanning the entire measured range of stimulus levels for ABR waves III (Fig. 15D, Table 4) and IV (Fig. 15F, Table 4).In contrast, neither central ABR wave amplitudes nor latencies were not found to be different between GC-B HET and GC-B WT mice at any measured stimulus level (Bonferroni's multiple comparisons test see Table 3 and Table 4).

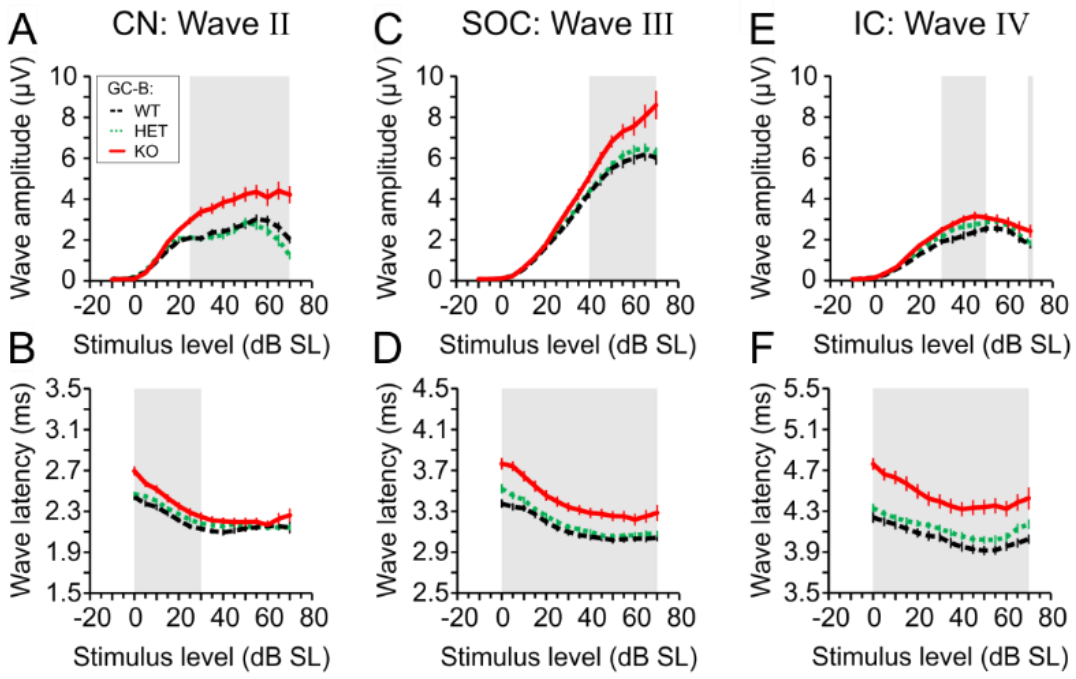

Fig. 15. **Click-evoked ABR wave II - IV were increased and progressively delayed in GC-B KO mice. (A,C,E, upper panels)** Mean ± S.E.M. I-O functions of maximum peak-to-peak amplitudes of ABR waves II **(A)**, III **(C)** and IV **(E)**. Summed neuronal activity of the CN, SOC and IC was significantly elevated in GC-B KO (**A, C, E**, red lines) compared to GC-B WT (black broken lines) and GC-B HET (green broken lines) mice. Note that ABR wave amplitudes are plotted from -10 to 70 dB SL (normalization to threshold). **(B,D,F; lower panels)** Mean ± S.E.M. I-O functions of ABR wave latencies corresponding to the analyzed peak amplitudes in the upper panels of the corresponding waves. ABR wave II **(B)**, III **(D)** and IV **(F)** latencies were significantly delayed in GC-B KO compared GC-B WT and GC-B HET mice. Note that latency is increasing along the afferent auditory pathway. Grey-shaded areas in **(A-F)** correspond to stimulus intensities with significant differences between GC-B WT and GC-B KO mice. Statistical comparisons are listed in detail in Table 3 and Table 4. The legend keys in **(A)** apply for **(A-F)**. *Modified from (Wolter et al. 2018)*.

Conclusion: Inconspicuous SP wave amplitudes and latencies indicate that the observed elevated hearing thresholds in GC-B KO mice are unlikely to be linked with possible sound transduction deficits in IHC (MET) channels. This finding strengthens further the assumption of functional and differentiated hair cells in GC-B KO mice as already predicted from findings shown in Fig. 10 and Fig. 11. From significantly elevated and progressively delayed early and central ABR waves in GC-B KO mice can be inferred, that not cochlear hair cell function but succeeding auditory signal processing may be affected, as for example the modulatory influence of retrocochlear feedback loops originating in the auditory brainstem.

3.3.3 Analysis of retrocochlear efferent modulation of cubic DPOAEs

Since efferent contacts onto OHCs and IHCs were reduced (see Fig. 12) and ABR wave III was significantly elevated and delayed in C-B KO mice (see Fig. 15), it can be hypothesized that retrocochlear feedback loops, radiating from the olivary nuclei in the auditory brainstem, are functionally affected in GC-B KO mice. It has been previously shown that dysfunctional MOC-efferent innervation of OHCs (Warr and Guinan 1979) led to an increase in hearing thresholds by up to 10 dB (Jäger and Kössl 2016), a threshold elevation comparable to that observed in GC-B KO mice (see Fig. 6 and Fig. 7). Further, activation of (mainly) ipsilateral MOC-neurons (Liberman et al. 1996) is discussed to play a role in suppression of OHC mechanoelectrical properties. Therefore, rapid (~100 ms) modulation of OHC electromotility by EF-MOC fibers was tested in a subgroup of GC-B KO, GC-B WT and GC-B HET mice by ipsilateral adaptation (Kujawa and Liberman 2001; Liberman et al. 1996) of DPOAE amplitudes during stimulus presentation (Maison et al. 2012) with the help of phase-varied primary pairs as elicitors (Dalhoff et al. 2015; Whitehead et al. 1996).

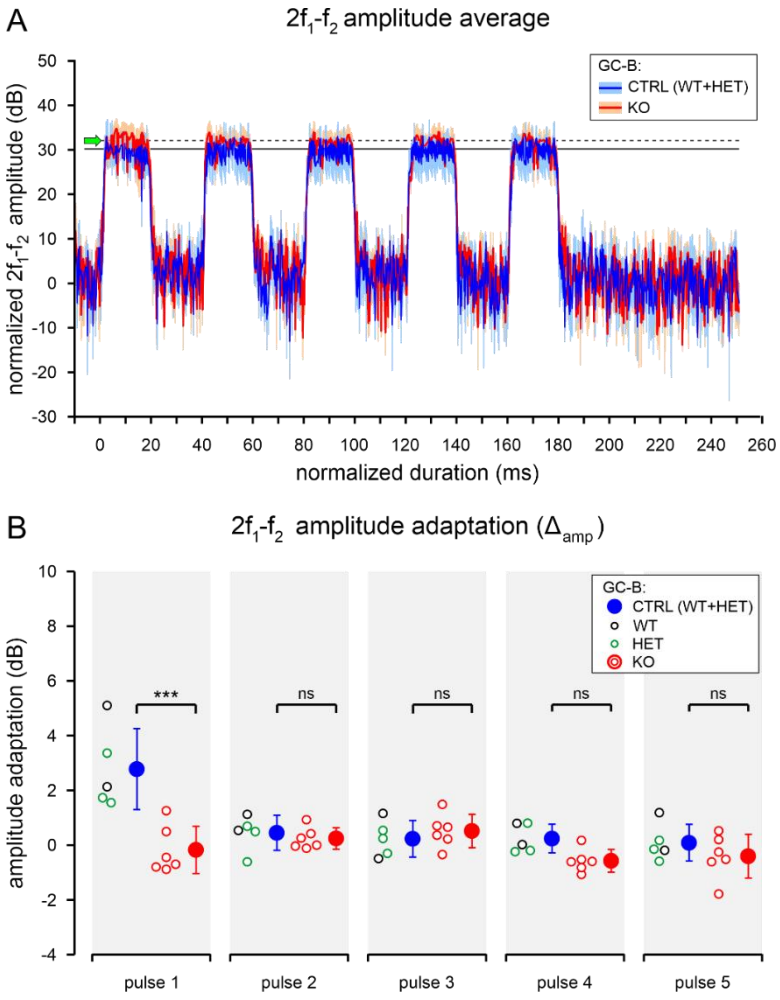

Fig. 16. Pulsed f_2 presentation resulted in absence of fast adaptation in GC-B KO mice. (A) Time course of $2f_1$-f_2 DPOAE amplitudes of GC-B CTRL (GC-B WT and GC-B HET mice, blue line and shade, mean ± S.E.M.) and GC-B KO mice (red line and shade, mean ± S.E.M.) after pulsed f_2 presentation (five f_2 pulses with 20 ms duration, f_2=11.3 kHz, L_1=60-70 dB). DPOAE amplitudes were normalized to noise level. The "baselines" of adapted DPOAE amplitudes are indicated for GC-B KO (dashed black line) and GC-B CTRL mice (black line). Adaptation of GC-B CTRL DPOAE amplitudes in the first pulse are indicated (lime-green arrow). **(B)** Mean ± S.D. Δ_{amp} amplitudes (filled circles and error bars) of the first f_2 pulse were significantly reduced in GC-B KO mice (red open dots: individual ears) when compared to GC-B CTRL mice (black open dots: individual GC-B WT ears, green open dots: individual GC-B HET ears).

In 9 GC-B CTRL mice (four GC-B WT and five GC-B HET mice combined as a control group) and in three GC-B KO mice, DPOAE amplitudes showed reduction over time (Wolter et al. 2018) when stimulated simultaneously by phase-varied primary pairs with f_1 stimulus SPLs ranging from 60-70 dB SPL (Kujawa and Liberman 2001). The initial maximal DPOAE (amp_{max}) amplitudes were significantly smaller in GC-B KO mice when compared to GC-B CTRL mice (Wolter et al. 2018). Further, a statistically non-significant trend for smaller amplitude adaptation in GC-B KO mice was observed when compared to GC-B CTRL mice (Wolter et al. 2018). Subsequently, five GC-B CTRL (two GC-B WT and three GC-B HET mice) and five GC-B KO mice were stimulated by phase-varied primary pairs with continuous presentation of the f_1 stimulus with L_1=60-70 dB SPL and pulsed presentation of the f_2 stimulus (Fig. 16). Amp_{max} amplitudes in response to each pulse were not significantly different between GC-B KO and GC-B CTRL mice (multiple t tests corrected for multiple comparisons after Bonferroni-Dunn for pulse 1: p>0.9999, pulse 2: p=0.5918, pulse 3: p=0.5399, pulse 4: p>0.9999 and pulse 5: p>0.9999). Strikingly, the averaged adapted (amp_{adapt}) amplitudes of the first f_2 pulse differed significantly between GC-B KO and GC-B CTRL mice (multiple t tests corrected for multiple comparisons after Bonferroni-Dunn: p<0.0001). On the other hand, amp_{adapt} amplitudes were not significantly different for the four subsequent f_2 pulses (multiple t tests corrected for multiple comparisons after Bonferroni-Dunn for pulse 2: p>0.9999, pulse 3: p>0.9999, pulse 4: p=0.4097 and pulse 5: p>0.9999). The time course of amplitude adaptation was comparable for simultaneous and pulsed primary presentation experiments, as amplitudes decreased in a time window of roughly 20 ms and then stabilized on a plateau, while adaptation strength was more prominent when primaries were presented simultaneously (see Fig. 16 and (Wolter et al. 2018). The results of both experiments may indicate impaired MOC function but it cannot be excluded that middle ear muscle reflexes are changed in GC-B KO mice, which also are expected to change when auditory input is changed (Valero et al. 2016).

Conclusion: The $2f_1$-f_2 DPOAE amplitude curves for simultaneous (Wolter et al. 2018) and pulsed f_2 presentation (Fig. 16) indicate a fast and persisting adaptive response after onset of a loud sound stimulus (L_1=60-70 dB SPL) (Kujawa and Liberman 2001) in GC-B CTRL but not in GC-B KO mice. These results may point to impaired MOC function in GC-B KO mice but it cannot be excluded that middle ear muscle reflexes

are affected, which also are expected to change when auditory input is changed (Valero et al. 2016).

3.3.2 Analysis of central processing of amplitude-modulated stimuli (ASSR)

Progressively delayed ABR wave I-IV latencies and elevated ABR wave I-IV amplitudes in GC-B KO mice raised the question, if fast auditory processing with high acuity in temporal precision is changed in these mice. Amplitude-modulated stimuli were presented and ASSRs were recorded to test for proper integrity of auditory pathways, subcortical areas and the frontocentral cortex involved in processing of these stimuli (Engelien et al. 2000). The neurons in these auditory pathways respond to amplitude-modulated stimuli with phase-locked action potential generation according to the modulation frequency of acoustic stimuli (Kuwada et al. 2002). Therefore, a wide range of modulation frequencies, modulation indices (depth), and stimulus levels (I-O function) was tested in a subgroup of GC-B KO (*n*=8), GC-B WT (*n*=8) and GC-B HET (*n*=10) mice (Fig. 17 and (Wolter et al. 2018)).

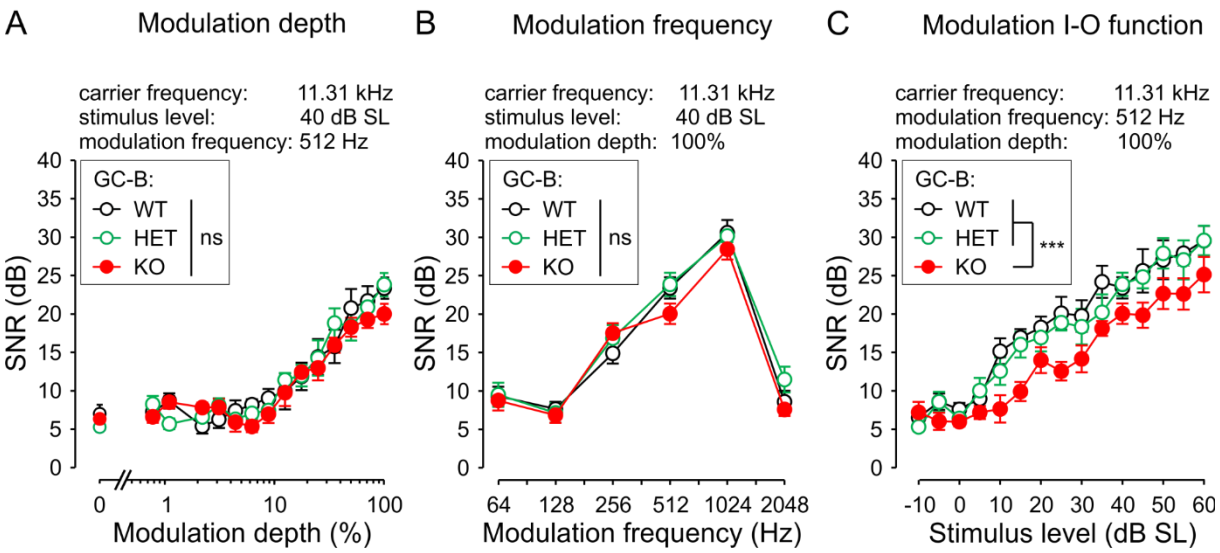

Fig. 17. ASSR I-O function was reduced in GC-B KO mice. (A) Mean ± S.E.M. signal-to-noise ratio (SNR) modulation depth response (CF: 11.3 kHz; MF: 512 Hz; SL: 40 dB above threshold) was not significantly different between genotypes. **(B**) Mean ± S.E.M. SNR of the response to increasing MF of GC-B WT (black open circles), GC-B HET (green open circles) and GC-B KO mice (red filled circles) did not differ between genotypes. **(C)** Mean ± S.E.M. SNR modulation I-O function of an amplitude-modulated tone (CF: 11.3 kHz; MF: 512 Hz; 100 % modulation depth). GC-B KO I-O function was significantly reduced compared to GC-B WT and GC-B HET mice. *From (Wolter et al. 2018)*.

Amplitude-modulated stimuli were designed using 11.3 kHz as the carrier frequency in all experiments, as this frequency is affected in GC-B KO mice (see Fig. 6, Fig. 7 and

Fig. 8). First, modulation frequency was fixed at 512 Hz, stimulus level was fixed at 40 dB SL and modulation depth was varied (contrasts: 0.78-100 % and 0 %). Responses were not significantly different between genotypes (Fig. 17A, 2-way ANOVA, p=0.1853, F(2,345)=1.694). Next, modulation depth was fixed at 100 % modulation, stimulus level was fixed at 40 dB SL and modulation frequency was varied between 64 and 2048 Hz. Responses were also not significantly different between genotypes (Fig. 17B, 2-way ANOVA, p=0.1240, F(2,138)=2.119). Last, modulation frequency was fixed again at 512 Hz, modulation depth was fixed at 100 % and stimulus level was varied between -10 and 60 dB SL. The calculated ASSR I-O functions were significantly different between genotypes (Fig. 17C, 2-way ANOVA, p<0.0001, F(2,344)=28.49). *Post hoc* tests revealed significantly reduced ASSRs, in particular at stimulus levels close to detection threshold in GC-B KO mice when compared to GC-B WT and GC-B HET mice (Table 5). On the other hand, no significant difference was found between GC-B WT and GC-B HET mice at any tested stimulus level (Table 5).

Conclusion: Unchanged modulation depth and modulation frequency for stimulus levels at 40 dB SL in GC-B KO compared to GC-B WT and GC-B HET mice indicate, that central auditory circuits could properly respond to amplitude-modulated stimuli. However, the significantly reduced ASSR I-O growth functions in GC-B KO mice may demonstrate a reduced capability to detect amplitude-modulated sounds close to detection threshold.

3.3.4 Analysis of features of the acoustic startle response (ASR) and prepulse inhibition (PPI)

The cochlear root neurons are a cluster of afferent auditory neurons with their nuclei located in the CN, which were shown to be involved in generation of the ASR (Gomez-Nieto et al. 2014; Lingenhohl and Friauf 1994). The ASR is one of the fastest reflexes found in the mammalian CNS (Lauer et al. 2017) and a well-established behavioral test in awake animals for testing of very fast auditory processing (Steube et al. 2016). Therefore, it was investigated in a subgroup of GC-B WT (n=5) and GC-B KO (n=7) mice, whether impaired AN branching affects proper function of the ASR.

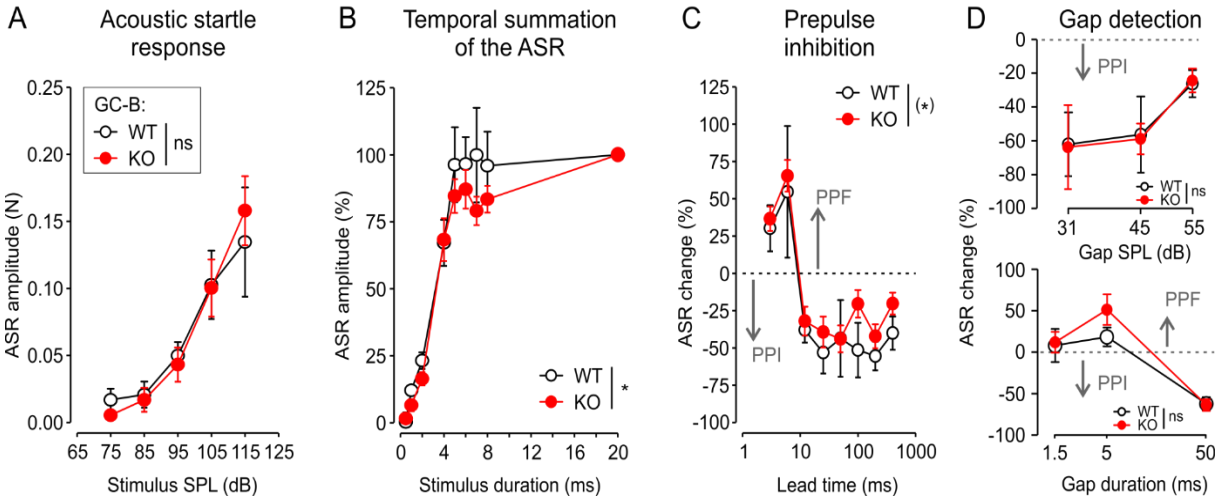

Fig. 18. GC-B KO mice maintained subtle changes of temporal features of the acoustic startle response (ASR) and prepulse inhibition (PPI). (A) Mean ± S.E.M. ASR amplitude growth of GC-B WT (black open circles and lines) and GC-B KO (red filled circles and lines) mice shown for increasing startle stimulus SPL. There was no significant difference between genotypes for stimulus SPLs between 75-115 dB SPL. **(B)** In both genotypes ASR amplitude increased with increasing stimulus durations between 0.5-20 ms. The mean ± S.E.M. maximum ASR was similar for stimulus durations up to 4 ms in both genotypes but smaller for stimulus durations between 5-8 ms in GC-B KO compared to GC-B WT mice. This reduction in temporal summation was significant. **(C)** A prepulse with different lead time was presented before the startle stimulus, which elicited prepulse facilitation of the ASR (PPF, 3-6 ms lead time) or prepulse inhibition of the ASR (PPI, 12-400 ms lead time). The broken line marks the zero line for ASR change; values above this line correspond to increase of the ASR (PPF), values below the broken line correspond to reduction of the ASR (PPI). Mean ± S.E.M. change of the ASR resulted in a statistically non-significant trend (p=0.0935) for reduction of PPI in GC-B KO compared to GC-B WT mice. **(D)** Presenting a gap in noise as a startle response modulating prepulse (gap-detection) resulted in similar PPI or PPF in GC-B WT and GC-B KO mice across the explored gap SPL (upper panel) and gap duration (lower panel). *From (Wolter et al. 2018)*.

Analysis of ASR amplitudes revealed no significant difference in the ASR growth function with increasing stimulus SPL between genotypes (Fig. 18A, 2-way ANOVA, p=0.991, F(1,50)=0.0001). However, startle thresholds were increased in GC-B KO mice, as only 29 % of the tested individuals showed a significant ASR at 75 dB SPL compared to 60 % GC-B WT mice and only 71 % GC-B KO mice had a response significantly different from spontaneous motor activity at 85 dB SPL, while 100 % GC-B WT mice showed a significant ASR at this stimulus level (one-sample t-tests, p<0.05). ASR amplitudes typically increase with increasing startle stimulus durations up to 8 ms (Blaszczyk 2003). In fact, ASR amplitudes increased with prolonged startle stimuli (2-way ANOVA, p<0.0001, F(7,80)=57.2), when normalized to the saturated, maximal ASR amplitude (20 ms stimulus duration, Fig. 18B). The ASR amplitude increase was significantly different between GC-B KO and GC-B WT mice (Fig. 18B, 2-way ANOVA, p=0.0358, F(1,80)=4.56). For startle stimulus durations between 0.5-

4 ms, the ASR increased in an indistinguishable way in both genotypes. While the ASR was already saturated in GC-B WT mice at startle stimulus durations of 5 ms, saturation of the ASR was not yet reached even at 8 ms in GC-B KO mice, indicating changed properties of the underlying neuronal circuitry. The ASR increased, when a second acoustic pulse (prepulse) was given 3-6 ms prior to the startle stimulus (prepulse facilitation, PPF) and decreased, when prepulses were presented 12-400 ms prior to the startle stimulus (prepulse inhibition, PPI, Fig. 18C, 2-way ANOVA, $p<0.001$, $F(7,80)=15.6$). GC-B KO mice exhibited a nonsignificant trend for reduced PPI (2-way ANOVA, $p=0.0935$, $F(1,80)=2.88$). When a gap in noise (65 dB SPL) with 50 ms leadtime before startle stimulus presentation was used to modulate the ASR no significant difference was found between GC-B KO and GC-B WT mice, neither for different gap durations tested between 1.5-50 ms (Fig. 18D, upper panel, 2-way ANOVA, $p=0.319$, $F(1,30)=1.03$) nor for different gap SPL tested between 31-55 dB SPL (Fig. 18D, lower panel, 2-way ANOVA, $p=0.931$, $F(1,30)=0.01$).

Conclusion: ASR amplitudes in GC-B KO mice were indistinguishable from those in GC-B WT mice, indicating that the circuitry involved in execution of a sufficient motor response is not affected or can compensate for the significantly changed cochlear output (see Fig. 14) and evoked activity in involved brainstem nuclei (Fig. 15) when bifurcation of AN fibers is absent. Nevertheless, significantly reduced temporal summation of the ASR and tendencies for a reduced PPI indicate possible deficits in temporal integration in the ASR pathway or in the ASR-modulating PPI circuitry.

3.4 Basal hearing function analysis of Npr2$^{fl/fl}$;Wnt1^{Cre} and cGKI$^{fl/fl}$;Wnt1^{Cre} mice

To confirm that the auditory threshold phenotype found in the constitutive knockout model (GC-B KO, *Npr2$^{LacZ/LacZ}$*) is specific for effects caused by loss of GC-B function in SGNs, the same measurements were performed in mice with a conditional knockout of either GC-B (*Npr2$^{fl/fl}$;Wnt1^{Cre}*) or its downstream target cGKI (*cGKI$^{fl/fl}$;Wnt1^{Cre}*).

3.4.1 Analysis of naso-anal length

Naso-anal length of *Npr2$^{fl/fl}$;Wnt1^{Cre}* but not of *cGKI$^{fl/fl}$;Wnt1^{Cre}* was determined as cGKII and not cGKI is involved in cGMP-dependent signaling of endochondral bone growth (Hofmann et al. 2006) and because the tested *cGKI$^{fl/fl}$;Wnt1^{Cre}*mice were totally inconspicuous in respect to body size.

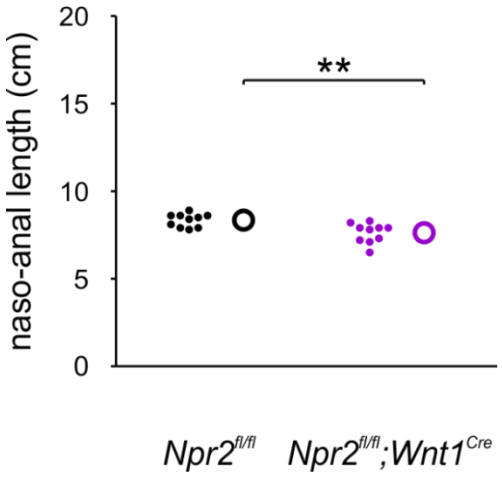

Fig. 19. *Npr2$^{fl/fl}$;Wnt1^{Cre}* mice maintain a slight but significant reduction in body size. Mean ± S.D. naso-anal lengths were significantly different for *Npr2$^{fl/fl}$;Wnt1^{Cre}* (purple open circle) compared to *Npr2$^{fl/fl}$* (black open circle) mice. Filled dots represent individual mice.

Npr2$^{fl/fl}$;Wnt1^{Cre} mice maintained a very marginal but still significant bone growth phenotype (Fig. 19), which was not reported before (Tröster et al. 2018). For quantification, naso-anal length of 1-to-2-month-old mice was measured (*Npr2$^{fl/fl}$*: 1.5±0.3 months, *n*=10; *Npr2$^{fl/fl}$;Wnt1^{Cre}*: 1.4±0.3 months, *n*=10). *Npr2$^{fl/fl}$;Wnt1^{Cre}* mice were significantly smaller when compared to *Npr2$^{fl/fl}$* mice (t test, $t(18)=3.062$, $p=0.0067$, $F(9,9)=1.988$). In average, *Npr2$^{fl/fl}$;Wnt1^{Cre}* mice were 0.7 cm shorter when compared to *Npr2$^{fl/fl}$* mice.

Conclusion: The severe impact of constitutive GC-B knockout on bone growth is absent in the conditional knockout models for GC-B and its downstream target cGKI. The observed minor reduction in naso-anal length is probably related to loss of GC-B function in sensory ganglion neurons.

3.4.2 Analysis of ABR thresholds

For ABR measurements, conditional GC-B knockout mice (*Npr2*$^{fl/fl}$;*Wnt1*^{Cre}: *n*=9 mice) and their controls (*Npr2*$^{fl/fl}$: *n*=10 mice), as well as conditional cGKI knockout mice (*cGKI*$^{fl/fl}$;*Wnt1*^{Cre}: *n*=5 mice) and their controls (*cGKI*$^{fl/fl}$: *n*=4 mice) were used. *Npr2*$^{fl/fl}$;*Wnt1*^{Cre} mice exhibited mildly elevated ABR thresholds when compared to their *Npr2*$^{fl/fl}$ controls for click- and noise burst-evoked ABRs (Fig. 20A left, click: average threshold loss of 4.8 dB, Mann-Whitney test: *p*=0.0220, Fig. 20A right, noise: average threshold loss of 5.7 dB, Mann-Whitney test: *p*=0.0057). In line, *cGKI*$^{fl/fl}$;*Wnt1*^{Cre} mice showed comparable elevation of ABR thresholds when compared to their respective *cGKI*$^{fl/fl}$ controls for click- and noise burst-evoked ABRs (Fig. 20B left, click: threshold loss average of 4.4 dB, t test: *t*(7)=3.443, *p*=0.0108, *F*(3,4)=1.088, Fig. 20B right, noise: threshold loss average of 4.8 dB, Mann-Whitney test: *p*=0.0317).

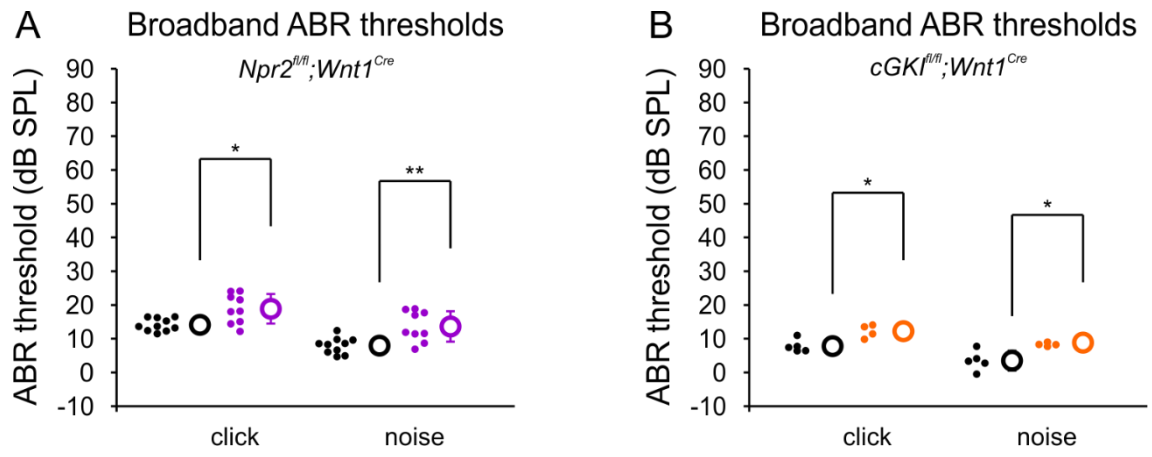

Fig. 20. Mild elevation of ABR thresholds in *Npr2*$^{fl/fl}$;*Wnt1*^{Cre} and *cGKI*$^{fl/fl}$;*Wnt1*^{Cre} mice. Broadband ABR thresholds were significantly different for click- and noise-evoked stimuli for **(A)** *Npr2*$^{fl/fl}$;*Wnt1*^{Cre} (purple) compared to *Npr2*$^{fl/fl}$ (black) mice and for **(B)** *cGKI*$^{fl/fl}$;*Wnt1*^{Cre} (orange) compared to *cGKI*$^{fl/fl}$ (black) mice. **(A)** Mean ± S.D. click- and noise-evoked ABR thresholds were significantly elevated for *Npr2*$^{fl/fl}$;*Wnt1*^{Cre} (purple open circle) compared to *Npr2*$^{fl/fl}$ (black open circle) mice. **(B)** Mean ± S.D. click- and noise-evoked ABR thresholds were significantly elevated for *cGKI*$^{fl/fl}$;*Wnt1*^{Cre} (orange open circle) compared to *cGKI*$^{fl/fl}$ (black open circle) mice. Filled dots in **(A and B)** represent thresholds of individual mice.

Conclusion: The observed elevation in ABR thresholds in constitutive GC-B KO mice was reproduced in two distinct conditional models of the GC-B/cGMP/cGKI signaling cascade involved in sensory axon bifurcation. Despite low *n*, the elevation of click- and noise-evoked ABR thresholds was still significant in *Npr2*$^{fl/fl}$;*Wnt1*^{Cre} and *cGKI*$^{fl/fl}$;*Wnt1*^{Cre} mice, underpinning a deficit to detect acoustic stimuli when AN axons fail to innervate target neurons in the CN.

3.4.3 Analysis of DPOAE thresholds

As a next step, DPOAE thresholds of the same mice as for the ABR measurements were analyzed. *Npr2$^{fl/fl}$;Wnt1^{Cre}* mice exhibited mildly elevated $2f_1$-f_2 DPAOE thresholds at the stimulus frequency f_2=11.3 kHz when compared to their *Npr2$^{fl/fl}$* controls (Fig. 21A, average threshold loss of 14.6 dB, Mann-Whitney test: p=0.0061). In contrast, *cGKI$^{fl/fl}$;Wnt1^{Cre}* mice showed no elevation of $2f_1$-f_2 DPAOE thresholds at the stimulus frequency f_2=11.3 kHz when compared to their respective *cGKI$^{fl/fl}$* controls (Fig. 21B, average threshold loss of 3.6 dB, t test: $t(7)$=1.092, p=0.3110, $F(3,4)$=2.464).

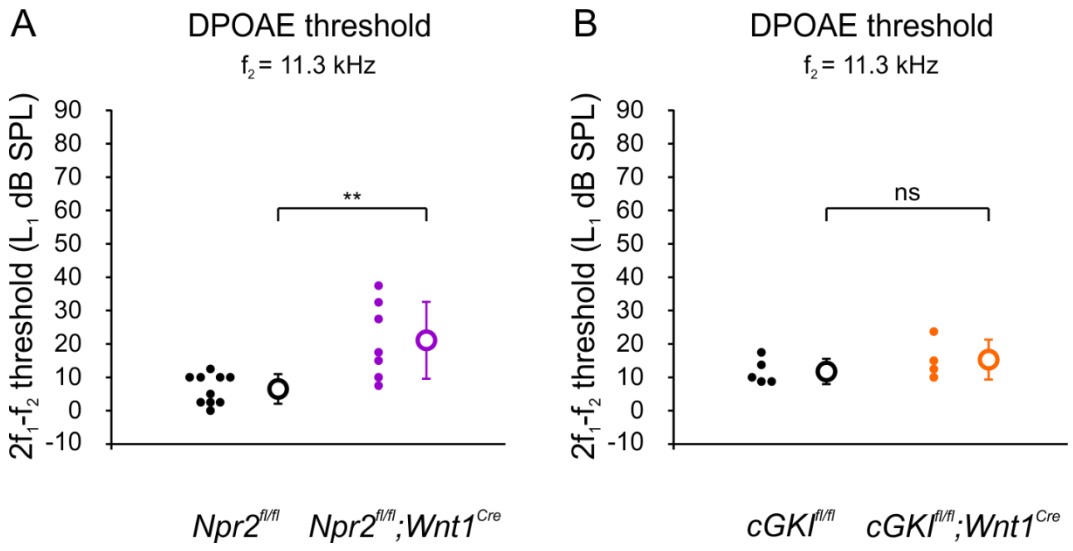

Fig. 21. Mild elevation of ABR thresholds in *Npr2$^{fl/fl}$;Wnt1^{Cre}* but not in *cGKI$^{fl/fl}$;Wnt1^{Cre}* mice. **(A)** Mean ± S.D. $2f_1$-f_2 DPOAE threshold (open circles with error bars) at the stimulus frequency f_2=11.3 kHz of *Npr2$^{fl/fl}$;Wnt1^{Cre}* (purple) was significantly elevated compared to *Npr2$^{fl/fl}$* (black) mice .**(B)** Mean ± S.D. $2f_1$-f_2 DPOAE threshold at the stimulus frequency f_2=11.3 kHz of *cGKI$^{fl/fl}$;Wnt1^{Cre}* (orange) mice was not statistically different compared to *cGKI$^{fl/fl}$* mice (black). Filled dots in **(A and B)** represent thresholds of individual mice.

Conclusion: The observed elevated ABR thresholds in *Npr2$^{fl/fl}$;Wnt1^{Cre}* mice may be associated with reduced detection sensitivity of OHCs following sound stimulation, whereas the reduced capability to detect sound cannot be clearly associated with OHC function in *cGKI$^{fl/fl}$;Wnt1^{Cre}* mice. Further studies are needed to test efferent modulation of IHC and OHC activity in these conditional GC-B knockout mouse lines.

3.4.4 Outlook

The implications of profound changes in fast temporal processing on sound localization and speech understanding are not completely understood. Sound localization is essential for interindividual communication and also for navigation, as natural environment is loaded with noise and (fearful) stimuli which have to be recognized, weighed and responded to. It can be expected that loss of AN bifurcation, which is already influencing basal hearing and processing of fast stimuli, is affecting localization and recognition of speech (or vocalization in case of mice). Further studies are needed in the future to confirm the results reported here and in (Wolter et al. 2018). First experiments with conditional GC-B KO mice showed clearly, that the conditional GC-B knockout models maintained significantly elevated ABR thresholds (see Fig. 6 and Fig. 20). Interestingly, *cGKI$^{fl/fl}$;Wnt1^{Cre}* mice can compensate for elevated ABR thresholds on the level of OHCs (Fig. 21). If the reported elevated auditory thresholds of conditional GC-B knockout mice result from impaired retrocochlear feedback onto IHCs or OHCs and the specific role of cGKI in these processes needs further investigation. Also, the question whether AF type I undergo final maturation (proper development of fibers with high-SR/low-threshold characteristics) when they lack a precise and reliable retrocochlear efferent system is still not answered, as it also could explain the impaired cochlear gain observed in GC-B KO mice. A possible way to test for integrity of low- and high-SR fibers is to challenge the auditory system of conditional GC-B knockout mice with ototoxic noise, as low- and high-SR fibers maintain different vulnerability to damaging noise.

4. Discussion

The present study aimed to provide new insights into the role of proper AN bifurcation on auditory processing with focus on the auditory brainstem and retrocochlear feedback loops. It has been shown, that impaired AN bifurcation during embryonal development impacts tonotopic representation within the CN (Lu et al. 2014), but the consequences for higher order auditory processing are still unknown. It was shown, that adult GC-B KO (*Npr2*$^{LacZ/LacZ}$) mice, which maintain an impaired bifurcation of central AN axons (Ter-Avetisyan et al. 2014), exhibited significant effects on basal hearing function and features of fast temporal processing. A slight increase in ABR thresholds was abundant which could be linked to reduced active cochlear amplification due to reduced OHC sensitivity. A contribution of transmission impairments within the middle ear could be excluded judged by anatomical and functional analysis. The lack of *GC-B* expression within cell types of the sensory epithelium of the cochlea and the manifested innervation phenotype of the CN strengthen the hypothesis of impaired retrocochlear feedback control. In fact, a combination of reduced marker proteins for efferent OHCs (and IHCs) innervation and changed MOC-efferent-controlled suppression of OHC motility supports this argument. Further, evoked activity within the ascending auditory pathway was found to be increased and delayed in GC-B KO mice judged from ABR fine structure analysis. Temporal processing deficits were shown by impaired efficiency to follow amplitude-modulated stimuli close to auditory threshold and by a significant behavioral inaccuracy of temporal summation of the acoustic startle response. In the following chapter, these findings are discussed in the context of being a result of impaired AN bifurcation and the resulting cochlear output inexactness linked to impaired efferent gain control. None of the reported results was found in GC-B HET mice underpinning that the observed effects are a consequence of the bifurcation deficit. Loss of one unfunctional *GC-B* allele can be compensated by the remaining wildtype allele since bifurcation is completely normal in GC-B HET mice (Ter-Avetisyan et al. 2014).

4.1 Role of GC-B for maturation of cochlear hair cells

In contrast to recent analysis of another *GC-B* mutant mouse line (*Npr2*$^{cn/cn}$, (Tsuji and Kunieda 2005)) with reported disturbed tonotopic organization in the CN and normal hearing thresholds (Lu et al., 2014) this study found for the first time, that a loss of function mutation of the *GC-B* gene lead to a basal hearing phenotype (Fig. 6, Fig. 7 and (Wolter et al. 2018)) as detected by ABR and DPOAE threshold analysis. First, possible sound conduction impairments in the middle ear were excluded since GC-B KO mice suffer from short stature (Fig. 5) which may affect form and arrangement of the skull and the bony middle ear. Instead, elevation of hearing thresholds was very likely to be caused by changed OHC sensitivity to sound stimulation but not by impaired sound conduction through the middle ear (Fig. 8) and (Gehr et al. 2004; Qin et al. 2010; Turcanu et al. 2009; Wolter et al. 2018). Since embryonal and mature postnatal *GC-B* gene expression is absent in the sensory epithelium of GC-B KO mice (Fig. 9 and (Wolter et al. 2018)) and since OHCs differentiated into a mature state (Fig. 10 and (Wolter et al. 2018)) as judged from expression analysis of prestin (Dallos 2008) and KCNQ4 (Holt et al. 2007; Kharkovets et al. 2006; Marcotti and Kros 1999; Weber et al. 2002) a significant direct action of *GC-B* gene deletion on the hair cell level is very unlikely. This was also confirmed for IHCs where normal expression of otoferlin (Fig. 11 and (Duncker et al. 2013; Hams et al. 2017; Wolter et al. 2018)), BK (Fig. 11 and (Wolter et al. 2018)) and vGlut3 (Fig. 12 and (Ruel et al. 2008; Seal et al. 2008; Wolter et al. 2018)) suggests intact IHC function (Lee et al. 2015; Yu et al. 2016). Further, CtBP2/Ribeye-positive synaptic contacts with SGN afferent fibers (Becker et al. 2018; Sheets et al. 2017) as well as SP amplitudes and latencies (Barral and Martin 2011; Durrant et al. 1998) were indistinguishable between GC-B KO,GC-B HET and GC-B WT mice (Fig. 11C, Fig. 14 and (Wolter et al. 2018)), suggesting a functional IHC synapse.

Conclusion: Morphological and functional analysis of the sensory epithelium strongly suggests fully developed and functional hair cells. Therefore, the observed elevated auditory thresholds and the changed facets of sound processing in the auditory brainstem are more likely to be linked to modulation of hair cell function and cochlear output.

4.2 Role of GC-B for retrocochlear efferent feedback

Given the normal development of IHCs and OHCs but significant reduction of the efferent marker protein VAMP2 below IHCs (Fig. 12A-D and (Wolter et al. 2018)) and OHCs (Fig. 12E+G and (Wolter et al. 2018)), as well as significant reduction of the efferent marker protein ChAT below OHCs (Fig. 12F+H and (Wolter et al. 2018)), it can be hypothesized, that impaired basal hearing function of GC-B KO mice may be a consequence of changed efferent modulation of cochlear hair cells arising from the SOC in the auditory brainstem. Direct involvement of *GC-B* for formation and maturation of these efferent neurons could be excluded, because no *LacZ* staining could be found in any of the auditory nuclei in the lower auditory brainstem (see (Wolter et al. 2018)). Cholinergic efferent modulation of OHC electromotility underlies Ca^{2+} influx through α9/α10-nicotinic receptors (nAChR) in the OHC membrane, triggering Ca^{2+}-dependent K^+ channel (SK2) opening, which finally leads to a dampening effect (Guinan 2006). Recently it was shown, that changed expression of nAChRs in OHCs could be associated with alterations in morphology of OHC efferent synapses and their modulatory influence on OHC electromotility (Fuchs et al. 2014; Vetter et al. 2007). Further, nAChR deletion resulted in disturbed tonotopic organization of SOC auditory circuits (Clause et al. 2014), a phenotype which is quite comparable to the disturbed tonotopic organization of SGN axons in *Npr2*$^{cn/cn}$ mice (Lu et al. 2014). It was also reported, that increased size of efferent synaptic contacts onto OHCs could be related to enhanced and prolonged modulatory activity, resulting in prolonged MOC-efferent suppression (Wedemeyer et al. 2018). Conversely, it can be concluded that smaller OHC efferent synapses (Fig. 12E-H and (Wolter et al. 2018)) may indicate a reduction of MOC-efferent feedback, possibly contributing to the elevated DPOAE thresholds found in GC-B KO mice (Fig. 7 and (Wolter et al. 2018)). Indeed, electrical stimulation of the olivocochlear bundle can lead to reduced DPOAE amplitudes (Maison et al. 2007) and as a result, reduced cochlear gain (Guinan 2006). A drop of $2f_1$-f_2 DPOAE amplitudes by about 10 dB was also observed after lidocaine injections into the contralateral auditory cortex (Jäger and Kössl 2016), which is probably caused by impaired noise cancellation mediated by MOC-efferent fibers (Hienz et al. 1998; Huang and May 1996; Lustig 2006; Millman et al. 2017). Indeed, functional analysis of fast adaptation of $2f_1$-f_2 DPOAE amplitudes after ipsilateral stimulation in GC-B KO mice

revealed a tendency for reduced modulatory action on OHCs (Fig. 16 and (Wolter et al. 2018)).

It must be mentioned that other studies have shown that unfunctional MOC-efferent synapses were accompanied by disturbed expression patterns of otoferlin, BK, and CtBP2/Ribeye on the IHC level (S. L. Johnson et al. 2013; Knipper et al. 2015; Sendin et al. 2014), a phenotype which could not be confirmed in this study (Fig. 11 and (Wolter et al. 2018)). Activity of fully differentiated and mature IHCs is modulated by axo-dendritic LOC-efferent input onto SGN dendrites and mediated by a number of neurotransmitters, including dopamine, acetylcholine, γ-aminobutyric acid (GABA), enkephalins, dynorphins, and calcitonin gene-related peptide (Safieddine and Eybalin 1992; Safieddine et al. 1997). Recently it was shown, that auditory thresholds were elevated after pharmacological elimination of dopaminergic axo-dendritic LOC-efferent synapses and genetic deletion of $GABA_A$ receptor subunits β2 in AN fibers (Maison et al. 2006; Ruel et al. 2001). Taken together, the elevated audiometric thresholds, the reduced fast adaptation of $2f_1$-f_2 DPOAE amplitudes and the reduced efferent contacts with IHCs and OHCs in GC-B KO mice point to a combined impairment of LOC- and MOC-efferent feedback.

Conclusion: A combination of molecular and electrophysiological methods revealed a possible relation of elevated DPOAE thresholds (reduced cochlear gain) and changed morphology and function of efferent synaptic contacts with cochlear hair cells, (changed retrocochlear feedback control), but further studies are needed to investigate, how impaired tonotopic organization on the level of CN affects precision of retrocochlear feedback on the level of the SOC in GC-B KO mice.

4.3 Role of GC-B for fast auditory processing

In the next step it was investigated how elevated audiometric thresholds and changed efferent feedback control interfere with fast auditory processing, since binaural hearing relies on temporal integrity of signal processing along the auditory pathway. Functional analysis of sound processing along the auditory pathway revealed significant elevation and delay of evoked activity in the AN (Fig. 14 and (Wolter et al. 2018)) and subsequently along the ascending auditory pathway (Fig. 15 and (Wolter et al. 2018)). Sound information is coded by distinct AN fiber types, namely those with low spontaneous firing rates (SR) and a high threshold (low- to medium-SR fibers) and

those with high SR and low thresholds (high-SR fibers). Maximal activation of high-SR fibers is already reached close to hearing threshold, while low-SR fibers reach saturation at higher SPLs (about 20-40 dB). This enables for coding of sound information over a wide SPL range, called dynamic range (Sachs and Abbas 1974; Yates 1991). Differentiation of low-SR fibers occurs during development and even prior to hearing onset, when low-SR fibers are driven by spontaneous Ca^{2+} spikes, a process which is under control of efferent axo-somatic cholinergic input (Knipper et al. 2015). In contrast, characteristics of high-SR fibers develop delayed with or after hearing onset (Grant et al. 2010), when low-SR fibers switch to evoked activity patterns. After hearing onset, high-SR fibers contribute to the compound action potential threshold of the AN, equivalent to ABR wave I, while low-SR fibers don't (Bourien et al. 2014). Tonic dopaminergic axo-dendritic efferent modulation is discussed to play a role in this process (Knipper et al. 2015; Ruel et al. 2001). The loss of proper AN bifurcation in GC-B KO mice leads to elevated auditory thresholds and to elevated ABR wave I, which can be therefore associated to response property changes of high-SR fibers and possibly to a failure of setting proper thresholds, eventually caused by impaired critical efferent input. This is supported by the increased late ABR wave latencies in GC-B KO mice (Fig. 15B,D,F and (Wolter et al. 2018)), which can be explained by latency properties of auditory fiber types in the auditory system, where high-SR fibers have the shortest latencies and low-SR fibers have the longest latencies at any given characteristic frequency place (Rhode and Smith 1986). Future studies are needed to clarify how changes in properties of AN fibers lead to increase in threshold and if this is accompanied with changes in characteristic frequencies of high-SR and the dynamic range in general (el Barbary 1991; Ohlemiller and Echteler 1990; Taberner and Liberman 2005).

The significantly increased and delayed ABR wave IV in GC-B KO mice (Fig. 15E,F and (Wolter et al. 2018)) points to impaired auditory input into the IC (see Fig. 13 and (Wolter et al. 2018)), the auditory midbrain, where a large proportion of modulation-sensitive neurons is located (Schreiner and Langner 1988). These neurons are organized in a comparable topographic map (Schreiner and Langner 1988) as the frequency-coding neurons within the CN (and IC), a structuring which was compromised in *Npr2*$^{cn/cn}$ mice (Lu et al. 2014). In fact, GC-B KO mice maintained reduced sensitivity to respond to amplitude modulated tones (Fig. 17 and (Wolter et al.

2018)). Since low-SR fibers are a key contributor to the ASSR in terms of following envelopes of amplitude-modulated stimuli with synchronized spiking patterns (Joris et al. 2004) and because the dynamic range of low-SR may be affected in GC-B KO mice (as discussed in the previous section), it can be assumed that unrestrained dynamic ranges in low-SR fibers are a prerequisite for proper coding of amplitude-modulated stimuli. This is supported by the recent finding, that IHC synaptopathy, induced by deafferentation of the vulnerable low-SR fibers, is correlated with reduced coding of the temporal envelope of acoustic stimuli (Liberman et al. 2016; Liberman and Kujawa 2017).

Further, very fast auditory processing was tested using acoustic startle behavior in awake mice. The ASR is a conserved reflex reaction across mammalian species to harmful acoustic stimuli, is subject to negative selective pressure, and is one of the fastest reflexes found in the mammalian CNS (Lauer et al. 2017). It was investigated, if the observed deficits of GC-B KO mice in processing of auditory information affect reliance of this vital behavior. Interestingly, the basic ASR was unchanged as ASR amplitudes increased in the same way with increasing stimulus SPL when compared to GC-B WT mice (Fig. 18A and (Wolter et al. 2018)), suggesting a quite normal motor component of the ASR. Increased ASR thresholds were observed at the lowest startle stimulus SPLs (75 and 85 dB) in GC-B KO mice, going hand in hand with the observed elevated hearing thresholds (Fig. 6, Fig. 7 and (Wolter et al. 2018)). Despite normal ASR amplitudes, the prepulse length needed to trigger maximal ASR amplitudes was shifted to longer stimulus durations in GC-B KO mice (Fig. 18B and (Wolter et al. 2018)), suggesting reduced input to integrating neurons, thus resulting in a subtle inefficiency of temporal integration, especially for very short startle stimuli. Modification of the ASR by presenting a predictive prepulse (PPI paradigm) resulted in a, yet not statistically significant, trend for reduced capability of the startle circuits in GC-B KO mice to predict the startle stimuli (Fig. 18C and (Wolter et al. 2018)). Interestingly, an exchange of the pure tone prepulse with a gap in noise resulted in no statistical difference between GC-B KO and GC-B WT mice for the measured gap SPL and gap duration (Fig. 18D and (Wolter et al. 2018)). This indicates that the auditory circuits involved in PPI processing can compensate for, or are not affected by the bifurcation deficit in GC-B KO mice.

Conclusion: The findings of this study indicate that the significantly delayed late ABRs in GC-B KO mice (Fig. 14D, Fig. 15B,D,F and (Wolter et al. 2018)) result from increased activity in the AN even at lower stimulus levels (Fig. 14C and (Wolter et al. 2018)) with lowered temporal envelope resolution. Compromised activity in the AN results in reliance deficits, reduced sensitivity and poor coding of temporal envelopes in the nuclei of the auditory brainstem as indicated by subtle changes of processing of amplitude-modulated stimuli especially close to detection threshold (Fig. 17 and (Wolter et al. 2018)) and by changed features of the ASR and PPI (Fig. 18 and (Wolter et al. 2018)).

4.4 Reproduction of the basal hearing phenotype in two conditional GC-B knockout mouse models

The observed minor but still significant reduction in naso-anal length in *Npr2$^{fl/fl}$;Wnt1^{Cre}* mice was comparable to the significant difference between constitutive GC-B WT and GC-B HET mice (taking into consideration that the measured constitutive GC-B mice were significantly older than the conditional GC-B knockout mice). Further, overall appearance of *Npr2$^{fl/fl}$;Wnt1^{Cre}* mice was indistinguishable from that of *Npr2$^{fl/fl}$* mice. The distribution of the sexes was slightly inhomogeneous (female/male ratio for *Npr2$^{fl/fl}$;Wnt1^{Cre}*: 5/5 and *Npr2$^{fl/fl}$* : 7/3) in this study regarding that sex differences in size and weight were reported for a variety of GC-B knockout models (Geister et al. 2013; Tamura et al. 2004; Ter-Avetisyan et al. 2018; Tröster et al. 2018). Additionally, the age of *Npr2$^{fl/fl}$;Wnt1^{Cre}* and *Npr2$^{fl/fl}$* mice was quite spread and differed in average by 2 days due to distribution of genotypes in the litters (total range: P31 to P53). The observed difference in body size may also be an indirect effect, which could be correlated to decreased efficiency of food intake and digestion, as GC-B gene deletion has been recently shown to have an impact on biting force (Ter-Avetisyan et al. 2018) and nutrient uptake into the gastro-intestinal tract due to its changed motility (Sogawa et al. 2010). Taking all facts into consideration, the significant difference in naso-anal length in *Npr2$^{fl/fl}$;Wnt1^{Cre}* and *Npr2$^{fl/fl}$* mice is most likely not a result of a bone growth phenotype as observed in constitutive GC-B KO mice. The observed absence of the severe bone growth phenotype in the conditional GC-B/cGKI KO models is of advantage for the interpretation of the observed hearing phenotype of constitutive GC-B KO mice. In fact, the basal hearing phenotype was reproduced almost consistently for click- and noise-evoked ABR thresholds and f_2=11.3 kHz DPOAE thresholds even

with a very low *n*. Since the average increase in click- and noise-evoked ABR thresholds was significant and since the $2f_1$-f_2 thresholds for the stimulus frequency f_2=11.3 kHz are not significantly elevated in *cGKI$^{fl/fl}$;Wnt1^{Cre}* mice (Fig. 21B) it can be hypothesized that a knockout of the downstream kinase cGKI may enable for compensation mechanisms on the level of MOC-efferent feedback control. Future studies are needed to shed light onto fast temporal processing in the conditional knockout mouse models to confirm the disturbed efferent feedback control phenotype in the constitutive knockout model. Additionally, the conditional GC-B knockout mouse models enable for testing of sensitivity to sensorineural hearing loss following damaging noise overexposure. *Npr2$^{fl/fl}$;Wnt1^{Cre}* mice may be further a good model to disentangle the exact proportions for impaired retrocochlear feedback control on the IHCs and OHCs level.

4.5 Conclusion

The present study aimed to give new insights into the consequences of bifurcation loss of AN central axons in GC-B deficient mice and showed for the first time that, despite disturbed tonotopic representation of AN fibers in the CN (Lu et al. 2014), additional features of sound processing are profoundly changed. First, elevated ABR and DPOAE thresholds were observed which were not related to conduction deficits in middle ear sound transmission. Second, rapid MOC-efferent adaptive responses at the level of the OHCs was prominent. Thirdly, elevated AN activity was observed which is likely coupled to disinhibition of efferent feedback control on the OHC (and possibly IHC) level. Fourthly, progressively delayed ABR waves were observed, which could be linked to impaired LOC-efferent feedback onto IHCs. Fifth, changed responses to amplitude-modulated stimuli were observed which are likely linked to reduced reliance AN firing rates following acoustic stimulation (see also (Lu et al. 2014)). Sixthly, slight changes in very fast responses the ASR indicate deficits in temporal resolution of acoustic stimuli. Given the fact that specific features of auditory processing are spatially segregated on the level of the CN (Melcher and Kiang 1996; Zhao and Liang 1996) as well as the disturbed tonotopic representation of AN fibers in the CN (Lu et al. 2014; Ter-Avetisyan et al. 2014) and regarding that multipolar cells in the VCN maintained deficits in *Npr2$^{cn/cn}$* mice (Lu et al. 2014) which are discussed to be cholinergic EF-MOC feedback interneurons controlling cochlear amplification (de Venecia et al. 2005) it can be assumed that the evoked response of these interneurons is changed in case

of bifurcation loss, resulting in impaired retrocochlear feedback control. This hypothesis is strengthened by the finding that planar multipolar neurons in the VCN were found to terminate on MOC neurons in the ventral nucleus of the trapezoid body (MNTB) (Darrow et al. 2012). Further, the basic audiometric threshold loss was confirmed in conditional GC-B knockout mouse models underpinning the neuronal basis of the observed phenotypes in this study. More studies are needed to learn more about how segregation of low- and high-SR AN fibers is affected when proper development of the afferent auditory pathway is disturbed. Further, it is unknown until now how loss of AN nerve fiber bifurcation affects auditory synaptopathy and central processing disorders following noise overexposure (Basta et al. 2018; Gröschel et al. 2014)as well as death of cochlear neurons and its relevance for therapeutic intervention of hearing loss using cochlear implants (Wilkerson et al. 2017). The relevance for human patients is clear since reliable and precise temporal coding of auditory information is necessary for development and maintenance of proper speech perception (N. J. He et al. 2008; Shannon et al. 1995).

5. References

Avan, P., Buki, B., and Petit, C. (2013), 'Auditory distortions: origins and functions', *Physiol Rev,* 93 (4), 1563-619.

Barker, S. E., Lesperance, M. M., and Kileny, P. R. (2000), 'Outcome of newborn hearing screening by ABR compared with four different DPOAE pass criteria', *Am J Audiol,* 9 (2), 142-8.

Barral, J. and Martin, P. (2011), 'The physical basis of active mechanosensitivity by the hair-cell bundle', *Curr Opin Otolaryngol Head Neck Surg,* 19 (5), 369-75.

Barszczewski, M., et al. (2008), 'A novel site of action for alpha-SNAP in the SNARE conformational cycle controlling membrane fusion', *Mol Biol Cell,* 19 (3), 776-84.

Basta, D., Gröschel, M., and Ernst, A. (2018), '[Central and peripheral aspects of noise-induced hearing loss]', *HNO,* 66 (5), 342-49.

Becker, L., et al. (2018), 'The presynaptic ribbon maintains vesicle populations at the hair cell afferent fiber synapse', *Elife,* 7.

Beisel, K. W., et al. (2000), 'Longitudinal gradients of KCNQ4 expression in spiral ganglion and cochlear hair cells correlate with progressive hearing loss in DFNA2', *Brain Res Mol Brain Res,* 82 (1-2), 137-49.

Berglund, A. M. and Ryugo, D. K. (1987), 'Hair cell innervation by spiral ganglion neurons in the mouse', *J Comp Neurol,* 255 (4), 560-70.

Blaszczyk, J. W. (2003), 'Startle response to short acoustic stimuli in rats', *Acta Neurobiol Exp (Wars),* 63 (1), 25-30.

Bourien, J., et al. (2014), 'Contribution of auditory nerve fibers to compound action potential of the auditory nerve', *J Neurophysiol,* 112 (5), 1025-39.

Brand, A., et al. (2002), 'Precise inhibition is essential for microsecond interaural time difference coding', *Nature,* 417 (6888), 543-7.

Brawer, J. R., Morest, D. K., and Kane, E. C. (1974), 'The neuronal architecture of the cochlear nucleus of the cat', *J Comp Neurol,* 155 (3), 251-300.

Brownell, W. E. (1990), 'Outer hair cell electromotility and otoacoustic emissions', *Ear Hear,* 11 (2), 82-92.

Buran, B. N., et al. (2010), 'Onset Coding Is Degraded in Auditory Nerve Fibers from Mutant Mice Lacking Synaptic Ribbons', *Journal of Neuroscience,* 30 (22), 7587-97.

Burkard, R.F. and Don, M. (2007), 'The auditory brainstem response', in Burkard R.F., M. Don, and J.J. Eggermont (eds.), *Auditory Evoked Potentials: Basic Principles and Clinical Application* (Baltimore: Lippincott Williams & Wilkins), 229-50.

Cant, N. B. and Benson, C. G. (2003), 'Parallel auditory pathways: projection patterns of the different neuronal populations in the dorsal and ventral cochlear nuclei', *Brain Res Bull,* 60 (5-6), 457-74.

Clause, A., et al. (2014), 'The precise temporal pattern of prehearing spontaneous activity is necessary for tonotopic map refinement', *Neuron,* 82 (4), 822-35.

Dalhoff, Ernst, Zelle, Dennis, and Gummer, Anthony W. (2015), 'Ipsilateral medial olivocochlear reflex adaptation of the primary-source DPOAE component measured with pulsed tones', *AIP Conference Proceedings,* 1703 (1), 090009.

Dallos, P. (2008), 'Cochlear amplification, outer hair cells and prestin', *Curr Opin Neurobiol,* 18 (4), 370-6.

Danielian, P. S., et al. (1998), 'Modification of gene activity in mouse embryos in utero by a tamoxifen-inducible form of Cre recombinase', *Curr Biol,* 8 (24), 1323-6.

Darrow, K. N., Maison, S. F., and Liberman, M. C. (2006), 'Cochlear efferent feedback balances interaural sensitivity', *Nat Neurosci,* 9 (12), 1474-6.
--- (2007), 'Selective removal of lateral olivocochlear efferents increases vulnerability to acute acoustic injury', *J Neurophysiol,* 97 (2), 1775-85.
Darrow, K. N., Benson, T. E., and Brown, M. C. (2012), 'Planar multipolar cells in the cochlear nucleus project to medial olivocochlear neurons in mouse', *J Comp Neurol,* 520 (7), 1365-75.
de Venecia, R. K., et al. (2005), 'Medial olivocochlear reflex interneurons are located in the posteroventral cochlear nucleus: a kainic acid lesion study in guinea pigs', *J Comp Neurol,* 487 (4), 345-60.
Duncker, S. V., et al. (2013), 'Otoferlin couples to clathrin-mediated endocytosis in mature cochlear inner hair cells', *J Neurosci,* 33 (22), 9508-19.
Durrant, J. D., et al. (1998), 'Are inner or outer hair cells the source of summating potentials recorded from the round window?', *Journal of the Acoustical Society of America,* 104 (1), 370-77.
el Barbary, A. (1991), 'Auditory nerve of the normal and jaundiced rat. I. Spontaneous discharge rate and cochlear nerve histology', *Hear Res,* 54 (1), 75-90.
Elgoyhen, A. B. and Katz, E. (2012), 'The efferent medial olivocochlear-hair cell synapse', *J Physiol Paris,* 106 (1-2), 47-56.
Engel, J., et al. (2006), 'Two classes of outer hair cells along the tonotopic axis of the cochlea', *Neuroscience,* 143 (3), 837-49.
Engelien, A., et al. (2000), 'A combined functional in vivo measure for primary and secondary auditory cortices', *Hear Res,* 148 (1-2), 153-60.
Fettiplace, R. (2017), 'Hair Cell Transduction, Tuning, and Synaptic Transmission in the Mammalian Cochlea', *Compr Physiol,* 7 (4), 1197-227.
Friebe, A. and Koesling, D. (2003), 'Regulation of nitric oxide-sensitive guanylyl cyclase', *Circ Res,* 93 (2), 96-105.
Fuchs, P. A., Lehar, M., and Hiel, H. (2014), 'Ultrastructure of cisternal synapses on outer hair cells of the mouse cochlea', *J Comp Neurol,* 522 (3), 717-29.
G. Klumpp, R. and R. Eady, H. (1956), *Some Measurements of Interaural Time Difference Thresholds* (28).
Gehr, D. D., et al. (2004), 'Middle ear and cochlear disorders result in different DPOAE growth behaviour: implications for the differentiation of sound conductive and cochlear hearing loss', *Hear Res,* 193 (1-2), 9-19.
Geister, K. A., et al. (2013), 'A novel loss-of-function mutation in Npr2 clarifies primary role in female reproduction and reveals a potential therapy for acromesomelic dysplasia, Maroteaux type', *Human Molecular Genetics,* 22 (2), 345-57.
Glowatzki, E. and Fuchs, P. A. (2002), 'Transmitter release at the hair cell ribbon synapse', *Nat Neurosci,* 5 (2), 147-54.
Gomez-Nieto, R., et al. (2014), 'Origin and function of short-latency inputs to the neural substrates underlying the acoustic startle reflex', *Front Neurosci,* 8, 216.
Grant, L., Yi, E., and Glowatzki, E. (2010), 'Two modes of release shape the postsynaptic response at the inner hair cell ribbon synapse', *J Neurosci,* 30 (12), 4210-20.
Graydon, K., et al. (2019), 'Global burden of hearing impairment and ear disease', *J Laryngol Otol,* 133 (1), 18-25.
Gröschel, M., et al. (2014), 'Acute and long-term effects of noise exposure on the neuronal spontaneous activity in cochlear nucleus and inferior colliculus brain slices', *Biomed Res Int,* 2014, 909260.
Gu, J. W., et al. (2012), 'Brainstem auditory evoked potentials suggest a role for the ventral cochlear nucleus in tinnitus', *J Assoc Res Otolaryngol,* 13 (6), 819-33.

Guinan, J. J., Jr. (2006), 'Olivocochlear efferents: anatomy, physiology, function, and the measurement of efferent effects in humans', *Ear Hear,* 27 (6), 589-607.
--- (2010), 'Cochlear efferent innervation and function', *Curr Opin Otolaryngol Head Neck Surg,* 18 (5), 447-53.
--- (2018), 'Olivocochlear efferents: Their action, effects, measurement and uses, and the impact of the new conception of cochlear mechanical responses', *Hear Res,* 362, 38-47.
Hams, N., et al. (2017), 'Otoferlin is a multivalent calcium-sensitive scaffold linking SNAREs and calcium channels', *Proc Natl Acad Sci U S A,* 114 (30), 8023-28.
He, N. J., et al. (2008), 'Age-related differences in the temporal modulation transfer function with pure-tone carriers', *J Acoust Soc Am,* 124 (6), 3841-9.
He, S. and Yang, J. (2011), 'Maturation of neurotransmission in the developing rat cochlea: immunohistochemical evidence from differential expression of synaptophysin and synaptobrevin 2', *Eur J Histochem,* 55 (1), e2.
Hienz, R. D., Stiles, P., and May, B. J. (1998), 'Effects of bilateral olivocochlear lesions on vowel formant discrimination in cats', *Hear Res,* 116 (1-2), 10-20.
Hofmann, F., et al. (2006), 'Function of cGMP-dependent protein kinases as revealed by gene deletion', *Physiol Rev,* 86 (1), 1-23.
Holt, J. R., et al. (2007), 'Dominant-negative inhibition of M-like potassium conductances in hair cells of the mouse inner ear', *J Neurosci,* 27 (33), 8940-51.
Housley, G. D., Greenwood, D., and Ashmore, J. F. (1992), 'Localization of cholinergic and purinergic receptors on outer hair cells isolated from the guinea-pig cochlea', *Proc Biol Sci,* 249 (1326), 265-73.
Huang, A. Y. and May, B. J. (1996), 'Sound orientation behavior in cats. II. Mid-frequency spectral cues for sound localization', *J Acoust Soc Am,* 100 (2 Pt 1), 1070-80.
Jäger, K. and Kössl, M. (2016), 'Corticofugal Modulation of DPOAEs in Gerbils', *Hear Res,* 332, 61-72.
Jaumann, M., et al. (2012), 'cGMP-Prkg1 signaling and Pde5 inhibition shelter cochlear hair cells and hearing function', *Nat Med,* 18 (2), 252-9.
Jentsch, T. J., et al. (2000), 'Pathophysiology of KCNQ channels: neonatal epilepsy and progressive deafness', *Epilepsia,* 41 (8), 1068-9.
Johnson, D. H. and Kiang, N. Y. (1976), 'Analysis of discharges recorded simultaneously from pairs of auditory nerve fibers', *Biophys J,* 16 (7), 719-34.
Johnson, S. L., et al. (2013), 'Presynaptic maturation in auditory hair cells requires a critical period of sensory-independent spiking activity', *Proc Natl Acad Sci U S A,* 110 (21), 8720-5.
Joris, P. X., Schreiner, C. E., and Rees, A. (2004), 'Neural processing of amplitude-modulated sounds', *Physiol Rev,* 84 (2), 541-77.
Kawase, T., Delgutte, B., and Liberman, M. C. (1993), 'Antimasking effects of the olivocochlear reflex. II. Enhancement of auditory-nerve response to masked tones', *J Neurophysiol,* 70 (6), 2533-49.
Kemp-Harper, B. and Feil, R. (2008), 'Meeting report: cGMP matters', *Sci Signal,* 1 (9), pe12.
Kharkovets, T., et al. (2006), 'Mice with altered KCNQ4 K+ channels implicate sensory outer hair cells in human progressive deafness', *EMBO J,* 25 (3), 642-52.
Kiang, N. Y., et al. (1982), 'Hair-cell innervation by spiral ganglion cells in adult cats', *Science,* 217 (4555), 175-7.
Kitanishi, T., et al. (2013), 'Distinct localization of peripheral and central types of choline acetyltransferase in the rat cochlea', *Acta Histochem Cytochem,* 46 (5), 145-52.

Knipper, M., et al. (1996), 'Expression of neurotrophin receptor trkB in rat cochlear hair cells at time of rearrangement of innervation', *Cell Tissue Res,* 283 (3), 339-53.
Knipper, M., et al. (2013), 'Advances in the neurobiology of hearing disorders: recent developments regarding the basis of tinnitus and hyperacusis', *Prog Neurobiol,* 111, 17-33.
Knipper, M., et al. (2015), 'Specific synaptopathies diversify brain responses and hearing disorders: you lose the gain from early life', *Cell Tissue Res,* 361 (1), 77-93.
Knipper, M., et al. (2000), 'Thyroid hormone deficiency before the onset of hearing causes irreversible damage to peripheral and central auditory systems', *J. Neurophysiol.,* 83 (5), 3101-12.
Kuhn, M. (2003), 'Structure, regulation, and function of mammalian membrane guanylyl cyclase receptors, with a focus on guanylyl cyclase-A', *Circ Res,* 93 (8), 700-9.
--- (2009), 'Function and dysfunction of mammalian membrane guanylyl cyclase receptors: lessons from genetic mouse models and implications for human diseases', *Handb Exp Pharmacol,* (191), 47-69.
Kujawa, S. G. and Liberman, M. C. (2001), 'Effects of olivocochlear feedback on distortion product otoacoustic emissions in guinea pig', *J Assoc Res Otolaryngol,* 2 (3), 268-78.
--- (2009), 'Adding insult to injury: cochlear nerve degeneration after "temporary" noise-induced hearing loss', *J Neurosci,* 29 (45), 14077-85.
Kuwada, S., et al. (2002), 'Sources of the scalp-recorded amplitude-modulation following response', *J Am Acad Audiol,* 13 (4), 188-204.
Lauer, A. M., Behrens, D., and Klump, G. (2017), 'Acoustic startle modification as a tool for evaluating auditory function of the mouse: Progress, pitfalls, and potential', *Neurosci Biobehav Rev,* 77, 194-208.
Lee, Y., Kim, H. R., and Ahn, S. C. (2015), 'Vesicular glutamate transporter 3 is strongly upregulated in cochlear inner hair cells and spiral ganglion cells of developing circling mice', *Neurosci Lett,* 584, 320-4.
Leitner, M. G., et al. (2012), 'Restoration of ion channel function in deafness-causing KCNQ4 mutants by synthetic channel openers', *Br J Pharmacol,* 165 (7), 2244-59.
Liberman, M. C. (1978), 'Auditory-nerve response from cats raised in a low-noise chamber', *J Acoust Soc Am,* 63 (2), 442-55.
--- (1980), 'Morphological differences among radial afferent fibers in the cat cochlea: an electron-microscopic study of serial sections', *Hear Res,* 3 (1), 45-63.
Liberman, M. C. and Kujawa, S. G. (2017), 'Cochlear synaptopathy in acquired sensorineural hearing loss: Manifestations and mechanisms', *Hear Res,* 349, 138-47.
Liberman, M. C., Puria, S., and Guinan, J. J., Jr. (1996), 'The ipsilaterally evoked olivocochlear reflex causes rapid adaptation of the 2f1-f2 distortion product otoacoustic emission', *J Acoust Soc Am,* 99 (6), 3572-84.
Liberman, M. C., et al. (2016), 'Toward a Differential Diagnosis of Hidden Hearing Loss in Humans', *PLoS One,* 11 (9), e0162726.
Lingenhohl, K. and Friauf, E. (1994), 'Giant neurons in the rat reticular formation: a sensorimotor interface in the elementary acoustic startle circuit?', *J Neurosci,* 14 (3 Pt 1), 1176-94.
Lu, C. C., et al. (2014), 'Mutation of Npr2 Leads to Blurred Tonotopic Organization of Central Auditory Circuits in Mice', *Plos Genetics,* 10 (12).

Lustig, L. R. (2006), 'Nicotinic acetylcholine receptor structure and function in the efferent auditory system', *Anat Rec A Discov Mol Cell Evol Biol,* 288 (4), 424-34.
Maison, S. F., Usubuchi, H., and Liberman, M. C. (2013a), 'Efferent feedback minimizes cochlear neuropathy from moderate noise exposure', *J Neurosci,* 33 (13), 5542-52.
Maison, S. F., et al. (2006), 'Functional role of GABAergic innervation of the cochlea: phenotypic analysis of mice lacking GABA(A) receptor subunits alpha 1, alpha 2, alpha 5, alpha 6, beta 2, beta 3, or delta', *J Neurosci,* 26 (40), 10315-26.
Maison, S. F., et al. (2013b), 'Olivocochlear suppression of outer hair cells in vivo: evidence for combined action of BK and SK2 channels throughout the cochlea', *J Neurophysiol,* 109 (6), 1525-34.
Maison, S. F., et al. (2009), 'Loss of GABAB receptors in cochlear neurons: threshold elevation suggests modulation of outer hair cell function by type II afferent fibers', *J Assoc Res Otolaryngol,* 10 (1), 50-63.
Maison, S. F., et al. (2007), 'Overexpression of SK2 channels enhances efferent suppression of cochlear responses without enhancing noise resistance', *Journal of Neurophysiology,* 97 (4), 2930-36.
Maison, S. F., et al. (2012), 'Contralateral-noise effects on cochlear responses in anesthetized mice are dominated by feedback from an unknown pathway', *J Neurophysiol,* 108 (2), 491-500.
Malmierca, Manuel S. and Merchán, Miguel A. (2004), 'CHAPTER 31 - Auditory System', in George Paxinos (ed.), *The Rat Nervous System (Third Edition)* (Burlington: Academic Press), 997-1082.
Malmierca, Manuel S. and Ryugo, David K. (2012), 'Chapter 24 - Auditory System', in Charles Watson, George Paxinos, and Luis Puelles (eds.), *The Mouse Nervous System* (San Diego: Academic Press), 607-45.
Marcotti, W. (2012), 'Functional assembly of mammalian cochlear hair cells', *Exp Physiol,* 97 (4), 438-51.
Marcotti, W. and Kros, C. J. (1999), 'Developmental expression of the potassium current IK,n contributes to maturation of mouse outer hair cells', *J Physiol,* 520 Pt 3, 653-60.
Martinez-Monedero, R., et al. (2016), 'GluA2-Containing AMPA Receptors Distinguish Ribbon-Associated from Ribbonless Afferent Contacts on Rat Cochlear Hair Cells', *eNeuro,* 3 (2).
Mathers, Colin, Smith, Andrew, and Concha, Marisol (2000), *Global burden of hearing loss in the year 2000* (18).
Melcher, J. R. and Kiang, N. Y. S. (1996), 'Generators of the brainstem auditory evoked potential in cat .3. Identified cell populations', *Hearing Research,* 93 (1-2), 52-71.
Millman, R. E., et al. (2017), 'Magnified Neural Envelope Coding Predicts Deficits in Speech Perception in Noise', *J Neurosci,* 37 (32), 7727-36.
Möhrle, D., et al. (2016), 'Loss of auditory sensitivity from inner hair cell synaptopathy can be centrally compensated in the young but not old brain', *Neurobiol Aging,* 44, 173-84.
Möhrle, D., et al. (2017), 'NO-Sensitive Guanylate Cyclase Isoforms NO-GC1 and NO-GC2 Contribute to Noise-Induced Inner Hair Cell Synaptopathy', *Mol Pharmacol,* 92 (4), 375-88.
Moser, T., Brandt, A., and Lysakowski, A. (2006), 'Hair cell ribbon synapses', *Cell Tissue Res,* 326 (2), 347-59.

Nouvian, R., et al. (2006), 'Structure and function of the hair cell ribbon synapse', *J Membr Biol,* 209 (2-3), 153-65.
Ohinata, Y., Miller, J. M., and Schacht, J. (2003), 'Protection from noise-induced lipid peroxidation and hair cell loss in the cochlea', *Brain Res,* 966 (2), 265-73.
Ohlemiller, K. K. and Echteler, S. M. (1990), 'Functional correlates of characteristic frequency in single cochlear nerve fibers of the Mongolian gerbil', *J Comp Physiol A,* 167 (3), 329-38.
Patuzzi, R. B., Yates, G. K., and Johnstone, B. M. (1989), 'Outer hair cell receptor current and sensorineural hearing loss', *Hear Res,* 42 (1), 47-72.
Potter, L. R., Abbey-Hosch, S., and Dickey, D. M. (2006), 'Natriuretic peptides, their receptors, and cyclic guanosine monophosphate-dependent signaling functions', *Endocrine Reviews,* 27 (1), 47-72.
Qin, Z., Wood, M., and Rosowski, J. J. (2010), 'Measurement of conductive hearing loss in mice', *Hear Res,* 263 (1-2), 93-103.
Rabbitt, R. D. and Brownell, W. E. (2011), 'Efferent modulation of hair cell function', *Curr Opin Otolaryngol Head Neck Surg,* 19 (5), 376-81.
Rhode, W. S. and Smith, P. H. (1986), 'Encoding timing and intensity in the ventral cochlear nucleus of the cat', *J Neurophysiol,* 56 (2), 261-86.
Ruel, J., et al. (2001), 'Dopamine inhibition of auditory nerve activity in the adult mammalian cochlea', *Eur J Neurosci,* 14 (6), 977-86.
Ruel, J., et al. (2008), 'Impairment of SLC17A8 encoding vesicular glutamate transporter-3, VGLUT3, underlies nonsyndromic deafness DFNA25 and inner hair cell dysfunction in null mice', *Am J Hum Genet,* 83 (2), 278-92.
Russwurm, M. and Koesling, D. (2002), 'Isoforms of NO-sensitive guanylyl cyclase', *Mol Cell Biochem,* 230 (1-2), 159-64.
Rüttiger, L., Zimmermann, U., and Knipper, M. (2017), 'Biomarkers for Hearing Dysfunction: Facts and Outlook', *ORL J Otorhinolaryngol Relat Spec,* 79 (1-2), 93-111.
Rüttiger, L., et al. (2013), 'The reduced cochlear output and the failure to adapt the central auditory response causes tinnitus in noise exposed rats', *PLoS One,* 8 (3), e57247.
Sachs, M. B. and Abbas, P. J. (1974), 'Rate Versus Level Functions for Auditory-Nerve Fibers in Cats - Tone-Burst Stimuli', *Journal of the Acoustical Society of America,* 56 (6), 1835-47.
Safieddine, S. and Eybalin, M. (1992), 'Triple Immunofluorescence Evidence for the Coexistence of Acetylcholine, Enkephalins and Calcitonin Gene-related Peptide Within Efferent (Olivocochlear) Neurons of Rats and Guinea-pigs', *Eur J Neurosci,* 4 (10), 981-92.
Safieddine, S., Prior, A. M., and Eybalin, M. (1997), 'Choline acetyltransferase, glutamate decarboxylase, tyrosine hydroxylase, calcitonin gene-related peptide and opioid peptides coexist in lateral efferent neurons of rat and guinea-pig', *Eur J Neurosci,* 9 (2), 356-67.
Salvi, R. J., et al. (2000), 'A review of the effects of selective inner hair cell lesions on distortion product otoacoustic emissions, cochlear function and auditory evoked potentials', *Noise Health,* 2 (6), 9-26.
Schmidt, H. and Rathjen, F. G. (2010), 'Signalling mechanisms regulating axonal branching in vivo', *Bioessays,* 32 (11), 977-85.
--- (2011), 'DiI-labeling of DRG neurons to study axonal branching in a whole mount preparation of mouse embryonic spinal cord', *J Vis Exp,* (58).
Schmidt, H., et al. (2009), 'C-type natriuretic peptide (CNP) is a bifurcation factor for sensory neurons', *Proc Natl Acad Sci U S A,* 106 (39), 16847-52.

Schmidt, H., et al. (2007), 'The receptor guanylyl cyclase Npr2 is essential for sensory axon bifurcation within the spinal cord', *J Cell Biol,* 179 (2), 331-40.
Schreiner, C. E. and Langner, G. (1988), 'Periodicity coding in the inferior colliculus of the cat. II. Topographical organization', *J Neurophysiol,* 60 (6), 1823-40.
Schulz, S. (2005), 'C-type natriuretic peptide and guanylyl cyclase B receptor', *Peptides,* 26 (6), 1024-34.
Seal, R. P., et al. (2008), 'Sensorineural deafness and seizures in mice lacking vesicular glutamate transporter 3', *Neuron,* 57 (2), 263-75.
Sendin, G., et al. (2014), 'Spatiotemporal pattern of action potential firing in developing inner hair cells of the mouse cochlea', *Proc Natl Acad Sci U S A,* 111 (5), 1999-2004.
Shannon, R. V., et al. (1995), 'Speech recognition with primarily temporal cues', *Science,* 270 (5234), 303-4.
Sheets, L., et al. (2017), 'Enlargement of Ribbons in Zebrafish Hair Cells Increases Calcium Currents But Disrupts Afferent Spontaneous Activity and Timing of Stimulus Onset', *J Neurosci,* 37 (26), 6299-313.
Shen, J., Harada, N., and Yamashita, T. (2003), 'Nitric oxide inhibits adenosine 5'-triphosphate-induced Ca2+ response in inner hair cells of the guinea pig cochlea', *Neurosci Lett,* 337 (3), 135-8.
Shen, J., et al. (2005), 'Involvement of the nitric oxide-cyclic GMP pathway and neuronal nitric oxide synthase in ATP-induced Ca2+ signalling in cochlear inner hair cells', *Eur J Neurosci,* 21 (11), 2912-22.
Shen, J., et al. (2006), 'Role of nitric oxide on ATP-induced Ca2+ signaling in outer hair cells of the guinea pig cochlea', *Brain Res,* 1081 (1), 101-12.
Shi, X., Ren, T., and Nuttall, A. L. (2002), 'The electrochemical and fluorescence detection of nitric oxide in the cochlea and its increase following loud sound', *Hear Res,* 164 (1-2), 49-58.
Singer, W., et al. (2013), 'Noise-induced inner hair cell ribbon loss disturbs central arc mobilization: a novel molecular paradigm for understanding tinnitus', *Mol Neurobiol,* 47 (1), 261-79.
Sogawa, C., et al. (2010), 'Gastrointestinal tract disorder in natriuretic peptide receptor B gene mutant mice', *Am J Pathol,* 177 (2), 822-8.
Steube, N., et al. (2016), 'Dependence of the Startle Response on Temporal and Spectral Characteristics of Acoustic Modulatory Influences in Rats and Gerbils', *Front Behav Neurosci,* 10, 133.
Sun, F., et al. (2014), 'Expression patterns of atrial natriuretic peptide and its receptors within the cochlear spiral ganglion of the postnatal rat', *Hear Res,* 309, 103-12.
Taberner, A. M. and Liberman, M. C. (2005), 'Response properties of single auditory nerve fibers in the mouse', *J Neurophysiol,* 93 (1), 557-69.
Takeda-Nakazawa, H., et al. (2007), 'Hyposmotic stimulation-induced nitric oxide production in outer hair cells of the guinea pig cochlea', *Hear Res,* 230 (1-2), 93-104.
Takumida, M. and Anniko, M. (2002), 'Nitric oxide in the inner ear', *Curr Opin Neurol,* 15 (1), 11-5.
Tamura, N., et al. (2004), 'Critical roles of the guanylyl cyclase B receptor in endochondral ossification and development of female reproductive organs', *Proceedings of the National Academy of Sciences of the United States of America,* 101 (49), 17300-05.
Tan, J., et al. (2007), 'Tinnitus behavior and hearing function correlate with the reciprocal expression patterns of BDNF and Arg3.1/arc in auditory neurons following acoustic trauma', *Neuroscience,* 145 (2), 715-26.

Tasaki, I., Davis, H., and Eldredge, D. H. (1954), 'Exploration of cochlear potentials in guinea pig with a microelectrode', *J. Acoust. Soc. Am.,* 26 (765).
Ter-Avetisyan, G., Rathjen, F. G., and Schmidt, H. (2014), 'Bifurcation of Axons from Cranial Sensory Neurons Is Disabled in the Absence of Npr2-Induced cGMP Signaling', *Journal of Neuroscience,* 34 (3), 737-47.
Ter-Avetisyan, G., et al. (2018), 'Loss of Axon Bifurcation in Mesencephalic Trigeminal Neurons Impairs the Maximal Biting Force in Npr2-Deficient Mice', *Front Cell Neurosci,* 12, 153.
Tröster, P., et al. (2018), 'The Absence of Sensory Axon Bifurcation Affects Nociception and Termination Fields of Afferents in the Spinal Cord', *Front Mol Neurosci,* 11, 19.
Tsuji, T. and Kunieda, T. (2005), 'A loss-of-function mutation in natriuretic peptide receptor 2 (Npr2) gene is responsible for disproportionate dwarfism in cn/cn mouse', *Journal of Biological Chemistry,* 280 (14), 14288-92.
Turcanu, D., et al. (2009), 'Accuracy of velocity distortion product otoacoustic emissions for estimating mechanically based hearing loss', *Hear Res,* 251 (1-2), 17-28.
Valero, M. D., Hancock, K. E., and Liberman, M. C. (2016), 'The middle ear muscle reflex in the diagnosis of cochlear neuropathy', *Hear Res,* 332, 29-38.
Vetter, D. E., et al. (2007), 'The alpha10 nicotinic acetylcholine receptor subunit is required for normal synaptic function and integrity of the olivocochlear system', *Proc Natl Acad Sci U S A,* 104 (51), 20594-9.
Von Békésy, G. (1960), *Experiments in Hearing* 1-745.
Warr, W. Bruce and Guinan, John J. (1979), 'Efferent innervation of the organ of corti: two separate systems', *Brain Research,* 173 (1), 152-55.
Weber, T., et al. (2002), 'Thyroid hormone is a critical determinant for the regulation of the cochlear motor protein prestin', *Proc Natl Acad Sci U S A,* 99 (5), 2901-6.
Wedemeyer, C., et al. (2018), 'A Gain-of-Function Mutation in the alpha9 Nicotinic Acetylcholine Receptor Alters Medial Olivocochlear Efferent Short-Term Synaptic Plasticity', *J Neurosci,* 38 (16), 3939-54.
Wegener, J. W., et al. (2002), 'cGMP-dependent protein kinase I mediates the negative inotropic effect of cGMP in the murine myocardium', *Circ Res,* 90 (1), 18-20.
Whitehead, M. L., et al. (1996), 'Visualization of the onset of distortion-product otoacoustic emissions, and measurement of their latency', *Journal of the Acoustical Society of America,* 100 (3), 1663-79.
Whitfield, T. T. (2015), 'Development of the inner ear', *Curr Opin Genet Dev,* 32, 112-8.
Wilkerson, B. J., Porps, S. F., and Babu, S. C. (2017), 'The Impact of Comorbidities in the Aging Population on Cochlear Implant Outcomes', *Otology & Neurotology,* 38 (8), E285-E88.
Winter, H., et al. (2006), 'Thyroid hormone receptors TRalpha1 and TRbeta differentially regulate gene expression of Kcnq4 and prestin during final differentiation of outer hair cells', *J Cell Sci,* 119 (Pt 14), 2975-84.
Wolter, S., et al. (2018), 'GC-B Deficient Mice With Axon Bifurcation Loss Exhibit Compromised Auditory Processing', *Frontiers in Neural Circuits,* 12 (65).
Xia, Z. and Li, B. (1998), '[DPOAE in high-risk neonatal screening for hearing]', *Lin Chuang Er Bi Yan Hou Ke Za Zhi,* 12 (7), 306-8.
Yates, G. K. (1991), 'Auditory-nerve spontaneous rates vary predictably with threshold', *Hear Res,* 57 (1), 57-62.
Yu, F., et al. (2016), 'Mild Maternal Iron Deficiency Anemia Induces Hearing Impairment Associated with Reduction of Ribbon Synapse Density and

Dysregulation of VGLUT3, Myosin VIIa, and Prestin Expression in Young Guinea Pigs', *Neurotox Res,* 29 (4), 594-604.
Yukawa, H., et al. (2005), 'Acute effects of glucocorticoids on ATP-induced Ca2+ mobilization and nitric oxide production in cochlear spiral ganglion neurons', *Neuroscience,* 130 (2), 485-96.
Zampini, V., et al. (2010), 'Elementary properties of CaV1.3 Ca(2+) channels expressed in mouse cochlear inner hair cells', *J. Physiol.,* 588 (Pt 1), 187-99.
Zhao, H. B. and Liang, Z. A. (1996), 'Processing of modulation frequency in the dorsal cochlear nucleus of the guinea pig: sinusoidal frequency-modulated tones', *Hear Res,* 95 (1-2), 120-34.

6. Appendix

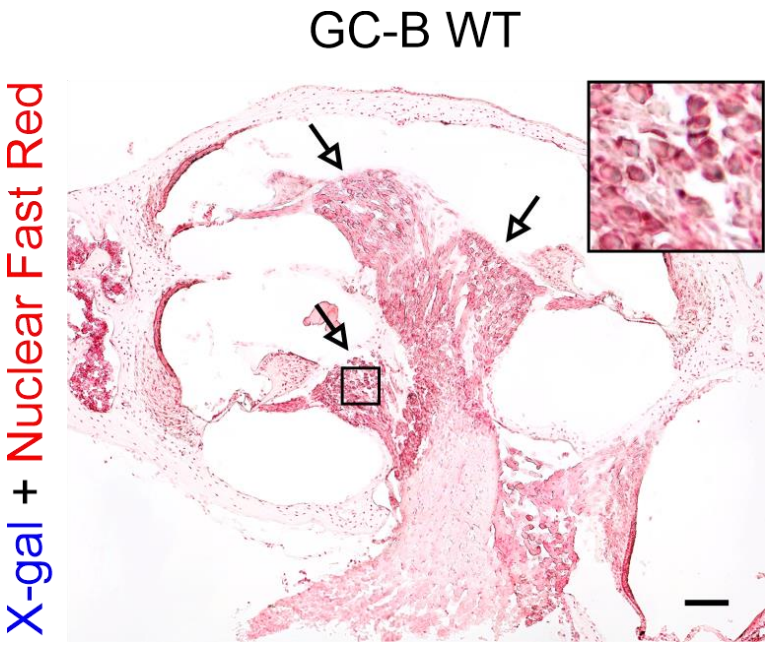

Fig. S1. GC-B expression analysis in the mature GC-B WT inner ear. Cochlear section of a 10-week-old GC-B WT mouse stained for X-gal (blue) and Nuclear Fast Red (red) with the apex oriented upwards. No X-gal staining was found in the SGNs and the OC. SGNs are indicated by open arrows. The inset shows a magnification from the boxed area in the midbasal cochlear turn. Scale bar: 25 µm.

Table 3. Statistical comparison of click-evoked ABR wave I-IV amplitudes from GC-B WT, GC-B HET and GC-B KO mice.

ABR wave I amplitudes																	
Stimulus level (dB SL)	**-10**	**-5**	**0**	**5**	**10**	**15**	**20**	**25**	**30**	**35**	**40**	**45**	**50**	**55**	**60**	**65**	**70**
WT (n=19-32) **vs KO** (n=18-31)	>0.999 n.s.	>0.999 n.s.	>0.999 n.s.	>0.999 n.s.	>0.999 n.s.	0.2098 n.s.	0.0094 **	<0.0001 ***	<0.0001 ***	<0.0001 ***	<0.0001 ***	<0.0001 ***	<0.0001 ***	<0.0001 ***	<0.0001 ***	<0.0001 ***	<0.0001 ***
HET (n=18-33) **vs KO** (n=18-31)	>0.999 n.s.	>0.999 n.s.	>0.999 n.s.	>0.999 n.s.	>0.999 n.s.	0.3469 n.s.	0.0639 n.s.	0.0011 ***	<0.0001 ***	<0.0001 ***	<0.0001 ***	<0.0001 ***	<0.0001 ***	<0.0001 ***	<0.0001 ***	<0.0001 ***	<0.0001 ***
WT (n=19-32) **vs HET** (n=18-33)	>0.999 n.s.	>0.999 n.s.	>0.999 n.s.	>0.999 n.s.	>0.999 n.s.	>0.999 n.s.	>0.999 n.s.	>0.999 n.s.	0.6377 n.s.	0.8076 n.s.	0.4795 n.s.	0.3358 n.s.	0.2750 n.s.	0.1224 n.s.	0.2378 n.s.	0.0891 n.s.	0.0132 *
ABR wave II amplitudes																	
WT (n=8-27) **vs KO** (n=12-23)	>0.999 n.s.	>0.999 n.s.	>0.999 n.s.	>0.999 n.s.	>0.999 n.s.	0.3825 n.s.	0.1153 n.s.	0.0035 **	<0.0001 ***	<0.0001 ***	<0.0001 ***	<0.0001 ***	<0.0001 ***	<0.0001 ***	0.0002 ***	<0.0001 ***	<0.0001 ***
HET (n=15-30) **vs KO** (n=18-31)	>0.999 n.s.	>0.999 n.s.	>0.999 n.s.	>0.999 n.s.	>0.999 n.s.	>0.999 n.s.	0.3029 n.s.	0.0032 **	<0.0001 ***	<0.0001 ***	<0.0001 ***	<0.0001 ***	<0.0001 ***	<0.0001 ***	<0.0001 ***	<0.0001 ***	<0.0001 ***
WT (n=8-27) **vs HET** (n=15-30)	>0.999 n.s.	>0.999 n.s.	>0.999 n.s.	>0.999 n.s.	>0.999 n.s.	>0.999 n.s.	>0.999 n.s.	>0.999 n.s.	>0.999 n.s.	>0.999 n.s.	>0.999 n.s.	>0.999 n.s.	>0.999 n.s.	0.7584 n.s.	0.2268 n.s.	0.1610 n.s.	0.1449 n.s.

ABR wave III amplitudes																
WT (n=16-32) **vs KO** (n=18-31)	>0.999 n.s.	>0.999 n.s.	>0.999 n.s.	>0.999 n.s.	>0.999 n.s.	>0.999 n.s.	>0.999 n.s.	0.6248 n.s.	0.1776 n.s.	0.0975 n.s.	0.0426 *	0.0026 **	0.0001 ***	<0.0001 ***	<0.0001 ***	<0.0001 ***
HET (n=18-33) **vs KO** (n=18-31)	>0.999 n.s.	>0.999 n.s.	>0.999 n.s.	>0.999 n.s.	>0.999 n.s.	>0.999 n.s.	>0.999 n.s.	>0.999 n.s.	0.4091 n.s.	0.2441 n.s.	0.0735 n.s.	0.0070 **	0.0008 ***	0.0008 ***	0.0012 ***	<0.0001 ***
WT (n=16-32) **vs HET** (n=18-33)	>0.999 n.s.	>0.999 n.s.	>0.999 n.s.	>0.999 n.s.	>0.999 n.s.	>0.999 n.s.	>0.999 n.s.	>0.999 n.s.	>0.999 n.s.	>0.999 n.s.	>0.999 n.s.	>0.999 n.s.	>0.999 n.s.	0.8749 n.s.	0.5705 n.s.	>0.999 n.s.
Table ABR wave IV amplitudes																
WT (n=17-32) **vs KO** (n=18-31)	>0.999 n.s.	>0.999 n.s.	>0.999 n.s.	>0.999 n.s.	>0.999 n.s.	0.4212 n.s.	0.1429 n.s.	0.0639 n.s.	0.0340 *	0.0024 **	0.0007 ***	0.0011 **	0.0436 *	0.1613 n.s.	0.2914 n.s.	0.0713 n.s.
HET (n=18-33) **vs KO** (n=18-31)	>0.999 n.s.	>0.999 n.s.	>0.999 n.s.	>0.999 n.s.	>0.999 n.s.	>0.999 n.s.	0.4123 n.s.	>0.999 n.s.	0.3436 n.s.	0.6301 n.s.	0.3128 n.s.	0.1288 n.s.	0.8820 n.s.	>0.999 n.s.	>0.999 n.s.	0.4124 n.s.
WT (n=17-32) **vs HET** (n=18-31)	>0.999 n.s.	>0.999 n.s.	>0.999 n.s.	>0.999 n.s.	>0.999 n.s.	>0.999 n.s.	>0.999 n.s.	0.4028 n.s.	0.9769 n.s.	0.0942 n.s.	0.1058 n.s.	0.3348 n.s.	0.4405 n.s.	0.3348 n.s.	0.8676 n.s.	>0.999 n.s.

Bonferroni corrected *p* values: ***$p<0.001$, **$p<0.01$, *$p<0.05$, n.s. not significant; *n* = number of ears

Table 4. Statistical comparison of click-evoked ABR wave I-IV latencies from GC-B WT, GC-B HET and GC-B KO mice.

ABR wave I latencies															
Stimulus level (dB SL)	**0**	**5**	**10**	**15**	**20**	**25**	**30**	**35**	**40**	**45**	**50**	**55**	**60**	**65**	**70**
WT (n=29-32) **vs KO** (n=18-31)	0.0042 ****	0.0034 ****	0.0320 *	0.0302 *	0.0302 *	0.0857 n.s.	0.1976 n.s.	0.0820 n.s.	0.1976 n.s.	0.0340 *	0.0123 *	0.0041 **	0.0050 **	0.0005 ***	0.0002 ***
HET (n=31-33) **vs KO** (n=18-31)	0.0386 *	0.0786 n.s.	0.4144 n.s.	0.4144 n.s.	>0.999 n.s.	0.7980 n.s.	0.7980 n.s.	>0.999 n.s.	0.8088 n.s.	0.0860 n.s.	0.2045 n.s.	0.0343 *	0.0373 *	0.0018 **	0.0050 **
WT (n=29-32) **vs HET** (n=31-33)	>0.999 n.s.	0.8102 n.s.	0.7980 n.s.	0.7864 n.s.	0.1852 n.s.	0.7980 n.s.	>0.999 n.s.	0.4048 n.s.	>0.999 n.s.	>0.999 n.s.	0.8209 n.s.	>0.999 n.s.	>0.999 n.s.	>0.999 n.s.	0.8335 n.s.
ABR wave II latencies															
WT (n=8-27) **vs KO** (n=12-23)	<0.0001 ***	0.0001 ***	0.0002 ***	0.0028 **	0.0061 **	0.0075 **	0.0328 *	0.1133 n.s.	0.0627 n.s.	0.2030 n.s.	0.4654 n.s.	0.6530 n.s.	>0.999 n.s.	0.5573 n.s.	0.2984 n.s.
HET (n=15-30) **vs KO** (n=12-23)	<0.0001 ***	0.0202 *	0.0202 *	0.0715 n.s.	0.2116 n.s.	0.3543 n.s.	0.3543 n.s.	0.7925 n.s.	0.8029 n.s.	>0.999 n.s.	0.8328 n.s.	0.8255 n.s.	>0.999 n.s	0.3498 n.s.	0.1568 n.s.
WT (n=8-27) **vs HET** (n=15-30)	>0.999 n.s.	0.3049 n.s.	0.4690 n.s.	0.7122 n.s.	0.4690 n.s.	0.3049 n.s.	0.7573 n.s.	0.7925 n.s.	0.5341 n.s.	0.5681 n.s..	>0.999 n.s.	>0.999 n.s.	>0.999 n.s.	>0.999 n.s.	>0.999 n.s.

ABR wave III latencies															
WT (n=29-32) **vs KO** (n=18-31)	<0.0001 ***	<0.0001 ***	<0.0001 ***	<0.0001 ***	<0.0001 ***	<0.0001 ***	<0.0001 ***	<0.0001 ***	0.0002 ***	0.0002 ***	0.0002 ***	0.0005 ***	0.0042 **	0.0010 ***	0.0011 **
HET (n=29-33) **vs KO** (n=18-31)	0.0002 ***	<0.0001 ***	0.0002 ***	0.0002 ***	0.0013 **	0.0013 **	0.0025 **	0.0025 **	0.0047 **	0.0008 ***	0.0015 **	0.0031 **	0.0329 *	0.0168 *	0.0085 **
WT (n=29-32) **vs HET** (n=29-33)	0.0540 n.s.	0.1713 n.s.	0.4668 n.s.	>0.999 n.s.	>0.999 n.s.	>0.999 n.s.	>0.999 n.s.	>0.999 n.s.	>0.999 n.s.	>0.999 n.s.	>0.999 n.s.	>0.999 n.s.	>0.999 n.s.	>0.999 n.s.	>0.999 n.s.
ABR wave IV latencies															
WT (n=29-32) **vs KO** (n=18-31)	<0.0001 ***	<0.0001 ***	<0.0001 ***	<0.0001 ***	<0.0001 ***	<0.0001 ***	<0.0001 ***	<0.0001 ***	<0.0001 ***	<0.0001 ***	<0.0001 ***	<0.0001 ***	<0.0001 ***	<0.0001 ***	<0.0001 ***
HET (n=28-33) **vs KO** (n=18-31)	<0.0001 ***	<0.0001 ***	<0.0001 ***	<0.0001 ***	0.0001 ***	0.0017 **	0.0010 **	0.0017 **	0.0017 **	0.0002 ***	<0.0001 ***	<0.0001 ***	0.0020 **	0.0094 *	0.0127 *
WT (n=29-32) **vs HET** (n=28-33)	0.7618 n.s.	>0.999 n.s.	>0.999 n.s.	>0.999 n.s.	0.6816 n.s.	0.5391 n.s.	0.8492 n.s.	0.5391 n.s.	0.4200 n.s.	0.5391 n.s.	0.4200 n.s.	0.5391 n.s.	0.7035 n.s.	0.2287 n.s.	0.2360 n.s.

Bonferroni corrected *p* values: ***$p<0.001$, **$p<0.01$, *$p<0.05$, n.s. not significant; *n* = number of ears

Table 5. Statistical comparison of ASSR I-O functions from GC-B WT, GC-B HET and GC-B KO mice,evoked by an amplitude-modulated tone composed of a 11.3 kHz carrier modulated with 512 Hz at 100 % modulation depth.

SNR															
Stimulus level (dB SL)	**-10**	**-5**	**0**	**5**	**10**	**15**	**20**	**25**	**30**	**35**	**40**	**45**	**50**	**55**	**60**
WT (n=8) **vs KO** (n=8)	>0.999	0.9130	>0.999	>0.999	0.0082	0.0151	0.2673	0.0080	0.0768	0.0457	0.5337	0.0626	0.2362	0.1022	0.2642
	n.s.	n.s.	n.s.	n.s.	**	*	n.s.	**	n.s.	*	n.s.	n.s.	n.s.	n.s.	n.s.
HET (n=10) **vs KO** (n=8)	>0.999	0.8519	>0.999	0.6881	0.1136	0.0301	0.6406	0.0234	0.2324	>0.999	0.3176	0.1089	0.0815	0.1864	0.2140
	n.s.	n.s.	n.s.	n.s.	n.s.	*	n.s.	*	n.s.	n.s.	n.s.	n.s.	n.s.	n.s.	n.s.
WT (n=8) **vs HET** (n=10)	>0.999	>0.999	>0.999	>0.999	0.8224	>0.999	>0.999	>0.999	>0.999	0.2812	>0.999	>0.999	>0.999	>0.999	>0.999
	n.s.	n.s.	n.s.	n.s.	n.s.	n.s.	n.s.	n.s.	n.s.	n.s.	n.s.	n.s.	n.s.	n.s.	n.s.

Bonferroni corrected *p* values: *** $p<0.001$, ** $p<0.01$, * $p<0.05$, n.s. not significant, *n* number of mice